DEVELOPMENT OF MRI TECHNIQUES FOR MEASURING CEREBRAL BLOOD VOLUME, BLOOD FLOW, AND BLOOD OXYGENATION WITHIN A SINGLE SCAN

by
Ying Cheng

A dissertation submitted to Johns Hopkins University in conformity with the requirements for the degree of Doctor of Philosophy

Baltimore, Maryland
August, 2015

ABSTRACT

Functional MRI (fMRI) is commonly performed using the blood-oxygenation-level-dependent (BOLD) approach, which is sensitive to ensemble changes in cerebral blood volume (CBV), cerebral blood flow (CBF), and cerebral metabolic rate of oxygen ($CMRO_2$). In order to understand and quantify the BOLD fMRI signal, it is essential to design multi-modal fMRI approaches that are sensitized to these individual hemodynamic parameters, and to further determine the oxygen metabolism. This dissertation aims to develop and improve current quantitative fMRI techniques to detect relaxation times T_2^*, cerebral blood volume (CBV), cerebral blood flow (CBF), blood oxygenation level hemodynamics, oxygen extraction fraction (OEF), and $CMRO_2$ during neuronal activation in a time efficient manner.

Total and extravascular R_2^* values in the parenchyma in human visual cortex are measured by combining multi-echo BOLD and vascular-space-occupancy (VASO) fMRI with visual stimulation at 7T. The VASO method is expected to suppress the intravascular signals in the microvessels. Both the absolute parenchymal extravascular R_2^* and R_2^* changes (ΔR_2^*) upon activation are determined, and the ratio of extravascular ΔR_2^* to total ΔR_2^* is calculated, confirming a predominant contribution from the extravascular component of the BOLD effect at 7T. Parenchymal OEF during stimulation is also estimated based on these measurements, the value of which is consistent with those reported at lower field strengths.

While normally in most of the quantitative fMRI approaches, BOLD, CBV, and CBF measurements are separately performed to estimate $CMRO_2$ dynamics, the ability to acquire these physiological parameters simultaneously would be very useful to improve

image acquisition efficiency, and more importantly reduce the sensitivity to temporal variations due to factors such as subject head motion, task performance, and physiologic fluctuations between the fMRI experiments. A large portion of this dissertation is devoted to design single-scan approaches to detect changes in the multi-modal hemodynamic signals. First, a novel 3D whole-brain MRI pulse sequence, dubbed 3D VASO-FAIR, is proposed to detect CBV and CBF responses in a single scan. Second, a new 3D acquisition strategy that extends VASO-FAIR and incorporates a 3D T2-preparation gradient-echo (GRE) BOLD method is implemented to simultaneously measure BOLD, CBV, and CBF reactivity during functional stimulation. Compared to individually performed multi-modal fMRI scans, similar image quality, activation patterns, relative signal changes (ΔS/S), tSNRs and CNRs can be achieved using the proposed combined sequences. Finally, based on the BOLD, CBV, and CBF responses obtained from the combined sequence, the oxygen metabolism alterations (OEF and CMRO2) are quantified.

First Reader and Supervisor:

Peter C.M. van Zijl, Ph.D.

Professor

Department of Radiology and Radiological Science, Johns Hopkins University

Department of Biophysics and Biophysical Chemistry, Johns Hopkins University

Department of Oncology, Johns Hopkins University

Director

F.M. Kirby Research Center for Functional Brain Imaging

Second Reader:

James J. Pekar, Ph.D.

Associate Professor

Department of Radiology and Radiological Science, Johns Hopkins University

Manager and Research Coordinator

F.M. Kirby Research Center for Functional Brain Imaging

Defense Committee (in alphabetic order):

Peter Barker, D.Phil.

Daniel Herzka, Ph.D.

James J. Pekar, Ph.D.

Peter C.M. van Zijl, Ph.D.

ACKNOWLEDGEMENT

This dissertation work would not have been possible without the guidance and support from numerous individuals at every step of the way.

First, I would like to thank my Ph.D. advisor, Dr. Peter van Zijl, who has always given me constant support, encouragement, and freedom to work on my projects, and has taught me the importance of thinking independently and critically. His wisdom, intuition, knowledge, creativity, and friendliness are contagious, and I have learnt many lessons from him not only about magnetic resonance and science, but also life. I am also grateful for Peter's constant supportiveness in sending me to various international conferences, workshops, and industry course trainings, even when I first got to lab and knew little about MR. Before every presentation I need to give at a conference, Peter was always there sitting in the audience, comforting me to relax and to speak slowly, and ready to take bullets for me whenever there is a tough question that I cannot handle myself. Peter is the best advisor I could possibly ask for, and it has truly been a great honor and privilege to work closely with him.

The work presented in this dissertation took place in the F. M. Kirby Research Center for Functional Brain Imaging, where I have spent the best five years of my life and have been lucky to have been surrounded by people who have generously provided a great deal of assistance and guidance to me, both in terms of professionalism as well as friendship. I owe my special thanks to Dr. Jun Hua, who has always been my go-to person and has given me numerous hands-on help and advices on pulse sequence programming and image post-processing, and spent countless days revising my manuscripts and ISMRM presentation slides. Specifically, I wish to thank Dr. James

Pekar, who served on my thesis committee board and officiated my wedding, for his tremendous help and advices on my Ph.D. study. I want to give my special thanks to Dr. Alan Huang, who picked me up from the BWI airport after I landed in this new country for the very first time in my life, and has been the most caring 'big sib' ever since. I am grateful for the experimental assistance provided to me by the MR technologists Terri Brawner, Kathleen Kahl, and Ivana Kusevic, all of whom have always been keen to help in my research projects. I am also grateful to Joe Gillen for his continued assistance in programming and all the IT-related problems. Other members of the Kirby Center who have helped me in every possible ways are Drs. Qin Qin, Nirbhay Yadav, Craig Jones, Feng Xu, Xiang Xu, Kannie Chan, Jiadi Xu, Xu Li, Issel Lim, Ann Choe, Haifeng Zeng, Wenbo Li, and Guanshu Liu. I also would like to thank Candace Herbster and Heather Mackey for always addressing administrative matters quickly and professionally. Kirby Center is like a big family to me. The environment created by Peter and the wonderful people above has made me coming to work every day like a privilege, and I will never forget what the members of the Kirby Center have given me.

I am grateful to Dr. Peter Barker, who accepted me as his first graduate student for a research rotation, and introduced me to the world of MRI and MRS. I would like to thank Dr. Barker for his invaluable advices and insightful inputs on my thesis research. I also wish to thank Dr. Richard Edden, who helped with my first MRI experiment, and gave me the very first lecture on MR pulse sequence development. I sincerely thank Dr. Daniel Herkza for his participation in both my GBO and my thesis committee, for his helpful comments on my dissertation work, and for all the stimulating MRI lectures he

TABLE OF CONTENTS

LIST OF TABLES

LIST OF FIGURES

Chapter 1: Introduction and Motivations

1.1. Basic Principles of Magnetic Resonance Imaging

Unlike CT and PET which rely on ionizing radiation, MRI uses non-ionizing radiofrequency (RF) pulses for generating image contrast, making it a much safer alternative. The true utility of MRI, however, is its flexibility. CT and PET are generally limited in their capacity to generating images and studying basic metabolism. Conversely, MRI is derived from the manipulation of proton spins by RF pulses and can be achieved in incredibly diverse ways. Different combinations of pulses can sensitize MR contrast to a variety of different physiological processes.

The first successful nuclear magnetic resonance experiment was independently performed by Purcell (Purcell et al. 1946) at Harvard and Bloch (Bloch et al. 1946) at Stanford in 1946, respectively, in which they measured the resonance of nuclei in bulk matter. The experiments of Bloch and Purcell laid the groundwork for the field of NMR as a method for probing the structure of chemical compounds. They received the Nobel prize in 1952. Paul Lauterbur demonstrated how to localize regions of interest within the NMR sample by using a weak magnetic field combined with a magnetic field gradient to induce a spatially varying resonant frequency. He generated the first MR images using a projection reconstruction technique (Lauterbur 1973) similar to current CT image reconstruction methods. Richard Ernst developed spatially encoding mechanisms for the NMR signal and applied Fourier transform to interpret the frequency data (Nagayama et al. 1977; Ernst 1987). Peter Mansfield similarly formulated mathematical approaches for generating images from detectable MR frequencies and also developed a fast imaging

technique called *echo planar imaging* (EPI) (Mansfield et al. 1978). Over the past few decades, MRI has become a primary non-invasive imaging modality to probe the anatomical and functional information of the human body. In 2003, Lauterbur and Mansfield were awarded the Nobel Prize for the invention of MRI.

Classical description of NMR

At thermal equilibrium, when there is no external magnetic field applied, no net magnetic field exists around an object. When the object sample is placed in a strong external magnetic field ($\vec{B}_0$), it will be polarized such that its bulk magnetization will align with the direction of the external magnetic field. The external $\vec{B}_0$ field is usually defined to be along the z-axis, so at equilibrium the net magnetization vector $\vec{M}$ points along the positive direction of the z-axis, and its magnitude is

$$M_z^0 = \left|\vec{M}\right| = \frac{\gamma^2 \hbar B_0 N_s}{4KT_s}$$
[1.1]

where γ is the gyromagnetic ratio for certain nucleus, $\hbar$ is the Planck's constant h divided by 2π, N_s is the total number of spins in the sample, K is the Boltzmann constant, T_s is the absolute temperature of the sample. Equation [1.1] indicates that the magnitude of $\vec{M}$ is directly proportional to the external magnetic field strength B_0. Thus, the net magnetization increases as the strength of $\vec{B}_0$ increases. For most clinical MRI systems, $\vec{B}_0$ ranges from 0.5 to 3 T.

If in some way the net magnetization $\vec{M}$ is perturbed away from $\vec{B}_0$, it will experience a torque. The motion of $\vec{M}$ can be described by the following equation:

2

$$\omega_0 = \gamma B_0 \qquad\qquad [1.2]$$

If $\vec{B}_0$ is along z-axis, the magnetization vector $\vec{M}$ will precess about the z-axis with the angular frequency of $\omega_0 = \gamma B_0$, which is also called the Larmor frequency. Therefore, in the presence of a magnetic field, the net magnetization vector will precess at an angular frequency proportional to the gyromagnetic ratio of the nuclei in the sample and the strength of the external magnetic field.

A detectable MR signal is achieved by applying an additional time varying magnetic field $\vec{B}_1$ perpendicular to the static magnetic field $\vec{B}_0$ to perturb the magnetization. In contrast to the primary magnetic field $\vec{B}_0$, the external field is much weaker (e.g., B_1 = 50 mT while B_0 = 1.5 T). Moreover, $\vec{B}_1$ is oscillating at the Larmor frequency ω_0 of the proton sample (resonant with $\vec{B}_0$). According to Eq. [1.2], the net magnetization vector $\vec{M}$ will simultaneously precess about $\vec{B}_0$ at ω_0 and $\vec{B}_1$ at $\omega_1 = \gamma B_1$. It is often conceptually simpler to think in terms of the frame of reference of $\vec{B}_1$ that is rotating at the Larmor frequency ω_0 of the sample. In this rotating frame, the magnetization is simply tipped away from z-axis by $\vec{B}_1$. If the duration of the $\vec{B}_1$ excitation pulse is t, the magnetization vector $\vec{M}$ will rotate by a flip angle (FA) of $\theta = \omega_1 t$. When an appropriate $\vec{B}_1$ excitation is applied, the magnetization vector can be tipped by 90° to lie entirely in the transverse plane, where its evolution can then be detected.

When $\vec{B}_1$ is removed, the magnetization vector will gradually return to the equilibrium state. This process is characterized by a precession of $\vec{M}$ about the $\vec{B}_0$ field,

called *free precession*; a recovery of the longitudinal magnetization M_z, called *longitudinal relaxation*; and the destruction of the transverse magnetization M_{xy}, called *transverse relaxation*, the latter two are different, independent processes. Longitudinal relaxation is an exponential process characterized by the time constant T_1 and is caused by the interaction of the excited spins with surrounding randomly fluctuating magnetic fields of spins in the lattice. Thus T_1 relaxation is often called *spin-lattice* relaxation and increase with field strength.

The transverse relaxation is also an exponential process, and is characterized by the time constant T_2. It occurs since the fluctuating spins in the sample each generate a slightly different magnetic field that changes the phase of the spins of interest. Therefore T_2 is also called *spin-spin* relaxation time. To detect the transverse magnetization is difficult as the spins in the transverse plane will see slightly different local fields thus different frequencies of precession, leading to a loss of phase coherence of the transverse component and ultimately a decay of the detectable MRI signal. This T_2 relaxation is an irreversible process as it is caused by random fluctuations of the magnetic fields of spins in the sample.

It is worth mentioning that certain mechanisms that cause phase dispersion can be reversed. B_0 field inhomogeneity will cause spins in different locations to accumulate phase relative to each other, leading to an exponential decay of signal described by the time constant T_2'. The combined effect of T_2 and T_2' is described by the effective transverse relaxation time T_2^* ($\frac{1}{T_2^*} = \frac{1}{T_2} + \frac{1}{T_2'}$). It has been shown that dephasing in static inhomogeneous magnetic fields can be reversed by applying a 180° RF pulse to invert the phase of the spins following the initial evolution after excitation. In this so-called *spin*

echo experiment, the time between the excitation and when the spins are again in phase is the echo time (TE), and the 180° RF pulse is applied at time TE/2. Spin echo experiments therefore effectively correct for T_2' decay, allowing for more signal to be present at the time of acquisition, and in turn the possibility for longer signal acquisition times.

The time-dependent behavior of the magnetization vector $\vec{M}$ can be described quantitatively by the empirical Bloch equation, named after Felix Bloch:

$$\frac{d\vec{M}}{dt} = \gamma \vec{M} \times \vec{B} + \frac{1}{T_1}(M_0 - M_z)\hat{z} - \frac{1}{T_2}\vec{M}_{xy} \qquad [1.3]$$

where B is the applied, external magnetic field, M_z is the longitudinal magnetization and M is the transverse (x,y) magnetization. The Bloch equation can be separated into transverse and longitudinal components:

$$\frac{dM_x}{dt} = \omega_0 M_y - \frac{M_x}{T_2}$$
$$\frac{dM_y}{dt} = -\omega_0 M_x - \frac{M_y}{T_2} \qquad [1.4]$$
$$\frac{dM_z}{dt} = \frac{(M_0 - M_z)}{T_1}$$

the general solutions are,

$$M_x = e^{-t/T_2}(M_x(0)\cos\omega_0 t + M_y(0)\sin\omega_0 t)$$
$$M_y = e^{-t/T_2}(M_y(0)\cos\omega_0 t - M_x(0)\sin\omega_0 t)$$
$$M_z = M_z(0)e^{-t/T_1} + M_0(1 - e^{-t/T_1}) \qquad [1.5]$$

Note that in the above equations, the transverse (T_2) and longitudinal (T_1) relaxation times are completely independent of one another.

Spatial encoding and imaging

Finally, MR *imaging* is achieved through application of spatially varying magnetic fields (gradients) in addition to the $\vec{B}_0$ and $\vec{B}_1$ fields. There are generally three separate gradient coils that produce linear variations in the magnetic field along the x, y and z direction, so-called field gradients (G_x, G_y, and G_z). Therefore, the gradient field, in combination with the $\vec{B}_0$ field, can be used to create a region of spins with a distinct resonant frequency at a specific location; then spatially selective excitation can be achieved by tuning $\vec{B}_1$ to this frequency.

The strength of the magnetic field at any given position can be written as

$$B = B_0 + G_x r_x + G_y r_y + G_z r_z$$

[1.6]

where G_x, G_y, and G_z denote the gradient strengths and r_x, r_y and r_z describe the corresponding location. In the absence of the gradient fields, having denoted the number of spins at a particular location (x,y,z) with the spin density $\rho(x,y,z)$, the signal from the sample can be written as

$$s = \iiint dx\, dy\, dz \rho(x,y,z)$$

[1.7]

However, when the spatially varying gradients exist, protons at different locations will have non-equal phases. Therefore, an additional term to account for the different phases produced by the gradients must be introduced,

$$s(k_x, k_y, k_z) = \iiint dx\, dy\, dz \rho(x,y,z) e^{-2\pi i (k_x x + k_y y + k_z z)} = F[\rho(x,y,z)]$$

[1.8]

where,

$$k_x(t) = \frac{\gamma}{2\pi} \int_0^t G_x(t')dt'$$

$$k_y(t) = \frac{\gamma}{2\pi} \int_0^t G_y(t')dt'$$

$$k_z(t) = \frac{\gamma}{2\pi} \int_0^t G_z(t')dt'$$

[1.9]

The above formula suggests that there is a Fourier relationship between the detected MR signal and spin density of the sample being imaged, and the signal is described with a spatial frequency parameter given by $\vec{k} = k_x\hat{x} + k_y\hat{y} + k_z\hat{z}$. Therefore, if spatial frequency information is sampled, an image of $\rho(x,y,z)$ can be generated by taking the inverse Fourier transform of all of the spatial frequency-space or so called k-space.

There are different ways that have been developed for sampling k-space. In general the idea is to detect the frequency of the imaging sample during a time course of gradient applications. The resolution of the image depends on the extent of k-space that is sampled. Sampling schemes with different k-space trajectories include Cartesian sampling, radial sampling, and spiral sampling.

Image contrast and pulse sequence

An MRI pulse sequence is a programmed set of RF pulses and magnetic field gradients with careful choice of timings. The contrast in an MR image is strongly dependent upon the pulse sequence. It is possible to highlight different components in the object being imaged, based on properties such as water (spin) density, T_1, and T_2 relaxation time.

7

The basis of MR image contrast is the spin density throughout the object. There will be no NMR signal at all if there are no spins present in a region. The majority of MRI scans utilize the hydrogen nuclei (i.e., protons) as the signal sources, which are found in abundance in the human body in water molecules. Therefore proton spin densities depend on water content, and vary in different human tissues. When such difference in tissues is small, additional contrast mechanisms must be employed. These are generated based on the variation in T_1 and T_2 values for different tissues.

T_1 weighted images are usually generated using a so-called inversion recovery (IR) pulse sequence, in which a RF pulse with flip angle of 180° that inverts the magnetization is followed by a 90° RF pulse that flips the residual longitudinal magnetization into the transverse plane where it can be detected by an RF coil. After the 180° inversion pulse, the longitudinal magnetization M_z will recover for a period of time, namely the inversion time (TI), before acquiring the images. The amount of signal available by the time of signal detection will depend on the T_1 relaxation time of the sample. If the sample has spins with several different T_1, it is possible to choose a suitable TI such that the signal from spins with one recovery rate is nulled, while giving a good contrast among spins with other recovery rates. In order to calculate the values of T_1 to create a T_1 map, it is necessary to acquire several points along the magnetization recovery curve and then fit the points to the inversion recovery equation derived from the Bloch equation for M_z:

$$M_z(TI) = M(0) \cdot (1 - 2e^{-TI/T_1} + e^{-TR/T_1})$$

[1.10]

The most straightforward way is to repeat the inversion recovery sequence for a number of values of TI.

As briefly mentioned earlier, a spin echo (SE) sequence can be used to obtain images with dominant T_2 contrast. A spin echo is formed by applying a 180° pulse to invert the phase of the spins following the initial evolution after excitation. The time between the excitation and when the spins are again in phase is the echo time (TE), and the 180° RF pulse is applied at time TE/2. This has the effect of reversing the dephasing of the transverse magnetization of spins in the presence of field inhomogeneity. Since the spin-spin relaxation cannot be refocused in the spin echo, the contrast in the image is dependent on T_2. The echo time (TE) is the main timing parameter that can be adjusted to generate different T_2 weighted contrast. Similarly T_2 maps can be made from multi-echo images by using a series of 180° pulses and multiple imaging modules at each consecutive TE, and fitting to the T_2 decay equation derived from the Bloch equations:

$$S(TE) = S(0) \cdot e^{-TE/T_2}$$
[1.11]

The other type of echo, called gradient echo, can be generated by dephasing and rephasing the spins with a pair of oppositely polarized gradients. In a gradient echo pulse sequence, if the spins in a single voxel experience different magnetic fields, the loss of phase coherence from field inhomogeneity cannot be not reversed, which reduce the transverse magnetization magnitude in the same way as spin-spin relaxation does. As briefly mentioned earlier, the total effect of spin-spin relaxation and field inhomogeneity is characterized by T_2^*. The signal evolution is governed by an equation of exponential decay similar to Eqn. [1.11] with T_2 replaced by T_2^*. Similarly, maps of T_2^* values can be obtained by taking several images with different TEs and fitting to this equation.

Functional magnetic resonance imaging

Ever since its invention, MRI has been largely used in clinics as an anatomical imaging modality to non-invasively visualize the structure of human body. Nowadays it can also be used to probe functional and physiological information in various organs in the body, most commonly, in the brain. Functional MRI (fMRI) measures signal changes in the brain arising from hemodynamic responses upon neuronal activity, and is widely used for mapping spatial and temporal patterns of brain activity. The most common fMRI measurement is based on the blood oxygenation level dependent (BOLD) effect, which results from changes in local deoxyhemoglobin content (Ogawa et al., 1993). Deoxyhemoglobin serves as a paramagnetic agent that creates magnetic field distortions within and around blood vessels, thereby attenuating the MR signal by affecting the transverse relaxation times T_2 and T_2^*. A very important observation during brain activation is that the brain will have excess glucose and oxygen delivery compared to demand (Mintun et al., 2001; Powers et al., 1996) as the cerebral blood flow (CBF) increases more than the cerebral metabolic rate of oxygen ($CMRO_2$). Such overcompensation decreases the concentration of red blood cells carrying deoxyhemoglobin in the post-arterial vasculature (capillaries, venules and veins), resulting an increased value of proton T_2 and T_2^* relative to baseline, thus MR signals will increase during increased neuronal activity and this is the mechanism underlying BOLD fMRI contrast.

While BOLD fMRI is most commonly employed nowadays as a mapping tool for neuroscience studies, to interpret BOLD signal change in terms of neuronal activity is difficult because the BOLD effect is sensitive to ensemble changes in several physiological parameters including cerebral blood volume (CBV), cerebral blood flow

(CBF), and the cerebral metabolic rate of oxygen (CMRO2). Although this creates some difficulty in interpreting the signal, it also offers the possibility of estimating changes in oxygen metabolism when BOLD, CBF, and CBF measurements are combined.

1.2. Relationship between deoxyhemoglobin concentration and BOLD fMRI parameters

As briefly mentioned earlier, BOLD signal changes are related to changes in the concentration of deoxyhemoglobin, which acts as a paramagnetic contrast agent in capillary and venous blood. When the blood oxygenation fraction (Y) is changed, the concentration of deoxyhemoglobin changes, which affects the T_2 and T_2* values of spins inside the vasculature, as well as those of extravascular spins around capillaries and veins draining from activated cortex. Therefore BOLD fMRI will have both intravascular and extravascular contributions. The relative concentration of paramagnetic deoxyhemoglobin ([Hb]) to total hemoglobin ([Hb_{tot}]) in venous blood is (van Zijl et al., 1998):

$$[Hb]/[Hb_{tot}]=1-Y_v=1-Y_a+OEF\cdot Y_a \qquad [1.12]$$

Y_v and Y_a are the venous and arterial oxygen saturation fractions, respectively. OEF is the oxygen extraction fraction, describing the ratio between oxygen consumption and delivery:

$$OEF=\frac{CMRO_2}{C_a\cdot CBF}=\frac{CMRO_2}{[Hb_{tot}]\cdot Y_a\cdot CBF} \qquad [1.13]$$

The above equation reflects the so-called "coupling" between CMRO2 and CBF, and the BOLD effect is sensitive to arterial oxygen saturation fraction, Y_a, and the total hemoglobin concentration, [Hb_{tot}], which is directly related to the hematocrit fraction

11

(*Hct*). In most of the current fMRI literature, *Hct* and arterial oxygenation are assumed constant, and the approximation

$$1 - Y_v = OEF = \text{constant} \cdot CMRO_2 / CBF \qquad [1.14]$$

is used. When looking at changes in Y_v or OEF under these conditions, we have:

$$\left(1 + \frac{\Delta CMRO_2}{CMRO_2}\right) = \left(1 + \frac{\Delta CBF}{CBF}\right)\left(1 + \frac{\Delta OEF}{OEF}\right) = \left(1 + \frac{\Delta CBF}{CBF}\right) \cdot \left(1 - \frac{\Delta Y_v}{(1 - Y_v)}\right) \qquad [1.15]$$

This equation indicates that relative changes in $CMRO_2$ can be simply determined by measuring the relative changes in blood flow and venous blood oxygenation. Although BOLD fMRI signals only directly reflect changes in transverse relaxation time, the transverse relaxation time is a function of venous oxygenation level Y_v. The dependence of Y_v and intravascular $R_2 = 1/T_2$ and $R_2* = 1/T_2*$ can be calibrated using experiments on isolated blood phantoms under well-controlled physiological circumstances (Wright et al., 1991). The simple hyperbolic equation commonly used for intravascular BOLD is (Silvennoinen et al., 2003; Uludag et al., 2009; Zhao et al., 2007):

$$R_2^{(*)} = A^{(*)} + C^{(*)}(1 - Y_v)^2 \qquad [1.16]$$

in which (*) indicates either gradient echo or spin echo and $A^{(*)}$ and $C^{(*)}$ are diamagnetic and paramagnetic rate constants that are dependent on the magnetic field strength, the hematocrit, and the particular pulse sequence and echo spacing used. Values for these constants at various filed strengths have been published.

Expressions for the extravascular BOLD effect, on the other hand, is based on the dephasing of water in large field gradients caused by deoxyhemoglobin (Ogawa et al., 1993; Weisskoff et al., 1994; Yablonskiy and Haacke, 1994). Approximating a blood

vessel by a long cylinder, gradients around a randomly oriented vessel network of such cylinders can cause a frequency shift ($\delta\omega$):

$$\delta\omega = \gamma \cdot B_0 \cdot \frac{4}{3}\pi \cdot \Delta\chi_{deoxy} \cdot Hct \cdot (1 - Y_v) \qquad [1.17]$$

in which γ is the gyromagnetic ratio, B_0 the static magnetic field, and $\Delta\chi_{deoxy}$ the magnetic susceptibility difference between oxygenated and fully deoxygenated blood (~0.2-0.3ppm). The estimated hematocrit (*Hct*) in the microvasculature is about 85% of that in the large vessels.

In the most optimum situation where signals from CSF and some parts of larger vessels especially draining veins, are minimal, an imaging voxel would contain only parenchyma, i.e. gray matter and microvessels (arterioles, venules, and capillaries). For larger microvessels in which dephasing of water spins due to the presence of static magnetic field gradients around the vessels is much larger than the diffusional dephasing of the spins, using the so-called static dephasing regime theory proposed by (Yablonskiy and Haacke, 1994), the extravascular BOLD effect based on a gradient-echo (GRE) acquisition (T_2*-weighted) can be analytically described as:

$$R'_{2t,Hb} = x_v \cdot \gamma \cdot B_0 \cdot \frac{4}{3}\pi \cdot \Delta\chi_{deoxy} \cdot Hct \cdot CBV(1 - Y_v) \qquad [1.18]$$

where *t* denotes extravascular tissue, and $x_v = 0.7$ is the venous fraction in CBV when assuming a two-compartment microvascular model (arteriolar/venular) in which capillaries are included in the venular compartment.

For spin-echo (SE) acquisitions however, the extravascular BOLD effect is intrinsically different from the static dephasing regime, as the SE-BOLD contrast is dominated by intra- and extravascular diffusion-induced dynamic averaging rather than

static dephasing that is induced by the static magnetic field inhomogeneity. Therefore in larger vessels, SE-BOLD effect will be very small as the diffusion effect of water molecules or so-called dynamic averaging regime is negligible and the static dephasing is refocused by the refocusing pulses, whereas in smaller microvessels especially in capillaries, there will be enhanced water diffusion, leading to more pronounced extravascular BOLD effect in the parenchyma (Jochimsen et al., 2004).

1.3. Cerebral Blood Volume Imaging Using Vascular-Space-Occupancy

Cerebral blood volume (CBV), commonly expressed in mL of blood per 100 mL of brain tissue, is a vital physiological parameter. As discussed in Chapter 1.2, to measure local changes in CBV is essential for understanding the BOLD fMRI signal mechanism and CBV can serve as an important contrast for functional brain mapping. During increased neuronal activity, it is primarily the arteries and arterioles equipped with smooth muscle that are capable of actively dilating, as suggested by a large body of literature in neurovascular coupling. There is also evidence showing that pericytes may be responsible for the dilatation and constriction of the capillaries, as capillaries do not contain smooth muscle themselves (Peppiatt et al., 2006).

CBV-weighted MR images are generally acquired in humans by injecting a non-diffusible tracer such as Gd-DTPA and tracking its progression through the vasculature. However, this involves the injection of contrast agents, and is based on the assumption that the contrast agent only occupies the intravascular space and does not penetrate the blood-brain-barrier, which may not be the case in diseases such as brain tumor. For dynamic imaging of CBV changes, Mandeville and colleagues have used long blood half-

life contrast agent, monocrystalline iron oxide nanoparticle (MION) (Mandeville et al., 1998), the sensitivity of which was found to be higher than that of the BOLD technique. However in this approach, it is assumed that tissue T_2* (or T_2) change induced by the contrast agent is mainly extravascular thus approximately proportional to CBV, neglecting the intravascular effects. This assumption may not hold for tissue around microvessels and large vessels. In 2003, Lu et al. (Lu et al., 2003) proposed an inversion recovery based MRI method called "vascular-space-occupancy (VASO)", which exploits the T_1 difference between blood and brain tissue and acquire the images when the blood signal is nulled, thereby obtaining MR signals sensitized to microvascular CBV changes non-invasively. Figure 1.1 illustrates the VASO pulse sequence. In the original VASO technique, a spatially nonselective (i.e. global) inversion pulse is applied, after which both blood and tissue longitudinal magnetizations will recover at the their T_1 relaxation rates, respectively. Since blood has a longer T_1 than tissue (both gray and white matter), by the time the blood magnetization crosses zero, tissue signal will be positive. The zero-crossing inversion time (TI) for blood can be determined by the following equation,

$$M_{blood}(TR, TI) = 1 - 2 \cdot e^{-TI/T_{1,blood}} + e^{-TR/T_1, blood} = 0 \qquad [1.19]$$

and the residual extravascular tissue signal in a VASO spin echo experiment can be expressed as:

$$S \sim (C_{par} - CBV \cdot C_b) \cdot M_{tissue}(TR, TI) \cdot e^{-TE/T_{2,tissue}} \qquad [1.20]$$

where C_{par} ~0.89 mL water/mL parenchyma and is the water density of parenchyma, C_b~0.87 mL water/mL blood and is the water density of blood, $M_{tissue}(TR,TI)$ is the longitudinal magnetization of the extravascular tissue water. Notice that during increased neuronal activity, CBV will increase due to the vasodilatation of the arterioles and

capillaries, thus tissue signal will decrease. Therefore, in a VASO fMRI experiment, the detected VASO signal change will be negative upon functional stimulation.
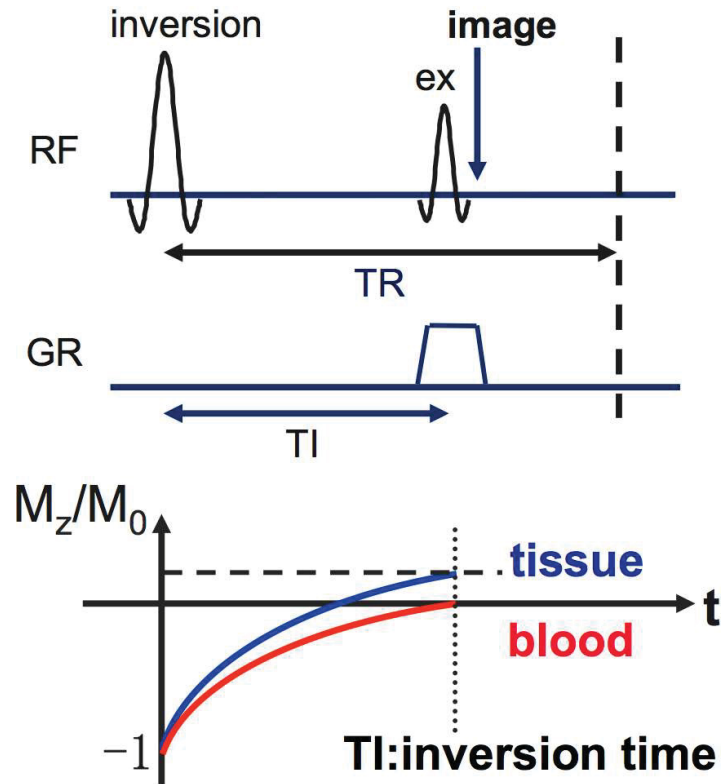
Fig. 1.1. Illustration of the VASO pulse sequence (top) and the inversion recovery process for tissue and blood magnetization (bottom). "RF" and "GR" represent RF pulse and gradient, respectively. "ex" indicates the excitation pulse after which the image is acquired. A spatially non-selective inversion pulse is applied and images are acquired at the blood nulling time when the tissue signal is positive.

Since activation-induced vasodilation is specific to small vessels rather than large sympathetically regulated vessels, VASO fMRI can spatially localize changes in the microvascular CBV, which is essential for localizing regions of neuronal activity and for performing functional brain mapping. Several imaging studies have also suggested an improved spatial specificity for VASO fMRI compared to BOLD fMRI. For example, a cat brain study conducted at high spatial resolution (Jin and Kim, 2008) convincingly showed that, across cortical layers, the peak VASO activation signal was observed in layer IV of the cortex where synapses are most abundant, showing a signal profile comparable to the MION CBV method used in the same animals, but distinctive from that of BOLD. BOLD activation patterns, on the other hand, covered broader areas of cortical layers and larger vessel regions, and did not manifest layer specificity. In human studies, the question of whether the VASO-activated voxels are predominantly located in brain parenchyma or large vessels can be probed by examining the T_1 properties of the voxel, because blood has a longer T_1 value than parenchyma tissue. It was found that T_1 of VASO-activated voxels was 1031 ± 20 ms (at 1.5 T), which is close to the tissue T_1 (Lu et al., 2003). However, the T_1 of BOLD-activated voxels were significantly ($p < 0.03$) longer (1103 ± 23 ms), suggesting an increased partial volume effect from blood or CSF. When VASO fMRI is performed at higher spatial resolution, the localization of the activated voxels becomes more apparent. Donahue et al. (Donahue et al., 2006a) performed VASO fMRI at resolution of $0.78\text{x}0.78\text{x}3\text{mm}^3$ and demonstrated that the activated voxels are mainly localized in the gray matter layer, with few voxels in the sulci between cortical banks (where the vessels are located). Huber et al. (Huber et al., 2015) performed a sub-millimeter resolution fMRI ($0.78\text{x}0.78\text{mm}^2$) study in human brain at 7

T, in which they reported that the highest BOLD activity is found at or outside the cortical surface, whereas VASO signal change has its peak 1-2 voxels (0.80-1.6 mm) deeper within GM, corresponding to the upper or middle cortical lamina.

Since a global inversion is applied in VASO MRI experiment, brain tissue signal will also be affected. Tissue T_1 is only slightly shorter than blood T_1, and depending on the repetition time (TR) used, only 10-20% of tissue signal is recovered after such nonselective inversion pulse at 3 Tesla. At higher magnetic fields, the residual tissue signal will be even lower since their T_1 values converge. Therefore, the signal-to-noise ratio (SNR) and contrast-to-noise ratio (CNR) of VASO is a lot lower when compared to BOLD, regardless of which field strength they are performed. To alleviate this problem, Hua *et al.* (Hua et al., 2009a) developed the magnetization transfer (MT)-enhanced VASO (MT-VASO) method, where a MT pre-pulse was applied immediately before or after the inversion pulses in the VASO sequence to prepare a smaller tissue magnetization or to speed up the tissue longitudinal magnetization recovery, respectively, thus achieving a higher residual tissue signal at the inversion time TI, and enhancing the inherently low SNR and CNR values for VASO MRI. When using moderate irradiation power ($\leq$3uT) and durations ($\leq$500ms), and a frequency offset sufficiently far away from water resonance ($\geq$40ppm), the MT prepulse has been shown to have negligible effect on blood signal so that same blood nulling TI can be used for VASO. It has been shown that the same magnitude of relative signal changes in MT-VASO were achieved as in VASO fMRI, meaning that the CBV sensitivity was preserved, while the SNR and CNR was enhanced by approximately 40% at 3 T. For this dissertation, all the VASO experiments we performed at 3 T were based on the MT-VASO approach.

One of the limitations of VASO MRI is the lower temporal resolution if pure CBV effects need to be studied. Donahue et al. showed that a CBF contribution will cause large negative VASO signal changes at short TR (≤3 s); using a TR of 5s or longer will considerably reduce the perfusion contribution. Also, the proton exchange between the tissue and the capillary compartment may alter the blood relaxation times, thus the nulling of blood spins in the capillary and initial part of venules may not be perfect. In the original VASO paper (Lu et al., 2003), the authors showed that such water exchange has negligible effects (about 0.02%) on the overall VASO signal by constructing a parenchymal model consisting of four pools (spins in blood and in tissue, spins exchanging from blood to tissue and from tissue to blood). Another confound comes from the actual inflow effects during the experiments. The VASO theory described above is based on the assumption that all blood spins within the imaging volume have reached the inversion steady state of approximately nulled signal before image acquisition. This assumption is only valid when the coverage of the RF transmission includes the entire body of the subject. However, even using a body coil for transmission, the effective inversion volume produced usually can only cover the lower neck and upper chest region. As a consequence, some fast-flowing blood spins may not have seen a sufficient number of inversion pulses to reach a steady state at the time of signal acquisition. Based on the time at which they enter the transmit coil, the non-steady-state inflowing blood spins can be categorized into three types: (I) spins flowing in before the end of readout of the previous TR; (II) spins flowing between the readout of the previous TR and the inversion pulse of the current TR; (III) spins flowing after the inversion pulse of the current TR. Lu (Lu, 2008) developed a 'magnetization reset' technique to eliminate type I non-steady-

state blood spins, where a spatially nonselective saturation module is applied immediately after each readout, and establishing a steady state for all blood spins entering the transmit coil after the first repetition time (TR). But this approach was found to only partially correct for the inflow effect. Fortunately, this effect is small when using body coils for RF transmission (Donahue et al., 2009b); More recently, Hua et al. (Hua et al., 2013a) proposed the use of motion-sensitized crushing gradients to suppress type II and III non-steady-state spins, where a spatially nonselective Carr-Purcell-Meiboom-Gill-based T_2 preparation module with inserted motion-sensitized crushing gradients are applied immediately before the readout. When these additional sequence components are not available, a TR of 5s or longer at 3 T (to minimize type I and II effects) and a large volume inversion (to minimize the type III effect) are recommended for predominant CBV contrast.

Since VASO MRI method is based on blood nulling, and theoretically there is only one nulling point during longitudinal relaxation, it appears that only one excitation pulse can be applied during each TR. Therefore, VASO fMRI was typically acquired in single-slice mode when it was first introduced (Lu et al., 2003). It is now possible to acquire multi-slice or three-dimensional (3D) volumes following one RF pulse. Multiple-Acquisition-with-Global-Inversion-Cycling (MAGIC) was proposed and further extended (Lu et al., 2004c; Scouten and Constable, 2007, 2008) to provide a multi-slice version of VASO. Single shot 3D gradient- and spin-echo (GRASE) acquisition scheme have been used for VASO acquisition (Poser and Norris, 2011). More recently, the fast 3D low-angle shot (FLASH) or fast gradient echo (GRE) acquisition (Cheng et al., 2014; Hua et al., 2013a) sequence was applied for VASO imaging both at 3T and 7T, where all k lines

of an imaging volume are sequentially acquired with short TR, short TE and low flip angle excitation pulses (<10°) following a single inversion. Such imaging scheme has been commonly used in high-resolution anatomical scans such as the Magnetization Prepared RApid Gradient Echo (MPRAGE) sequence (Hua et al., 2014; Mugler and Brookeman, 1990). A low-high (also known as "centric") phase encoding scheme was often used which is important for blood nulling in VASO. When compared to other commonly applied imaging sequences such as EPI, turbo SE and GRASE, the 3D fast GRE readout module can minimize BOLD contamination (short TE, 1.8ms) to the VASO contrast and reduce image distortion (susceptibility artifacts or spatial smoothing induced by the very long echo train) and power deposition.

1.4. Cerebral Blood Flow Imaging Using Arterial Spin Labeling

Cerebral blood flow (CBF) studies using ^{15}O-labeled water as the contrast agent have been used extensively for functional mapping with positron emission tomography (PET). To measure cerebral perfusion with MRI, there are two major approaches. The first is the application of an exogenous, intravascular, non-diffusible, and usually a gadolinium-based contrast agent, that emphasizes either the susceptibility effects on the signal, namely first-pass dynamic susceptibility contrast-enhanced (DSC) MR perfusion or the relaxivity effects on the signal, namely dynamic contrast-enhanced (DCE) MR perfusion. The second is using magnetically labeled arterial blood water as an endogenous, diffusible tracer that is capable of moving across the blood-brain barrier, applied in spin labeling (ASL) MR perfusion techniques (Essig et al., 2013).

ASL techniques involve the subtraction of two separately acquired images. First, the *label* acquisition is performed such that blood water spins outside the image slice are magnetically labeled by inverting their longitudinal magnetization relative to M_0. When these labeled blood water spins flow into the imaging slice and reach the capillary bed, they will exchange with extravascular tissue water and attenuate the tissue signal. In the second, *control* acquisition, the same slice is acquired with no preparatory inversion applied. A subtraction (*control - label*) will yield a difference image with intensity directly proportional to CBF. The inversion is done either adiabatically as the blood moves through a gradient field during a continuous or pseudo-continuous RF pulse in a continuous ASL (CASL) experiment, or by using a short RF pulse to invert a larger slab of blood water spins in a pulsed ASL (PASL) experiment. The labeling plane for CASL is typically at about the same location as the distal end of the labeling slab in PASL (Alsop et al., 2014).

One particular PASL method that we will be using in this dissertation is the flow-sensitive alternating recovery or FAIR technique (Kim, 1995; Kwong et al., 1995). It employs a frequency-selective inversion pulse with and without an accompanying slice-selection gradient to produce the tagged and the control images, respectively (Figure 1.2). When the inversion pulse is played with the slab-selective gradient, it inverts the spins within the imaging slab while leaving spins elsewhere virtually unaffected. When the gradient is either played with zero amplitude or played at a different time away from the inversion pulse, the inversion pulse inverts spins in the entire volume of the RF transmit coil. Therefore in the difference image the static tissue signals will be subtracted out, leaving the signals from the inflowing blood.
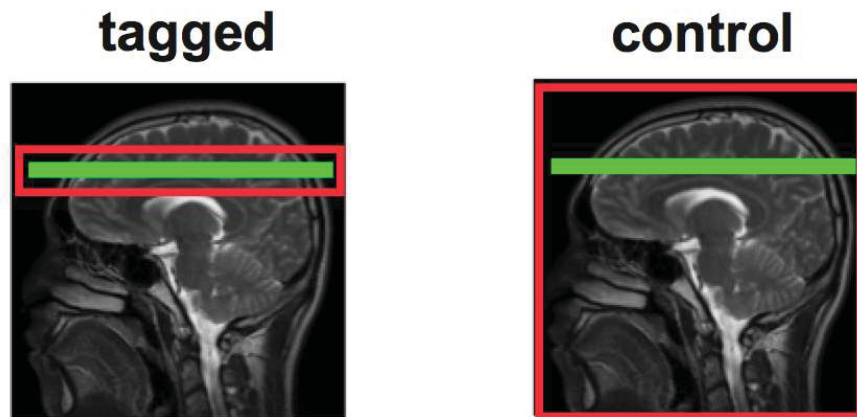
Fig. 1.2. Illustration of the FAIR-ASL experiment. A FAIR-ASL experiment consists of a *tagged* acquisition (left) in which only the water spins in the spatially-selective inversion slab (red), which includes the imaging slab (green), is inverted, followed by a *control* acquisition (right) where all the water spins in the transmit coil are inverted after the non-selective inversion pulses. When the *control* image is subtracted from the *tagged* image, we will get the so-called perfusion map, the image intensity of which is directly proportional to CBF value.

ASL perfusion MRI can be used to quantify the baseline CBF by solving a flow-modified Bloch equation, as well as to detect activation-dependent changes in CBF in a manner similar to BOLD fMRI. While the BOLD contrast primarily detects T_2 or T_2^* changes that indirectly reflect changes in CBF, ASL perfusion contrast is based on changes in T_1 induced directly by regional blood flow alterations. When compared to conventional BOLD fMRI, the perfusion signal is localized in parenchyma rather than draining veins, since most of the water molecules delivered to the capillary beds are extracted, and the inflow time in a typical ASL experiment is short, thus few if any of the tagged spins reach the venous side of the vasculature. Nevertheless, the greater spatial specificity of functional ASL is offset by its lower sensitivity due to the paired subtraction (Wong et al., 1997). Over longer timescales however, functional ASL has improved sensitivity as compared with BOLD fMRI since the low-frequency noise is eliminated by the paired subtraction (Detre et al., 2009).

1.5. Measurement of oxygen metabolism using multi-modal fMRI

In order to understand and quantify the BOLD fMRI signal, it is essential to design MRI approaches that are sensitized to the contributions from individual hemodynamic parameters such as CBV and CBF that have better spatial correspondence with the underlying neural activity, and to combine information from multi-modality fMRI experiments for determining oxygen metabolism especially in the brain parenchyma area.

By using a multi-compartment model for the parenchyma, one can combine CBF (ASL), CBV (VASO), and BOLD imaging to estimate alterations in $CMRO_2$ during a

physiological challenge or brain activation (Donahue et al., 2009a; Griffeth and Buxton, 2011; Hua et al., 2011c; Lu et al., 2004b; Uludag et al., 2009; van Zijl et al., 1998). When selecting only the subset of voxels that are activated in all methods, and because the VASO method is based on microvascular changes during challenges, it was concluded that this is the true parenchymal BOLD signal change (Lu et al., 2004b). A quantitative fMRI model for parenchyma needs to include arteriolar (a), capillary (c), venular (v), and tissue (t) compartments:

$$S \sim \sum_i x_i \cdot M_i \cdot e^{-R_{2i}^* TE}$$

[1.21]

in which M_i describes the well-known dependence on repetition (TR) and flip angle (FA), and x_i is the water fraction, that relates exactly to blood volume and tissue fractions via the water density. Using the static dephasing equations for the tissue relaxation (Eq. 1.18) and the intravascular calibration (Eq. 1.16) for intravascular BOLD, one can determine OEF and CMRO2 changes upon simple assumption of baseline CBV, Y_v, and $\Delta\chi_{deoxy}$.

The above-described quantitative BOLD approach normally needs separately performed BOLD, CBV, and CBF measurements during neuronal tasks in order to estimate CMRO2 dynamic. The ability to acquire these physiological parameters simultaneously would be potentially useful to improve image acquisition efficiency, and more importantly reduce the sensitivity to temporal variations due to factors such as subject head motion, task performance, and physiologic changes between the fMRI scans.

In this dissertation, we aim to design novel MRI methods to measure relaxation times T2*, cerebral blood volume (CBV), blood flow (CBF), blood oxygenation level hemodynamics, OEF and CMRO2 during neuronal activation in a time efficient manner.

In Chapter 2, multi-echo VASO and BOLD fMRI are exploited at 7T, which is able to quantify parenchymal total and extravascular T_2^* relaxation rates and estimate the extravascular fraction of the BOLD effect. In Chapter 3, a new MRI pulse sequence, dubbed as "VASO-FAIR", is proposed, which allows for three-dimensional whole-brain measurement of CBV and CBF dynamics in a single scan. In Chapter 4, an acquisition strategy that extends the 3D VASO-FAIR method and incorporates a T2-preparation module to induce the spin-echo BOLD contrast is presented, enabling the detection of CBV, CBF, and blood oxygenation-weighted signal changes in a single scan. Oxygen metabolism related parameters including oxygen extraction fraction (OEF) and cerebral metabolic rate of oxygen ($CMRO_2$) are also estimated based on the measured BOLD, CBV, and CBF reactivity from the combined sequence.

Chapter 2: Measurement of Parenchymal Extravascular R2* and Tissue Oxygen Extraction Fraction Using Multi-echo VASO MRI at 7 Tesla

2.1. Introduction

Parenchymal extravascular R_2^* is an important parameter for quantitative blood-oxygenation-level-dependent (BOLD) studies. It is well known that the BOLD effect increases with field strength, and the BOLD signal from extravascular tissue becomes more dominant at higher field, as the intravascular BOLD signal contribution is significantly reduced due to the faster R_2^* decay of venous blood (Duong et al., 2003; Gati et al., 1997; Ogawa et al., 1993; Song et al., 1996; Ugurbil et al., 1999; Ugurbil et al., 2003; Uludag et al., 2009; van der Zwaag et al., 2009; Yacoub et al., 2001). The relative contribution of the extravascular BOLD effect can be estimated using the ratio of extravascular and total R_2^* changes during neuronal activation. Furthermore, R_2^* changes can also be used to estimate changes in physiological parameters such as venous oxygenation (Y_v) and tissue oxygen extraction fraction (OEF) during brain activation.

Total and intravascular R_2^* values at various field strengths have been reported in a number of studies in animals and humans (Chen et al., 2004; Chien et al., 1994; Deistung et al., 2008; Donahue et al., 2011; Gati et al., 1997; Lee et al., 1999; Li et al., 1998; Li et al., 2006; Lu and van Zijl, 2005; Silvennoinen et al., 2003; Uludag et al., 2009; van der Zwaag et al., 2009; Wright et al., 1991; Yacoub et al., 2001; Yacoub et al., 2005; Zhao et al., 2004; Zhao et al., 2007). However, reports on extravascular R_2^* values remain scarce in the literature (Table 2.1), as it is not trivial to measure mainly due to the

difficulty to separate out the extravascular and intravascular signals in parenchyma. Duong et al. (Duong et al., 2003) used diffusion gradients to suppress the intravascular BOLD signal in order to investigate the microvascular contribution in the BOLD effects at 4T and 7T. Van der Zwaag et al. (van der Zwaag et al., 2009) excluded the intravascular BOLD effects in large veins using high resolution anatomical scans and reported R_2^* values in human motor cortex at 1.5, 3 and 7T at a spatial resolution of $1x1x3mm^3$. In the vascular-space-occupancy (VASO) approach, a spatially non-selective inversion pulse is applied", and the image is acquired at the inversion time (TI) when the longitudinal magnetization of blood is expected to be zero, while that of tissue is slightly positive based on different T_1 relaxation times of blood and tissue (Lu et al., 2003). Lu et al. (Lu and van Zijl, 2005) determined parenchymal extravascular R_2^* values at 1.5T and 3T using multi-echo VASO MRI, which eliminates the intravascular signal and is expected to isolate the extravascular tissue compartment in BOLD experiments. Donahue et al. (Donahue et al., 2011) employed bipolar crushing gradients to suppress fast flowing blood signal (intravascular), and measured extravascular R_2^* change (ΔR_2^*) during visual stimulation in human brain at 1.5T, 3T and 7T. To date, however, the combined BOLD/VASO method for determination of parenchymal extravascular R_2^* values (Lu and van Zijl, 2005) has not yet been used in human brain at 7T.

Table 2.1. Comparison of extravascular and total parenchymal R_2^* values at 1.5T, 3T and 7T.

		Resolution (mm^3)	Extravas. $R_{2,rest}^*$ (s^{-1})	Extravas. ΔR_2^* (s^{-1})[a]	Total $R_{2,rest}^*$ (s^{-1})	Total ΔR_2^* (s^{-1})	Extravas. ΔR_2^* fraction (%)[b]
1.5 T	Ref. (Lu and van Zijl, 2005)	2x2x2	16.14±0.64	-0.25±0.02	16.78±0.65	-0.57±0.10	47±7
	Ref. (Donahue et al., 2011)	3.5x3.5x3.5	---	-0.28±0.07	---	-0.61±0.10	45±13
	Ref. (van der Zwaag et al., 2009)	1x1x3	---	---	11.6±0.3	-0.51±0.06	---
3.0 T	Ref. (Lu and van Zijl, 2005)	2x2x2	21.15±0.66	-0.38±0.05	22.06±0.84	-0.58±0.09	67±6
	Ref. (Donahue et al., 2011)	3.5x3.5x3.5	---	-0.52±0.07	---	-0.74±0.05	70±11
	Ref. (van der Zwaag et al., 2009)	1x1x3	---	---	18.1±0.4	-0.98±0.08	---
7.0 T	Ref. (Donahue et al., 2011)	3.5x3.5x3.5	---	-1.25±0.11	---	-1.37±0.34	91±11
	Ref. (van der Zwaag et al., 2009)	1x1x3	---	---	30.8±1.0	-2.55±0.22	---
	This study	**2.5x2.5x2.5**	**44.66±1.55**	**-1.27±0.14**	**45.05±1.34**	**-1.40±0.16**	**91±3**

mean ± standard error (SEM)

[a] $\Delta R_2^* = R_{2,act}^* - R_{2,rest}^*$.

[b] Extravas. ΔR_2^* fraction = 100 x (Extravas. ΔR_2^* / Total ΔR_2^*) %.

In this chapter, we applied multi-echo BOLD and VASO fMRI with visual stimulation to measure total and extravascular R_2^* values in the visual cortex in human brain at 7T. By comparing total and extravascular ΔR_2^* during visual stimulation, the intra- and extravascular parenchymal contributions to the BOLD signal at 7T could be assessed. Y_v and OEF changes during activation were estimated from the R_2^* measurements.

2.2. Methods

The protocol was approved by the Internal Review Board of the Johns Hopkins University. Seven healthy subjects gave informed written consent before participating this study. From these, only six were included in the final report due to the fact that the relative extravascular ΔR_2^* from subject 7 was more than two standard deviations larger than the averaged value from the other six subjects. Experiments were performed on a 7T human MRI scanner (Philips Healthcare, Best, The Netherlands), using a quadrature transmit head coil (10 inch or 25.4 cm in foot-head coverage) and a 32-channel phased array receive coil (Nova Medical, Wilmington, MA, USA). A single slice was carefully placed to cover the calcarine fissure. Three pseudo-randomized fMRI scans including two VASO (repetition time or TR = 4 s, inversion time or TI = 1293 ms) and one BOLD (TR = 2 s) scans were performed on each participant with visual stimulation (yellow/blue flashing checkerboard, 40s off 24s on, 4 blocks, 1 extra off period in the end). The blood nulling TI in VASO was calculated using blood T1 = 2212 ms, measured from bovine blood with 79% oxygenation and Hematocrit (Hct) = 0.43 at 7T (Dobre et al., 2007). The spatially nonselective inversion pulse in VASO was optimized for 7T in previous work

31

(hyperbolic secant adiabatic pulse, duration = 20 ms, peak B1 = 15 µT, bandwidth = 1050Hz, >95% inversion at half of the maximum B1 in phantom and brain) (Hua et al., 2013a; Visser et al., 2010). A magnetization reset module (90° RF pulse followed by spoiler gradients) (Lu, 2008) was applied immediately after the readout in both VASO and BOLD scans to suppress inflow effects from non-inverted spins. For both BOLD and VASO fMRI, single-shot gradient echo (GE) echo-planar-imaging (EPI) readout was used with four echoes acquired at TE = 9, 27, 45 and 63 ms. Common imaging parameters included: flip angle (FA) = 67° (Ernst angle for BOLD scan based on a grey matter T1 of 2132 ms (Rooney et al., 2007)), field of view (FOV) = 192x192mm^2, spatial resolution = 2.5x2.5x2.5 mm^3, parallel imaging (SENSE) acceleration factor = 4, partial Fourier fraction = 0.6. Second-order shimming was applied in both BOLD and VASO scans, for which a water line width of <60Hz was achieved in all scans.

All fMRI images were corrected for motion and baseline drift using Statistical Parametric Mapping (SPM8, University College London, UK) and Matlab R2009b (Mathworks, Natick, MA, USA). BOLD and VASO images at different TEs were co-registered. The two VASO scans were averaged to improve signal-to-noise ratio (SNR) (Lu and van Zijl, 2005). VASO images from all four echoes were used to extrapolate to an effective TE of 0 ms to minimize BOLD contamination. A general linear model (GLM) was used to detect activated voxels in VASO (TE = 0 ms) and BOLD (TE = 27 ms, second echo) scans. Temporal SNR (tSNR) was calculated as the voxel-wised average signal divided by standard deviation along the time course during the rest periods (excluding the data acquired during 20 s at the start of each rest period). The criteria for activation were t-score > 1.5 (BOLD), t-score > 1 (VASO), adjusted p-value < 0.05,

cluster size > 4 and tSNR > 20 (Donahue et al., 2006a). Only voxels activated in both modalities were used for R_2^* calculation so that voxels containing large vessels are excluded and signals are predominantly localized in the parenchyma (Donahue et al., 2006a; Jin and Kim, 2008; Lu et al., 2003). Signal intensities (S) at the four echo times were numerically fitted as a function of TE (S = $S_0 \cdot exp(-TE \cdot R_2^*)$) to obtain S_0 and R_2^* values on a voxel-wise basis.

Using the calculated R_2^* values, Y_v and parenchymal OEF can be quantified using the equations for the static dephasing regime described in (Lu and van Zijl, 2005; Yablonskiy et al., 2000; Yablonskiy and Haacke, 1994):

$$\Delta R_{2t}^* \approx x_v \cdot \omega_0 \cdot \frac{4}{3} \pi \cdot \Delta \chi_{deoxy} \cdot Hct \cdot \{CBV^{act}(1-Y_v^{act}) - CBV^{rest}(1-Y_v^{rest})\} \qquad [2.1]$$

where $\Delta R_{2t}^* = R_{2t,act}^* - R_{2t,rest}^*$ (t denotes extravascular tissue), $x_v = 0.7$ is the venous fraction of cerebral blood volume (CBV) including capillaries (Lu and van Zijl, 2005), "act" and "rest" denote values during activation and rest, respectively. The reported susceptibility difference between fully oxygenated and deoxygenated blood ($\Delta \chi_{deoxy}$) varies from 0.18 ppm to more than 0.3ppm in the literature (Golay et al., 2001; Jain et al., 2012; Spees et al., 2001; Weisskoff and Kiihne, 1992; Yablonskiy and Haacke, 1994). Here, we adopted a value of 0.27 ppm from most recent studies (Jain et al., 2012; Spees et al., 2001). Other parameters assumed were: microvascular hematocrit (Hct) = 0.356 (Kuhl et al., 1980) which is 85% of that in the large vessels, and $CBV^{rest} = 0.052ml$ blood/ml tissue (Donahue et al., 2006a). CBV^{act} can be calculated from the VASO signal change (Lu et al., 2003). By assuming $Y_v^{rest} = 0.61$, Y_v^{act} can be calculated from Eq. [1], and OEF can be quantified using (van Zijl et al., 1998):

$$1-Y_v = 1 - Y_a + OEF \cdot Y_a \qquad [2.2]$$

where the arterial oxygenation (Y_a) was taken to be 0.98, corresponding to a resting state OEF of 0.38.

2.3. Results

Figs. 2.1a-b show representative activation maps (thresholded) superimposed on BOLD and VASO images from one subject. The VASO signal changes displayed are those found when extrapolating to TE = 0 ms. Figs. 2.1c-d show the corresponding t-score maps. Note that the t-scores for activated voxels in VASO (negative signal change upon activation) were positive as well, because the contrast itself was reversed when performing GLM analysis. The peak activated voxels were well localized in the visual cortex. For the purpose of this study, activations that were clearly outside the visual regions were excluded in the analysis. Figs. 2.1e-f show the time courses of fractional signal changes averaged over activated voxels in the BOLD and VASO scans, respectively. As expected, negative signal changes in VASO were observed upon neuronal activation because the concomitant vasodilatation results in tissue signal reduction at TE = 0ms (Lu et al., 2003).
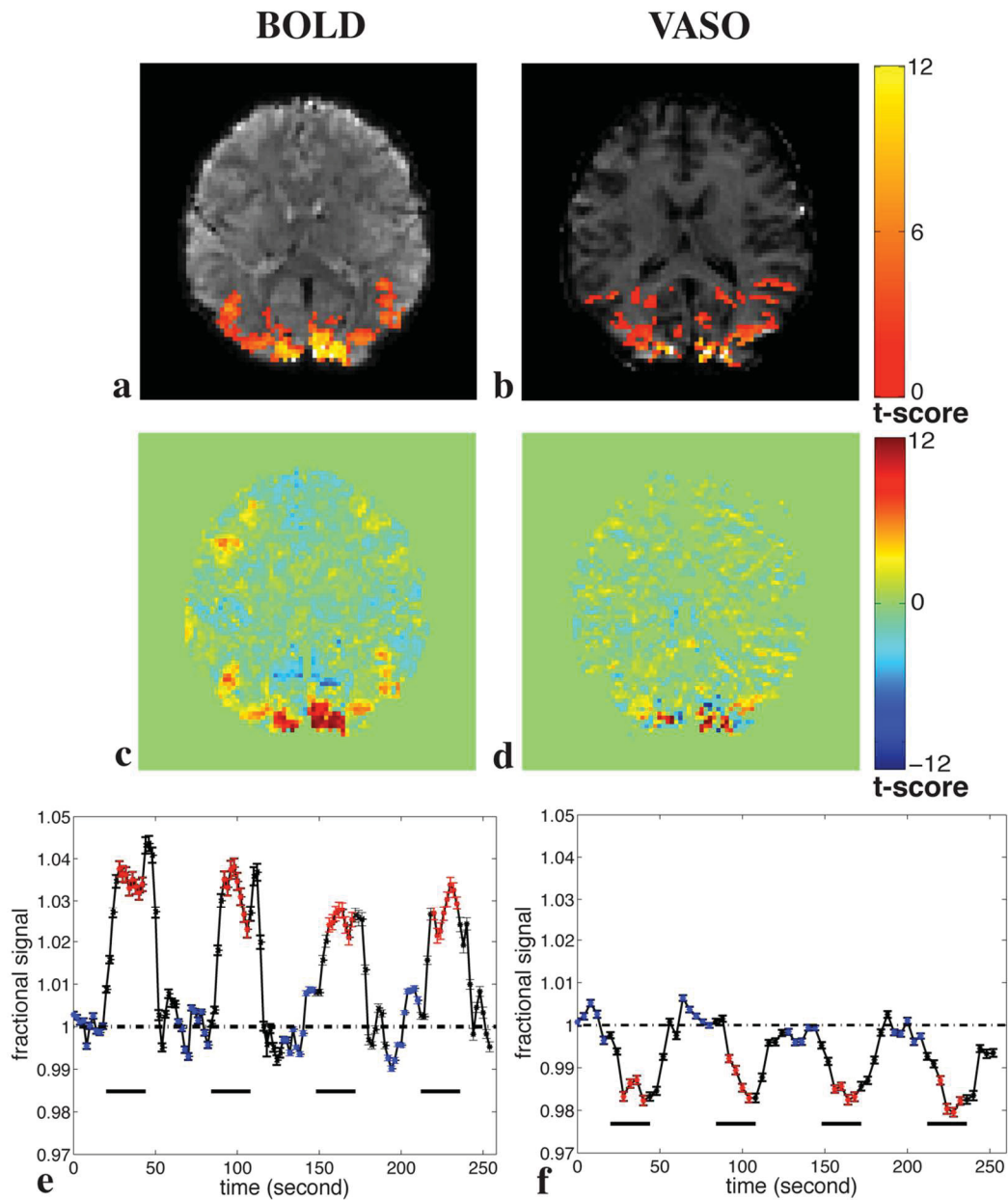
Fig. 2.1. Representative BOLD (TE = 27 ms) and VASO (extrapolated TE = 0 ms) fMRI results from one subject. a-b: Activation maps (thresholded) superimposed on BOLD and VASO images. c-d: Corresponding t-score maps. As the contrast in VASO and BOLD scans were reversed when performing GLM analysis, the t-scores for activated voxels in both scans were positive. e-f: Corresponding time courses of fractional signal changes

from BOLD and VASO activation maps. The horizontal bars indicate the periods of visual stimulation. The blue and red points were used to calculate signals during rest and activation, respectively. Error bars show standard error over the included voxels within this subject. Reproduced with permission from NMR in Biomedicine.

Typical BOLD and VASO images at all four echo times are shown in Figs. 2.2a-b. As second order shimming was applied, and a single slice was acquired in the occipital lobe (which has a relatively homogeneous B0 field), the distortion found in these images was small. In addition, images at different TEs were co-registered before further analysis. The average tSNR (n = 6) of images at the longest echo time (TE = 63ms) were 16.0±1.9 and 12.8±1.7 for BOLD and VASO, respectively, which is considered sufficient for robust R_2^* fitting. (Please note that the tSNR threshold of 20 mentioned in Methods was only applied on the extrapolated (TE = 0 ms) VASO images and BOLD images at the second echo time during functional analysis. Here, the tSNR of images at the longest TE shows that it is sufficient for R2* fitting.) Figs. 2.2c-d show the averaged result (n = 6) of TE-dependence curves of relative and absolute signal changes for both BOLD and VASO fMRI. Only the commonly activated voxels in both modalities were selected. The absolute BOLD signal change (Fig. 2.2d) was the largest at the second echo time (TE = 27 ms), consistent with the notion that the optimal TE for BOLD contrast should be around tissue T_2^* (Ugurbil et al., 1993). The well-known linear relationship between ΔS/S and TE in BOLD and VASO was fitted (Fig. 2.2c). The VASO signal change is negative for very short TE, but reverses sign at longer TEs. This is expected as the extravascular BOLD effects (positive) become quite large at longer TE, which counteract the negative VASO signals. This also stresses the importance of extrapolating to TE = 0 or using a readout with very short TE (Hua et al., 2013a) for VASO fMRI at 7T.
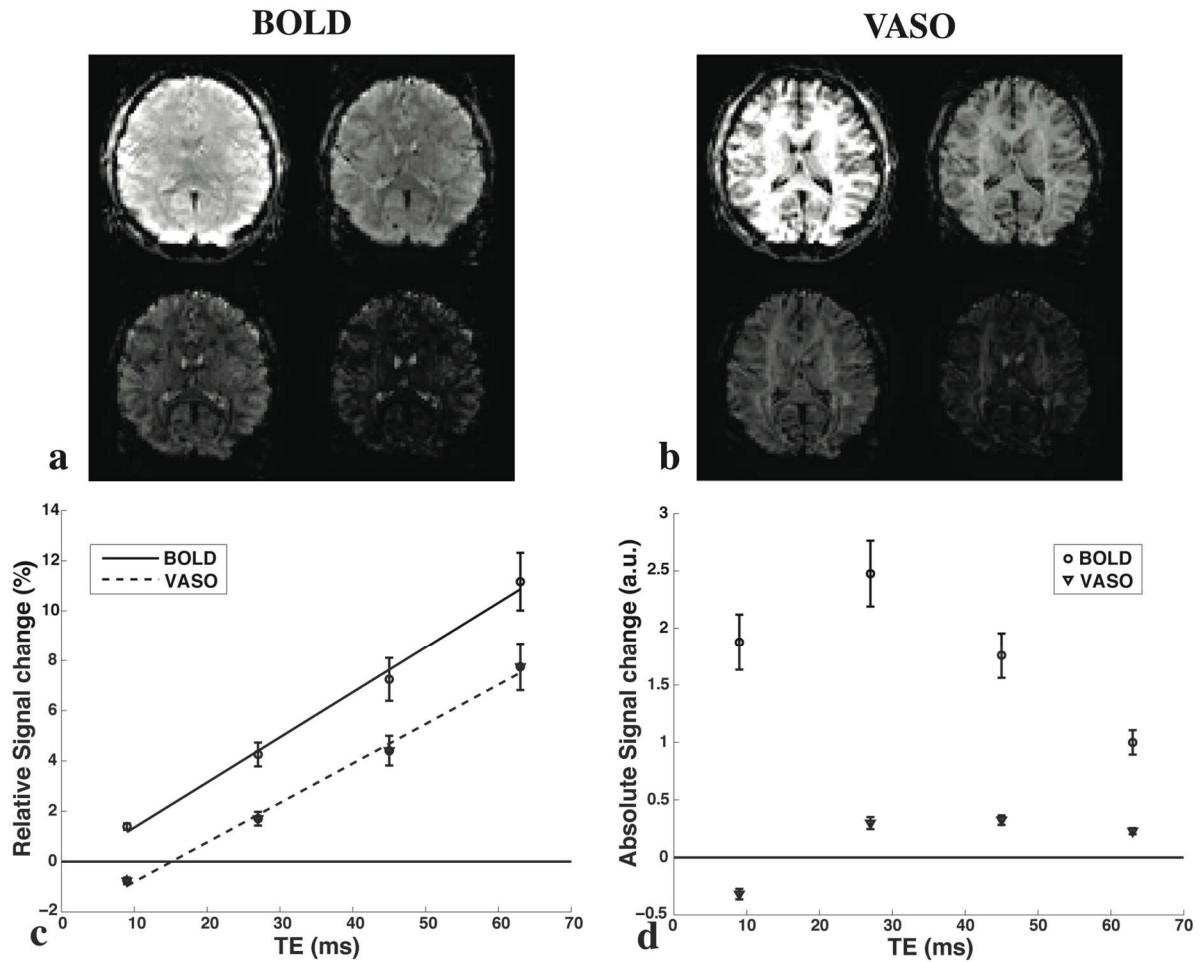
Fig. 2.2. Typical BOLD (a) and VASO (b) images at all four echoes (same scale). Group averaged (n = 6) relative (c, $\Delta S/S$) and absolute (d, arbitrary unit) fMRI signal changes versus TE in voxels that are both activated in BOLD (TE=27ms) and VASO (TE=0) methods. Error bars represent inter-subject variation. Lines in (c): results from linear fitting. Reproduced with permission from NMR in Biomedicine.

The fitted total and extravascular R_2^* values during rest and activation in six subjects are summarized in Table 2.2. Only the voxels that were activated in both BOLD and VASO scans were included. The ratio of extravascular ΔR_2^* to total ΔR_2^* was $91 \pm 3\%$ ($n = 6$, mean $\pm$ SEM). Figs. 2.3a-b show the R_2^* time courses from one subject.

Table 2.2. Extravascular and total BOLD effects measured in gray matter parenchyma at 7T.

	Extravas $R_{2,rest}^*$ (s^{-1})	Extravas. $R_{2,act}^*$ (s^{-1})	Extravas. ΔR_2^* $(s^{-1})^a$	Total $R_{2,rest}^*$ (s^{-1})	Total $R_{2,act}^*$ (s^{-1})	Total ΔR_2^* (s^{-1})	Extravas. ΔR_2^* fraction $(\%)^b$
Subject 1	40.38	39.08	-1.30	42.68	41.10	-1.57	83
Subject 2	46.61	45.16	-1.37	47.16	45.78	-1.45	95
Subject 3	40.46	39.73	-0.74	40.56	39.75	-0.81	91
Subject 4	45.18	43.89	-1.29	44.72	43.21	-1.51	86
Subject 5	45.02	43.26	-1.77	45.22	43.26	-1.96	90
Subject 6	50.34	49.17	-1.17	49.94	48.81	-1.13	103
Mean	**44.66**	**43.38**	**-1.27**	**45.05**	**43.65**	**-1.40**	**91**
SEM	**1.55**	**1.51**	**0.14**	**1.34**	**1.33**	**0.16**	**3**

SEM: inter-subject standard error.

[a] $\Delta R_2^* = R_{2,act}^* - R_{2,rest}^*$.

[b] Extravas. ΔR_2^* fraction = 100 x (Extravas. ΔR_2^* / Total ΔR_2^*) %.
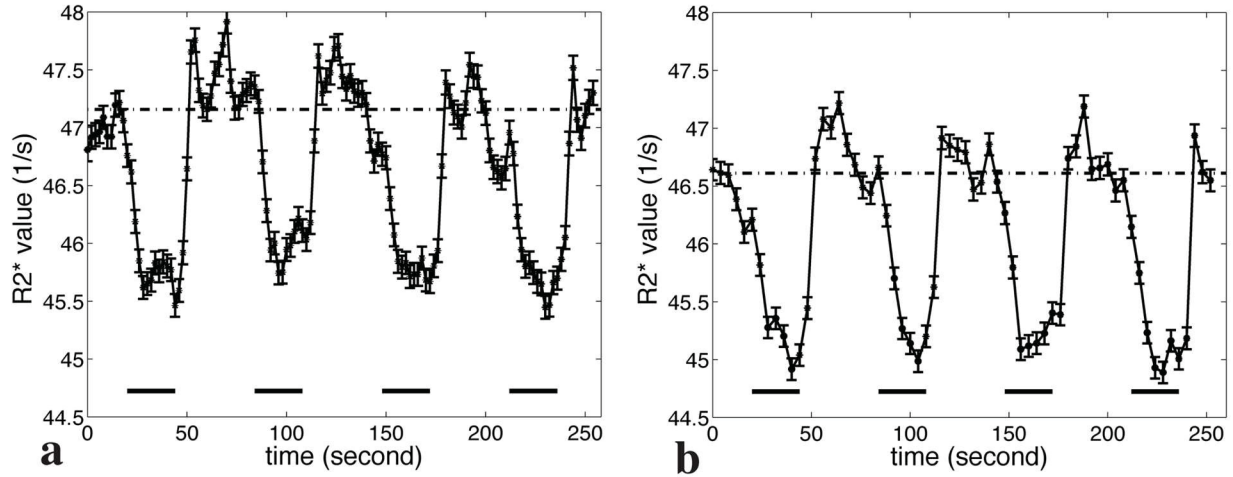
Fig. 2.3. Representative time courses of total (a) and extravascular (b) parenchymal R_2^* averaged over voxels activated in both BOLD (TE=27ms) and VASO (TE=0) scans from one subject. R_2^* values were fitted from data acquired at all four TEs. The horizontal bars indicate the periods of visual stimulation. Error bars show inter-voxel standard errors within the subject. The dash-dot lines depict average R_2^* values at baseline. Reproduced with permission from NMR in Biomedicine.

CBV increased by $35.8 \pm 3.2\%$ (n = 6, mean $\pm$ SEM) during visual stimulation, calculated from a $-1.94 \pm 0.17\%$ (n = 6, mean $\pm$ SEM) VASO signal change using the extrapolated VASO images at TE = 0 ms and assuming a baseline CBV value of 0.052ml blood/ml tissue(Donahue et al., 2006a). Using Eqs. 2.1, 2.2, Y_v^{act} and OEF during activation were quantified to be 0.75 ± 0.01 and 0.24 ± 0.01 (n = 6, mean $\pm$ SEM), respectively, indicating an approximately 37% OEF decrease during visual stimulation.

2.4. Discussion

In this study, we applied multi-echo VASO fMRI to remove the intravascular signal and measured the extravascular (tissue) R_2^* values in human visual cortex at 7T. Table 1 compares these data with the total and extravascular parenchymal R_2^* values reported at various field strengths (1.5T, 3T and 7T) in the literature. The R_2^* values measured here are in good agreement with the Donahue study (Donahue et al., 2011), but differ considerably from the ones reported in the van der Zwaag study (van der Zwaag et al., 2009). One plausible explanation may be that both the Donahue and current studies were conducted in the visual cortex with comparable spatial resolution, whereas the van der Zwaag study measured R_2^* values in the motor cortex with a much finer spatial resolution ($1 \times 1 \times 3$ mm^3). As expected, both total and extravascular R_2^* increase with field strength. The absolute and relative R_2^* changes (ΔR_2^* and $\Delta R_2^*/R_2^*$) during activation also increase with the field, indicating better sensitivity for BOLD fMRI as predicted. Extravascular ΔR_2^* shows a linear trend with field strength ($\Delta R_2^* = -0.196 \cdot B_0 + 0.114$, correlation coefficient = 0.99, p-value = 0.09), consistent with the theoretical calculations for extravascular BOLD effects in the static dephasing regime model proposed by

Yablonskiy and Haacke (Yablonskiy and Haacke, 1994). The relative contribution from the extravascular component in the total BOLD contrast becomes larger at higher field, as indicated by the larger ratio of extravascular ΔR_2^* to total ΔR_2^*. Our results showed that the BOLD effect is dominated by the extravascular component (91%) at 7T, in line with the results from Duong et al. (Duong et al., 2003) and Donahue et al. (Donahue et al., 2011) that used crushing gradients to suppress the intravascular signal. These experimental results are consistent with the theoretical calculations that the intravascular BOLD signal will be significantly reduced relative to the extravascular signal at higher field due to the faster R_2^* decay of venous blood (Duong et al., 2003; Gati et al., 1997; Ogawa et al., 1993; Song et al., 1996; Ugurbil et al., 1999; Ugurbil et al., 2003; Uludag et al., 2009; van der Zwaag et al., 2009; Yacoub et al., 2001). It is important to mention that the intravascular effects are actually larger than extravascular at short TE (Silvennoinen et al., 2003; Uludag et al., 2009; Zhao et al., 2007). However, when using typical TEs for BOLD fMRI (which are usually comparable to GM T2*), the relative contribution from the intravascular venous compartment to the overall parenchymal effect is small.

When assuming resting OEF and CBV values from the literature, multi-echo VASO fMRI also allows the measurement of changes in physiological parameters such as Y_v and OEF in the parenchyma during neuronal activation. OEF reduction upon visual stimulation measured here at 7T agrees reasonably well with previously reported values: 33% (Haacke et al., 1997; Oja et al., 1999), 39% (Lu and van Zijl, 2005), 53% (Golay et al., 2001) at 1.5T and 45% (Lu and van Zijl, 2005) at 3T. A number of neurophysiology studies suggest that the vasodilation during functional stimulation occurs predominantly in arterioles and capillaries that are very close to the active neural tissue (Koehler et al.,

2009), indicating an improved spatial specificity for CBV weighted VASO fMRI, as demonstrated by several animal and human fMRI studies (Donahue et al., 2006a; Jin and Kim, 2008; Lu et al., 2003). Therefore the OEF changes measured here were expected to be predominantly localized in the parenchyma by taking overlapping voxels activated in both BOLD and VASO scans, while some previous measurements were made mainly in the draining veins (Golay et al., 2001; Haacke et al., 1997; Lu and Ge, 2008; Lu et al., 2012; Oja et al., 1999; Qin et al., 2011; Xu et al., 2009).

In this 7T study, a blood T1 of 2212 ms was used to calculate the blood nulling time (TI) in VASO fMRI, which was measured from 79% oxygenation bovine blood (Hct = 0.43) at 7T(Dobre et al., 2007). Although this is within typical physiological range in normal human brains, it is known that blood T1 is sensitive to hematocrit and, to a lesser extent, to oxygenation (Blockley et al., 2008; Grgac et al., 2013; Lu et al., 2004a). This may affect the quantification of extravascular R_2^* values and relative CBV changes during functional activation. The oxygenation level of 79% corresponds mostly to an estimated average of the blood in capillaries and venules (Sharan et al., 1989; van Zijl et al., 1998). As only voxels activated from both the BOLD and VASO scans were used in the calculations, blood signals in veins should be largely excluded (if blood in veins is not completely nulled in VASO scans, it would reduce or cancel out the negative VASO changes during activation, thus be excluded in the voxel selection). Therefore, only incompletely nulled blood in arteries and arterioles is most likely to affect the extravascular R_2^* quantification. However, since the R_2^* values are comparable in arterial blood (about 40 s^{-1}, unpublished data, experimental setup same as in (Grgac et al., 2013)) and in extravascular tissue (Table 2.2) at 7T, this should not result in major biases in the

extravascular R_2^* estimation. Gu et al.(Gu et al., 2006) showed that the VASO signal change ($\Delta S/S$, thus ΔCBV) during visual stimulation plateaus over a range of about 150 ms around the theoretical blood nulling TI. Donahue et al.(Donahue et al., 2009d) also demonstrated that at typical spatial resolution for fMRI (around 3mm) and at relatively long TRs (>4s), the variation of blood T1 over a range of 100 ms has very limited influence on VASO signal change and ΔCBV estimation. It is therefore reasonable to expect that the blood T1 variation over typical physiological ranges in normal human brains should not have substantial effects on the ΔCBV estimation here. Moreover, the relative difference of T1 values decreases with field strength(Jin and Kim, 2008; Rooney et al., 2007), which should further reduce the potential biases in R_2^* and ΔCBV estimation resulted from blood T1 variations.

The contribution from physiological noises in fMRI signals has been shown to increase with field strength and voxel size (Triantafyllou et al., 2005). In order to check this for our study, we measured the coefficients of variation for the R2* values (Total R2*: 0.073; Extravascular R2*: 0.085), which were found to be comparable to those reported at 3T (Total R2*: 0.076; Extravascular R2*: 0.063) and 1.5T (Total R2*: 0.077; Extravascular R2*: 0.079) in a previous study adopting similar methodology (Lu and van Zijl, 2005). However, a larger voxel size was used in that study (2x2x5=20mm^3 versus 2.5x2.5x2.5=15.625mm^3 here). From this we conclude that the noise contribution in the R2* measurements at 7T would be larger than 3T and 1.5T if the same voxel size were used. We also noticed that the total R2* values measured in subjects 4 and 6 were slightly lower than the corresponding extravascular R2* values (total R2* is expected to be higher than extravascular R2* due to additional blood contributions), although the

difference was within noise range. This also occurred for one subject reported in previous 3T data but not 1.5T (Lu and van Zijl, 2005). We attribute this to the many possible contributions to R2*, making it difficult to measure this parameter with great accuracy. More repeats and averaging may be necessary for robust R2* measurement on a single-subject level.

A potential source of errors when estimating Y_v^{act} and OEF using Eqns. 1 and 2 comes from the literature values assumed for the model parameters. While this has been investigated in previous works (Donahue et al., 2009a; Hua et al., 2011c; Lu et al., 2004b), here again we performed an error analysis by estimating OEF using parameter values (assumed in Methods) over the normal physiological range: baseline CBV from 0.045 to 0.055 ml/ml, microvascular Hct from 0.38 to 0.46 and $\Delta\chi_{deoxy}$ from 0.20 to 0.27 ppm. Less than 8% estimated OEF differences were found between the two ends of both Hct and $\Delta\chi_{deoxy}$ ranges, whereas about 14% difference were observed when varying baseline CBV values. The assumed CBV^{rest} value of 0.052ml/ml in this study is approximated (Donahue et al., 2006a) based on the reported 0.048 - 0.055 ml/ml range in the literature (Brooks et al., 1985; Grandin et al., 2005; Leenders et al., 1990; Lu et al., 2005a; Rostrup et al., 2005). Although this error analysis shows that the estimated OEF values in this study are only moderately affected by these assumptions, the measurement of these physiological parameters in each participant would certainly improve the accuracy for OEF quantification.

2.5. Conclusions

Total and extravascular R_2^* values in the parenchyma in human visual cortex were

measured using multi-echo VASO and BOLD fMRI with visual stimulation at 7T. The parenchymal extravascular R_2^* value was 44.66 ± 1.55 s^{-1} at rest, and the ratio of extravascular ΔR_2^* to total ΔR_2^* was $91 \pm 3\%$ at 7T, confirming a predominant contribution from the extravascular component of the BOLD effect. A 37% decrease in parenchymal OEF during stimulation was estimated based on these measurements, consistent with values reported at lower field strengths.

Chapter 3: Three-dimensional Acquisition of Cerebral Blood Volume And Blood Flow Responses During Functional Stimulation In a Single Scan

3.1. Introduction

Cerebral blood volume (CBV) and cerebral blood flow (CBF) are two fundamental parameters in brain physiology. For instance, CBV and CBF responses during functional stimulation are required to quantify cerebral metabolic rate of oxygen (CMRO2) dynamics in most quantitative blood-oxygenation-level-dependent (BOLD) approaches, such as the calibrated BOLD approach (Blockley et al., 2013; Davis et al., 1998; Hoge et al., 1999; Lin et al., 2008, 2009; Lin et al., 2011) and other models (Donahue et al., 2009a; Hua et al., 2011c; Huber et al., 2013; Lin et al., 2008, 2009; Lin et al., 2011; Lu et al., 2004b; Uh et al., 2011). In the calibrated BOLD method using the Davis's model, CMRO2 change is estimated from BOLD and CBF changes measured during separate vascular and neuronal tasks, where the vascular stimulation is used as the calibration condition for BOLD signals. The extravascular BOLD effect of magnetic field gradients around the vessel network is approximated by a coefficient β determined from earlier simulations or measurement:

$$\text{BOLD } \frac{\Delta S}{S} = M\left(1 - \left(\frac{CMRO_2^{act}}{CMRO_2}\right)^{\beta}\left(\frac{CBF^{act}}{CBF}\right)^{\alpha-\beta}\right) \qquad [3.1]$$

where M is a constant, related to baseline physiolocial, vascular, and imaging parameters. Value for B of 1.5 is commonly assumed. A different BOLD model proposed by Lu and van Zijl (Lu et al., 2004b), and later used and refined by others, uses both intravascular

and extravascular compartments, and estimates CMRO2 change from separately measured BOLD, CBF and CBV responses during neuronal tasks (no vascular task is involved in this model). Accurate information about CBF and CBV dynamics is critical in both models. In the calibrated BOLD method, the CBV change is often derived from the measured CBF change using Grubb's equation with the constant exponent α (Grubb et al., 1974), which is commonly assumed to be identical in vascular and neuronal tasks:

$$CBV_1 = CBV_2 \cdot (CBF_1 / CBF_2)^{\alpha} \qquad [3.2]$$

However, recent studies have shown that this power-law relationship between CBF and CBV can vary substantially under different conditions (Blockley et al., 2009; Chen and Pike, 2009; Donahue et al., 2009e; Hua et al., 2010; Hua et al., 2011c; Ito et al., 2001; Lin et al., 2008; Rostrup et al., 2005). (Lin et al., 2008) demonstrated that using dynamic CBV measurements improves the accuracy for estimating $CMRO_2$ changes during functional stimulations, as compared with calculating CBV changes from CBF measurements and the Grubb's equation with an assumed constant. Therefore, it is important to measure both CBV and CBF dynamics to capture microvascular status alterations during functional stimulations.

The ability to detect CBV and CBF responses in one single scan is desirable as it will not only shorten total scan duration, but also reduce temporal variation due to factors such as subject motion, task performance, and physiologic changes between scans. The arterial spin labeling (ASL) technique can be used to measure CBF and CBV changes in the same scan by acquiring images at multiple post-labeling delays(Alsop et al., 2014; Brookes et al., 2007; Donahue et al., 2006b; Francis et al., 2008). However, the scan time of this method is relatively long compared to the typical temporal resolution in functional

studies. A number of MRI methods have been developed to measure CBV or CBF *separately*. For instance, CBV and CBF changes can be *separately* measured with vascular-space-occupancy (VASO) MRI (Lu et al., 2003) and flow-sensitive alternating inversion recovery (FAIR) arterial spin labeling (ASL) MRI (Kim, 1995; Kwong et al., 1995), respectively. Based on the T1 difference between blood and brain tissue, VASO MRI employs a spatially nonselective inversion pulse to invert both blood and tissue signals and acquires MR images at the time when blood signal recovers to zero (nulled), which can be used to calculate CBV changes (Lu et al., 2003). In FAIR ASL, an inversion pulse with and without spatially selective gradient is applied to produce the tagged and control images, respectively, from which CBF maps can be deduced (Kim, 1995; Kwong et al., 1995). Thus, a common feature in the pulse sequences of both methods is that an inversion pulse is exploited to perturb the blood water spins before image acquisition. The major difference, on the other hand, is that VASO images are always acquired at the blood nulling inversion time (TI), while FAIR ASL images need to be acquired at a much longer post-labeling delay (TI≈1.5-2s) (Alsop and Detre, 1996; Donahue et al., 2006a; Silva et al., 1997; Ye et al., 1997) to allow water exchange in the capillary bed to take place. Therefore, it is possible to combine VASO and FAIR MRI to share the same inversion pulse and acquire CBV and CBF weighted images at two different TIs in a single scan. Based on this principle, (Yang et al., 2004) previously devised an elegant technique for concurrent measurement of CBV, CBF and BOLD responses during functional stimulation. This method has recently been implemented on a 7T human MRI scanner by (Krieger et al., 2013). Another method for simultaneous measurement of CBV and CBF is the double-echo FAIR (DEFAIR) approach proposed

by (Thomas et al., 2001), in which CBF is measured with FAIR ASL and CBV is determined based on the different T_2 values calculated from the double echoes in the intra- and extravascular compartments. Both techniques were implemented in two-dimensional (2D) mode to acquire a single slice (Lin et al., 2008, 2009; Lin et al., 2011; Yang et al., 2004) or three slices (Gu et al., 2005) in one repetition time (TR).

Here, we propose a 3D MRI approach to measure CBV and CBF responses during functional stimulation in one single scan. It exploits the same principle as (Yang et al., 2004), which combines VASO and FAIR MRI with a common inversion pulse. A single-shot 3D fast gradient echo (GRE, also known as turbo field echo, TFE or TurboFLASH) sequence was used for image acquisition at two TIs. In addition, the magnetization pathways were simulated. The 3D VASO-FAIR sequence was implemented on a 3T human MRI scanner, and functional experiments with visual stimulation were performed on healthy volunteers to compare the data of the combined sequence and original separate scans in order to validate accuracy of the combined scan.

3.2. Materials and Methods

Pulse Sequence and Simulations

Figure 3.1 illustrates the combined 3D VASO-FAIR pulse sequence. Similar to the FAIR sequence, interleaving slab-selective (SS) and non-selective (NS) inversion preparation were employed. In each of the SS and NS scans, two image acquisition modules are deployed after the inversion at different TIs: TI_1 (blood nulling) and TI_2. CBV-weighted VASO images are obtained at TI_1 after NS inversion when the blood signal is nulled, and FAIR images are collected at a later time TI_2 in both SS and NS scans. These two FAIR

components are combined later to obtain the CBF-weighted signals. A single-shot 3D fast GRE sequence with centric (low-high) phase encoding profile was employed in all imaging modules. This readout has recently been used in VASO MRI, which showed minimal geometrical distortion and signal dropouts, low power deposition due to small flip angles, and negligible T_2^* contamination in VASO fMRI because of the very short echo time (TE) used (Hua et al., 2013a).
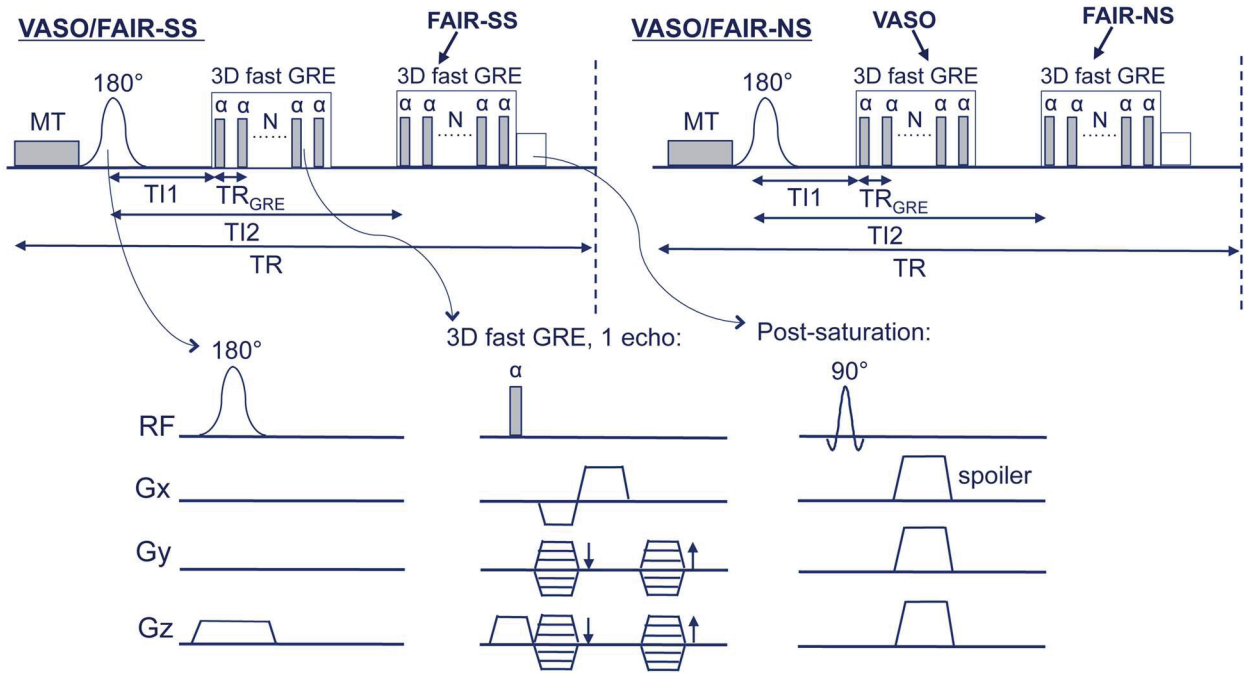
Fig. 3.1. Pulse sequence of the combined 3D VASO-FAIR approach. A pair of interleaving slice-selective (SS) and nonselective (NS) scans are shown. A magnetization transfer (MT) prepulse is added before the adiabatic FOCI inversion pulses. The imaging module used here is a 3D fast GRE readout for both VASO and FAIR ASL images, in which VASO signal is acquired at blood nulling time TI_1 and ASL signal at time TI_2. A post-saturation module comprising of a non-selective 90° saturation pulse and spoiler gradients is applied immediately after the FAIR ASL readout. Reproduced with permission from NeuroImage.

A magnetization transfer (MT) prepulse was applied immediately before the inversion pulses to prepare a smaller tissue magnetization, thus expediting the inversion recovery process so that the detectable tissue signals, and thus their signal-to-noise ratios (SNRs) are enhanced (Hua et al., 2009a; Hua et al., 2013a). When using moderate irradiation power and durations, and a frequency offset sufficiently far away from water resonance (40ppm or more), the MT prepulse has been shown to have negligible effect on blood signal so that the same blood nulling TI can be used for VASO(Balaban et al., 1991; Hua et al., 2009a; Hua et al., 2013a; Wolff and Balaban, 1989).

A spatially nonselective saturation (90° RF pulse followed by spoiler gradients) was deployed immediately after the second imaging module to set all residual magnetization (blood and tissue) to zero. The purpose for this post-saturation module is two-fold. First, it suppresses the inflow effect due to non-steady-state blood spins in VASO MRI by establishing a steady state for all blood spins entering the RF transmit coil after the first repetition time (TR) (Hua et al., 2013a; Lu, 2008; Wu et al., 2007a). Second, it ensures that blood spins in and outside the inversion slab applied in the SS scan will have the same steady-state blood nulling condition in the following NS scan. This is illustrated with Bloch simulations in Figure 2. Signal evolution during the 3D fast GRE readout was calculated using the same imaging parameters described in Experiments. Typical T_1 and T_2 values for blood, gray matter (GM), white matter (WM) and cerebrospinal fluid (CSF) in healthy human brain at 3T were used: $T_{1,blood}$ = 1624ms (Lu et al., 2004a), $T_{1,GM}$ = 1122ms (Lu et al., 2005b), $T_{1,WM}$ = 758ms (Lu et al., 2005b), $T_{1,CSF}$ = 3817ms (Lu et al., 2005b), $T_{2,GM}$ = 80ms (Lu et al., 2005b), $T_{2,WM}$ = 80ms (Lu et al., 2005b), $T_{2,blood}$ = 55ms (Zhao et al., 2007), $T_{2,CSF}$ = 1442ms (Donahue et al., 2006a). The

establishment of a steady state after the first TR with the post-saturation module applied immediately after the second readout, is illustrated in Figure 3.2a. For VASO, after the first pair of NS and SS scans, both blood in and outside the SS inversion slab will always have the same blood nulling time in the following NS scans, so that potential complications from inflowing blood are eliminated. For FAIR ASL, in-slab blood signals are identical at TI_2 in both NS and SS scans, which minimizes its contamination to the CBF measurement. On the other hand, signal from blood outside the inversion slab is higher at TI_2 in the SS scans, which is used to deduce CBF information upon subtraction of the NS and SS scans. Without the post-saturation module (Figure 3.2b), a steady state is not reached until the fourth TR in the simulations. Furthermore, even when this steady state is reached, the out-of-slab blood signal in VASO is still not properly nulled at TI_1 (Figure 3.2b inset), because the blood nulling times are different for in-slab and out-of-slab blood without the post-saturation module (effective TR is different). In-slab blood signals in the FAIR scans are still identical at TI_2 in both NS and SS scans during steady state.
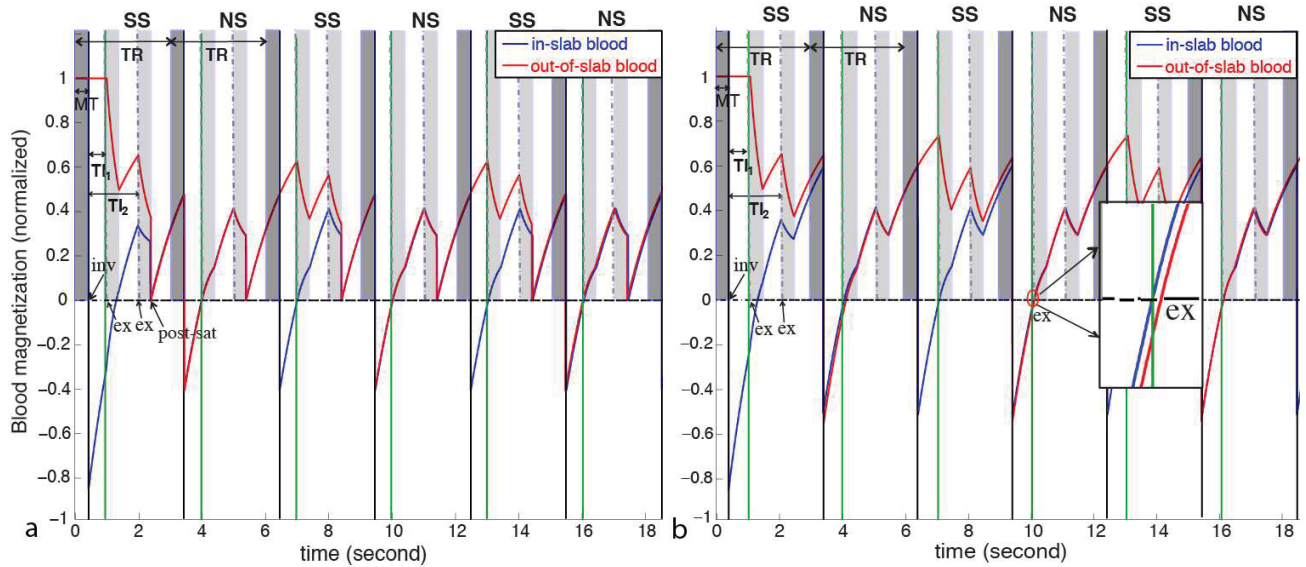
Fig. 3.2 Bloch simulations of the signal evolution for blood in (blue) and outside (red) the inversion slab applied in the slice-selective (SS) scan with (a) and without (b) the post-saturation module. The solid vertical black lines indicate the inversion pulses (labeled as "inv") in the interleaving slice-selective (SS) and non-selective (NS) scans. The short dashed vertical lines represent the first excitation pulses (labeled as "ex") in each image acquisition module, the durations of which are labeled in light shade. The MT period before the inversion pulse is labeled in dark shade. Steady state blood nulling time for VASO is marked as TI_1 (solid vertical green lines) and the post-labeling delay for FAIR as TI_2. **(a)** With the post-saturation module (labeled as "post-sat") applied immediately after the second readout, a steady state is built after the first TR, at which both blood in and outside the SS inversion slab is nulled at TI_1 in the NS scan. (b) When the post-saturation module is not applied, it takes three TRs for both in-slab and out-of-slab blood to reach steady state (for the experimental parameters used) and the out-of-slab blood is

not properly nulled even at steady state (zoomed inlet). Reproduced with permission from NeuroImage.

The same simulations were used to estimate blood nulling TIs in VASO scans and to evaluate GM and CSF signals. A 20% signal drop after the MT saturation pulse were assumed for GM (typical values under similar saturation schemes (Hua et al., 2009a)), and no MT effect for CSF. The steady state GM signals from the simulations were 23% (of the equilibrium signal) (separate) and 20% (combined) in the VASO scans, and 59% (separate) and 57% (combined) in the FAIR scans. The steady state CSF signals were -9% (separate) and -4% (combined) in the VASO scans, and 15% (separate) and 19% (combined) in the FAIR scans. Assuming a 30% increase of CBV upon activation, the relative VASO signal change from the simulations is -1.87% in a pure GM voxel for both separate and combined VASO scans, and is -1.90% (VASO in combined scan) and -1.92% (separate VASO scan) in a voxel with 5% CSF and 95% GM in volume.

Experiments

The protocol was approved by the Johns Hopkins Medicine Institutional Review Board. Subjects gave written informed consent before participating. Experiments were performed on a 3T human MRI scanner (Philips Healthcare, Best, The Netherlands), using a body coil for RF transmission and a 32-channel head coil for reception. Six healthy volunteers were scanned for this study. Three fMRI experiments with visual stimulation (yellow/blue flashing checkerboard, 24s visual stimulation interleaved with 42s cross-hair fixation, repeated 4 times) were performed on each participant: (a) 3D VASO-FAIR ($TR/TI_1/TI_2$=3/0.552/1.552s). A 400ms 2.5µT block-shaped MT prepulse with a frequency offset at -40 ppm (Hua et al., 2013a) was applied immediately before the inversion pulses in both NS and SS scans. (b) VASO (TR/TI = 3/0.743s). The same

MT prepulse and post-saturation module as in 3D VASO-FAIR were applied. (c) FAIR (TR/TI = 3/1.552s). The order of the experiments was counterbalanced across participants. Bloch simulations (described above) were performed to estimate steady state blood nulling times for VASO scans in order to account for the influence from the 3D fast GRE readout and the post-saturation module. Note that TI_1 in the combined 3D VASO-FAIR sequence is different from TI in VASO because of the different numbers of readouts, corresponding to different recovery times after the post-saturation module (before next inversion) in the two sequences (thus different steady states). Although this leads to different inflow times (TI) for VASO, it should not have a major influence on the VASO signals if the inflow effect (see Discussion) is largely suppressed by the post-saturation module. Frequency offset corrected inversion (FOCI) pulses (Ordidge et al., 1996) were used for inversion in all scans, which are expected to produce sharper edges for spatially selective inversion than hyperbolic secant (HS) pulses (Hua et al., 2011a; Hua et al., 2011b). Common imaging parameters: voxel size = 5mm isotropic, 16 slices, field of view (FOV) = 192x192 mm^2, TR_{GRE} (TR between two consecutive echoes in 3D GRE)/TE = 3.6/1.6ms, flip angle = 7°, turbo direction = radial, parallel imaging (SENSE) acceleration factor = 3x2 (APxFH), no partial Fourier sampling, readout duration for one image volume = 391 ms. Based on the thickness of the imaging volume (80mm), the thickness of the SS inversion slab was chosen to be 100 mm.

Data Processing

The Statistical Parametric Mapping (SPM 8, University College London, UK) software package and several in-house Matlab R2012a (Mathworks, Natick, MA, USA) routines

were used for data analysis. All fMRI images were corrected for motion and baseline drift. CBF-weighted images were obtained using a surround subtraction method, in which the SS/NS FAIR ASL images are subtracted with linear interpolation between the surrounding NS/SS images, respectively (Lu et al., 2006). A general linear model (GLM) was used to detect activated voxels (P < 0.01, t-score ≤ -1.5 for VASO and t-score ≥ 1.5 for FAIR). A SNR threshold of 20 for VASO images was used(Donahue et al., 2006b). Due to the low SNR in the subtracted FAIR ASL images, a SNR threshold of 1 was used. The relative signal change (ΔS/S) in each voxel was quantified as the difference between average signals during the baseline and activation periods normalized by the average baseline signal. In order to avoid the transitional periods when calculating average signals, images acquired during the first 18s and 6s during the baseline and activation periods, respectively, were excluded. Temporal SNR (tSNR) was calculated as the voxel-wise average baseline signal divided by the standard deviation along the time course during the baseline period. Contrast-to-noise ratio (CNR) per scan was defined as the product of absolute value of relative signal change (ΔS/S) and tSNR. CNR per unit time was taken as the product of CNR per scan and square root of number of image volumes acquired during the entire scan. In FAIR ASL, tSNR and CNR were calculated from the subtracted CBF-weighted images.

3.3. Results

Representative CBV-weighted and CBF-weighted (after surround subtraction) images from 3D VASO-FAIR are shown in Figures 3.3a,b, respectively. Figures 3.3c,d show the corresponding images from separate VASO and FAIR-ASL scans with the same

scales. The quality and contrast of the images are comparable between combined and separate scans.
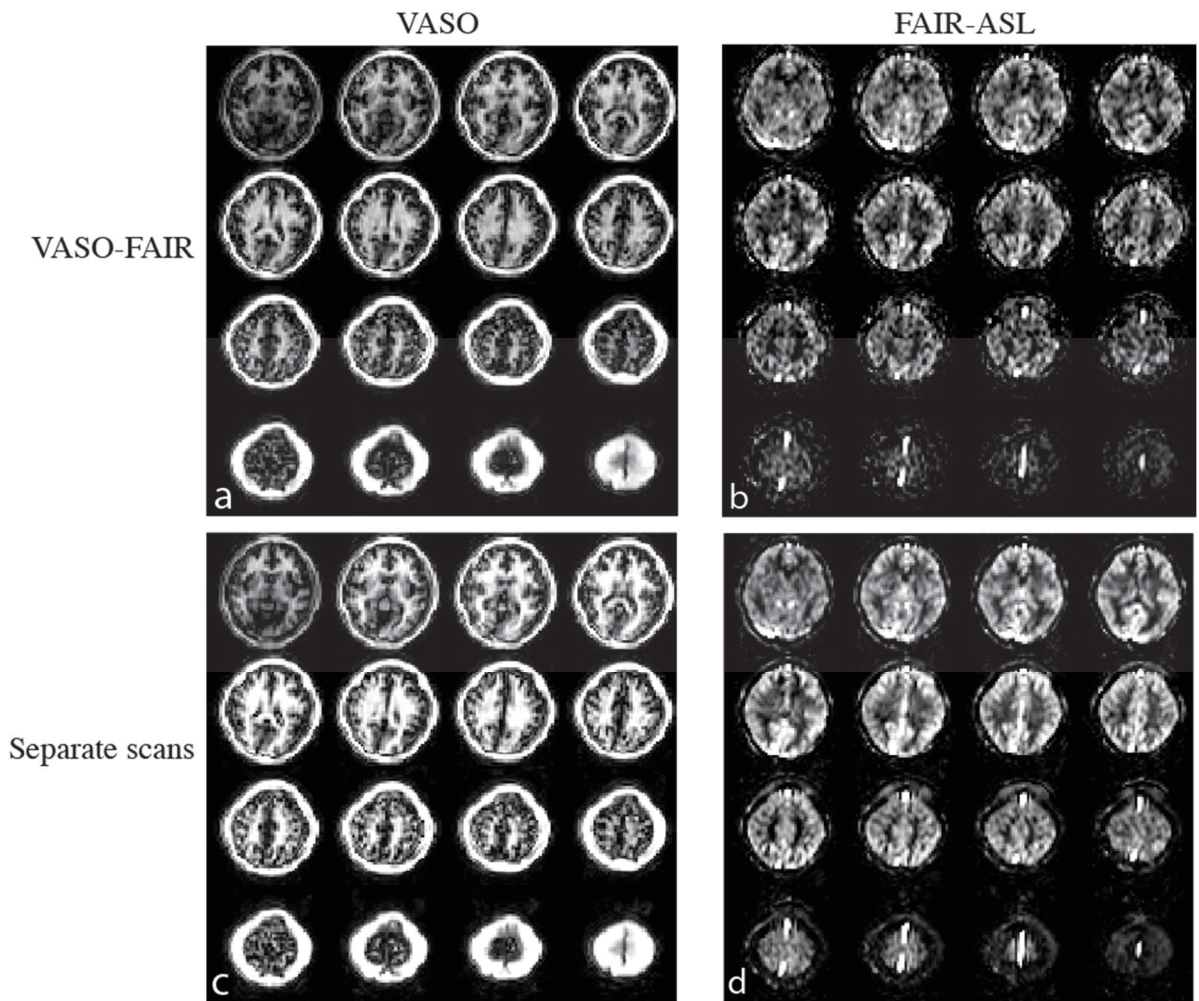
Fig. 3.3. Representative images from one subject. (a) Typical VASO images (3D fast GRE readout, 16 slices) from the 3D VASO-FAIR sequence. (b) Typical FAIR ASL difference maps (perfusion weighted images) in 3D VASO-FAIR. (c) Corresponding VASO images in the separate VASO scan. (d) Corresponding perfusion weighted images in the separate FAIR ASL scan. Images in (a) and (c), and (b) and (d) are on the same scales, respectively. Reproduced with permission from NeuroImage.

The fMRI results from the combined 3D VASO-FAIR scans and separate VASO and FAIR scans are compared further in Figure 3.4 and Table 3.1. The voxels meeting

activation criteria (highlighted with their t-scores) are mostly localized in the visual cortex (representative images for VASO in Figures 3.4a,b and for FAIR in Figures 3.4d,e; 16 slices acquired, 4 slices shown), and the spatial patterns of activation are similar between the combined and separate VASO and FAIR scans. A few spurious activations outside the visual regions were observed in some of the subjects, but these were excluded from further analysis as the focus of this study is to compare the separate and combined scans in the visual cortex. In the subsequent quantitative comparisons, only voxels that are activated in both separate and combined scans were used.

The time courses averaged over all slices and all subjects matched well between the separate and combined scans for both VASO (Figure 3.4c) and FAIR (Figure 3.4f). The relative signal changes ($\Delta S/S$), tSNR and CNR per scan were all statistically comparable ($P>0.1$) between combined and separate scans for VASO and FAIR, respectively. CNR per unit time for VASO was higher in the separate scan ($P<0.01$) than in the 3D VASO-FAIR scan, as only half of VASO scans were acquired in the combined scan. CNR per unit time for FAIR was comparable ($P>0.1$) between separate and combined scans.
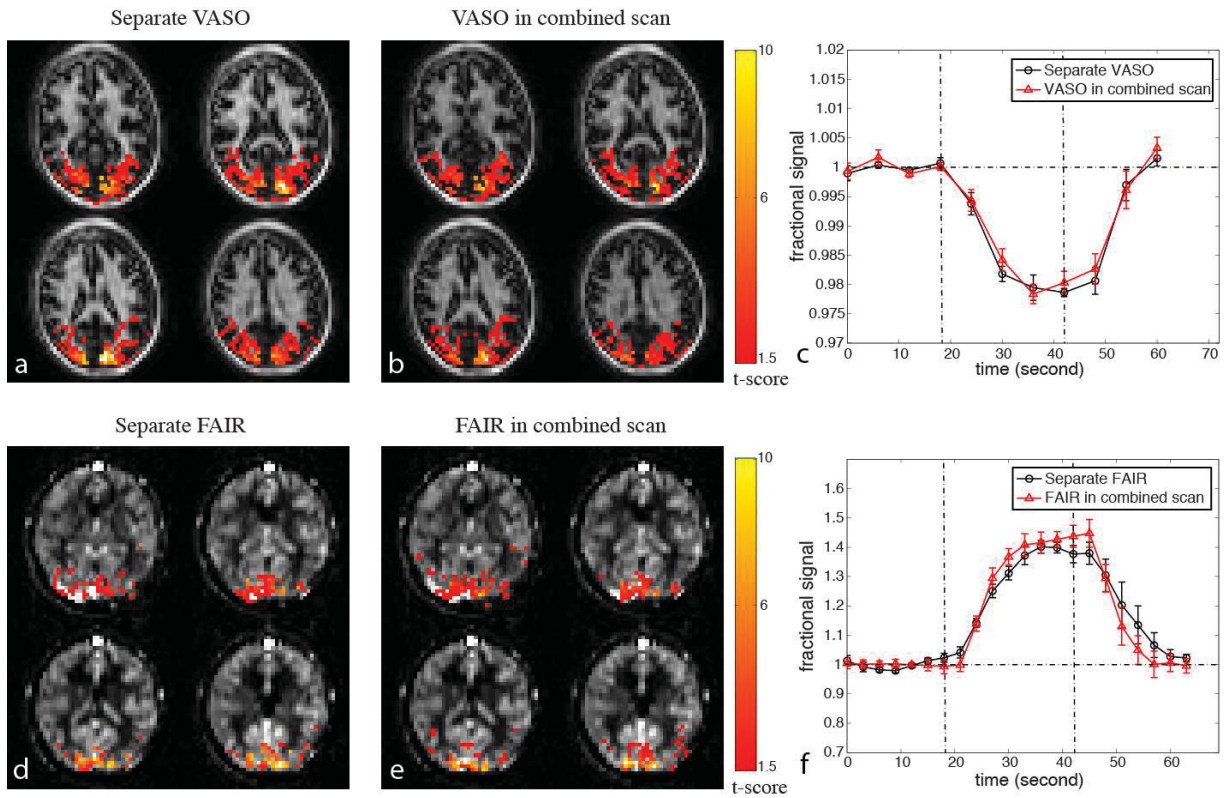
Fig. 3.4. Comparison of functional MRI results between the combined and separate scans. Representative activation maps from one subject for (a) separate VASO scan, (b) VASO in the combined 3D VASO-FAIR method; (d) separate FAIR ASL scan, and (e) FAIR ASL in the 3D VASO-FAIR scan are shown. The activated voxels are highlighted with their t-scores. Time courses averaged over common voxels activated in both separate (black circle) and combined (red triangle) scans (averaged over subjects, n = 6) for VASO and FAIR are shown in (c) and (f), respectively. Error bars represent inter-subject variations. The vertical dotted lines indicate the start and end of visual stimulation. Four blocks of baseline and stimulation periods were averaged to one block. Reproduced with permission from NeuroImage.

Table 3.1. Summary of quantitative fMRI results from all subjects (n = 6).

	Separate VASO	VASO in combined VASO-FAIR scan	Separate FAIR	FAIR in combined VASO-FAIR scan
ΔS/S (%)	-1.98±0.36	-1.86±0.45	38.6±6.1	42.7±8.3
tSNR	63.7±8.0	61.9±7.0	5.8±0.3	5.2±0.3
CNR per scan	1.26±0.20	1.14±0.21	2.24±0.27	2.23±0.39
CNR per unit time	12.8±2.1	8.2±1.5	22.6±2.7	22.5±3.9

Mean values ± standard deviation over all subjects. ΔS/S, tSNR and CNR were calculated as defined in Methods. Only common voxels activated in both separate and combined VASO or FAIR scans were included. All FAIR ASL results were calculated from the subtracted images (difference maps or perfusion weighted images).

Relative CBV and CBF changes upon visual stimulation were quantified based on the measured VASO and FAIR $\Delta S/S$, respectively. Using the theory and parameters from (Donahue et al., 2006a; Hua et al., 2011c; Lu et al., 2003), the relative CBV change was calculated as 37.1%±3.9% (separate scan) and 34.8%±6.3% (combined scan), whereas the relative CBF change was 38.6%±6.1% (separate scan) and 42.7% ± 8.3% (combined scan).

3.4. Discussion

We developed a 3D whole-brain imaging technique to simultaneously detect CBV and CBF responses upon functional stimulation in a single MRI scan. This is expected to be useful especially for the quantitative BOLD approaches in which concurrent CBV and CBF measurements are desired. Compared to sequentially obtaining CBV and CBF measurements using individual scans, this technique will not only improve the acquisition efficiency, but also reduce potential confounding effects resulting from head motion, task performance variation and physiologic fluctuations between MRI scans. Compared with the original separate VASO and FAIR scans, the proposed approach demonstrated similar image quality, activation patterns and relative signal changes ($\Delta S/S$) during functional stimulation, as well as comparable tSNR and CNR values per scan. The fact that $\Delta S/S$ in the separate and combined scans are consistent indicates that they are measuring the same contrast (CBV and CBF changes for VASO and FAIR, respectively). Bloch simulations demonstrated that the GM signals in the VASO and FAIR scans in the combined method are both slightly lower than those in the corresponding separate scans (VASO: 20% vs. 23%; FAIR: 57% vs. 59%). Nevertheless, tSNR and CNR per scan were all comparable

between the corresponding separate and combined scans in our data (Table 1). This can be explained by the fact that physiological noise is dominant in fMRI, thus a slight loss in MR signal might not lead to a decrease in tSNR (Gonzalez-Castillo et al., 2011; Kruger and Glover, 2001; Kruger et al., 2001; Triantafyllou et al., 2005). Indeed, we found that the noise levels (calculated as the standard deviation along the time course during the baseline period) were lower in the combined scans from all six subjects.

In the proposed approach, we adopted a 3D fast GRE imaging sequence, which has much less geometric distortion and fewer signal dropouts than the traditional GRE echo-planar-imaging (EPI) sequence and is commonly used in high-resolution anatomical scans such as the Magnetization Prepared RApid Gradient Echo (MPRAGE) sequence (Hua et al., 2013b; Mugler and Brookeman, 1990; Qin et al., 2014). For VASO fMRI, this readout minimizes the BOLD contamination by allowing a very short TE (< 2ms) to be used (Hua et al., 2013a). For CBF measurement, a 3D readout can eliminate the artifactual inter-slice variation of perfusion signals originating from slice-dependent post-labeling delay times in 2D acquisition methods (Gai et al., 2011; Gunther et al., 2005). A low-high (also known as "centric") phase encoding scheme was used in the 3D GRE readout. This means that the center of k-space (kz=ky=0 for 3D), which determines the gross signal intensity in the image, was acquired at the first echo. This is important for blood nulling in VASO (Hua et al., 2013a) and CBF quantification in ASL. Nevertheless, while the signal intensity in MRI images is dictated by the center of k-space, the evolution of magnetizations during the rest of the readout train when outer k-space lines are acquired would lead to a distorted point spread function (PSF), which causes blurring artifacts in the images (Epstein et al., 1996; Hua et al., 2013a; Lin and Bernstein, 2008).

For static spins (tissue), such artifacts are shown to be minimal when a low FA (<20º) is used in 3D fast GRE with short TR (Epstein et al., 1996). For inflowing spins (blood), a recent study using a similar 3D readout demonstrates that the blurring effects are small with vascular transit times ranging from 1.1 to 2.3 s (Nielsen and Hernandez-Garcia, 2013). The PSF for the sequence used in this study was calculated, which was only slightly distorted with maximum amplitude of the side lobes less than 5% of the main peak. This indicates that such blurring artifacts are minimal in our sequence with a FA of 7º and a short TR of 3.6 ms.

In this proof-of-concept study, we chose a spatial resolution of 5mm isotropic to boost the sensitivity (SNR) of the measurements, and to demonstrate the principles of the 3D VASO-FAIR method. This may lead to significant partial-volume effects from WM in the GM signals. WM is known to have much smaller CBV and CBF values, and a longer arterial transit time than GM, the change of which during a typical flashing checker board visual stimulation is known to be quite small (Leenders et al., 1990; van Gelderen et al., 2008; van Osch et al., 2009). This may bring down the overall perfusion signal changes in the large voxels measured in our data. Although this partial volume effect should not undermine the comparison between the separate and combined approaches here, for future quantitative physiological studies, finer spatial resolution, which can be achieved by adapting the readout pulse sequence and utilizing fast imaging techniques such as parallel imaging and partial Fourier sampling, may be used to alleviate this problem. Besides, a high resolution anatomical scan may be acquired for each subject in order to correct for such effects in the perfusion measurements.

In gray matter, CSF occupies about 10-15% of the voxel volume. The T_1 value of

CSF is long (~4300ms at 3T) as CSF contains few macromolecules. Consequently CSF magnetization is negative at the blood-nulling TI, which is opposite in sign to the gray/white matter magnetization. CSF partial volume effects can affect VASO fMRI by altering the baseline VASO signal, and thus CBV quantification. Some investigators have also suggested that the CSF volume fraction may change during brain activation, which could have further implications in VASO fMRI. As shown in several studies (Donahue et al., 2006a; Jin and Kim, 2010; Piechnik et al., 2009; Scouten and Constable, 2007, 2008) CSF contributions may influence the interpretation of VASO fMRI in two ways: impact on baseline VASO signal and impact on activation-induced signal change. First, the presence of CSF will lower the baseline VASO signal, as its magnetization is negative and will offset some of the positive tissue signals. Even in the absence of CSF volume changes upon activation, this effect may cause an over-estimation of relative CBV change. From the Bloch simulations (see Methods), the steady state CSF signals in the combined scan are less negative (-4% of the equilibrium signal) in VASO and more positive (19%) in FAIR ASL than the respective separate scans (VASO -9%, FAIR ASL 15%). Simulations also indicate that the CSF contamination in the VASO signal change is slightly smaller in the combined scan due to the less negative CSF signal, which may at least partially explain the less negative (albeit not statistically significant) $\Delta S/S$ in the combined VASO scan (Table 3.1). For FAIR ASL, as it is generally reasonable to assume comparable CSF signals in both label and control scans, this partial volume effect should not affect the difference signal (perfusion). Moreover, several studies have suggested that CSF volume may show a decrease upon activation (Donahue et al., 2006a; Jin and Kim, 2010; Piechnik et al., 2009; Scouten and Constable, 2007, 2008), which tends to cause a

signal increase in VASO fMRI, potentially overriding the VASO effect. There are also studies reporting an increase in CSF volume during hypercapnia (Scouten and Constable, 2008). The situation where CSF volume changes during activation was not simulated in this study, as it seems unclear so far whether and how much the CSF volume alters, which may need further investigation. Several techniques, such as VASO-FLAIR (Donahue et al., 2006a) and VASO ACDC (Scouten and Constable, 2007, 2008) may possibly be incorporated to suppress the CSF contamination in the VASO signals with careful design of the timing of pulse sequence.

The inflow effect in VASO MRI is suppressed by a post-saturation module in the 3D VASO-FAIR sequence. As shown in previous work (Hua et al., 2013a), the inflowing blood spins in VASO can be categorized into three different types depending on their times entering the transmit coil: I) spins flowing in before the end of readout of the previous TR; II) spins flowing in between the readout of previous TR and the inversion pulse of current TR; III) spins flowing after the inversion pulse of current TR. The post-saturation method only eliminates type I inflowing spins. Type II and III spins can be suppressed by the motion-sensitized driven equilibrium (MSDE) technique. In the current study, we did not apply MSDE in both the separate and combined scans for the following reasons: 1) The inflow effects from type II and III spins are relatively small when a body coil is used for RF transmit at 3T with a relatively long TR (Donahue et al., 2009b; Donahue et al., 2006a; Lu, 2008); 2) The main goal of this study is to compare the separate and combined scans with the same imaging parameters. However, this may result in larger VASO signal changes in our data due to residual type II and III spins, and the MSDE module (Hua et al., 2013a) should be applied in future quantitative studies.

Another confounding effect for CBF and CBV quantification comes from the alteration in vascular transit times upon functional stimulation. In VASO, a spatially non-selective inversion is used and the inflow effect, which is more prominent at short TR, is largely suppressed by the post-saturation module. Therefore, we expect that transit time changes upon stimulation have minor influence on the VASO signal changes with a relatively long TR used in this study. For FAIR ASL, it is well known that scans with a single post-labeling delay (TI) are more sensitive to bolus transit time changes, which is especially problematic for short TIs. With a relatively long TI used here for FAIR ASL, it has been shown that this confounding effect is quite small for typical transit time changes during functional stimulation in human brain (Alsop et al., 2014; Donahue et al., 2006b). In addition, the first readout pulse train in the 3D VASO-FAIR sequence may saturate some of the inflowing blood spins that will eventually contribute to the FAIR ASL signals acquired in the second readout. This would not affect the relative signal change in FAIR ASL if the vascular transit time does not change between baseline and activation. To evaluate the situation when the transit time does change, Bloch simulations were performed in which the signals from blood spins that reach the imaging volume after each excitation pulse in the first readout were calculated individually (because they see different numbers of excitation pulses), and the weighted sum of these blood signals (depending on transit times) was taken as the total blood signal when the FAIR ASL images are acquired in the second readout. The same imaging parameters described in Methods were used, and a baseline bolus arrival time of 400 ms with a 15% decrease upon visual stimulation (Hua et al., 2011a) was assumed. The results from simulation indicate that such a transit time effect will only increase the relative signal change in

FAIR ASL with <5% as compared to a pure CBF increase. To correct for these confounding effects in CBF quantification, methods such as QUIPPS II (Luh et al., 1999; Wong et al., 1998) and/or multiple post-labeling delays can be employed (Dai et al., 2012) in future studies, especially in certain physiological conditions where transit time changes drastically.

Taking these confounding effects together, the relative changes in FAIR ASL signals and CBF during visual stimulation in our data are relatively low compared to typical literature values. We attribute this mainly to a substantial partial volume effect from WM. On the other hand, the VASO signal changes and estimated CBV changes are comparable to literature values, which may be explained by the fact that counteracting confounding effects (partial volume effects from WM decreases the VASO signal changes; but CSF contamination and residual inflow effect increase the VASO signal changes) cancel out with each other on the final VASO signal change. Note that the proposed method is designed for functional studies where relative changes in CBF and CBV are of interest. The traditional VASO approach alone cannot measure absolute baseline CBV. For ASL, while it yields signals that are linearly proportional to CBF, absolute quantification of CBF requires careful evaluation of potential confounds which we feel is beyond the scope of the current study.

Power deposition does not seem to be a major limiting factor in the combined pulse sequence used here, mainly due to the low FA in the 3D GRE readout and the relatively long TR and readout duration. The specific absorption rate (SAR) is about 1.0 W/kg (<30% of the FDA limit for head exposure) for the proposed 3D VASO-FAIR sequence with the parameters used in this study. If the MT pre-pulse is turned off (with

other parameters identical), SAR will decrease to about 0.3 W/kg (<9% of the FDA limit). Note that the 400 ms 2.5 µT block-shaped MT prepulse can also be replaced by a pulse train to further lower the SAR level. With the same imaging parameters used here, the 3D VASO-FAIR sequence can acquire up to 30 slices with a SAR level less than 1.1 W/kg (<34% of the FDA limit) at 3T. In this case, the actual bottleneck is the long readout pulse train for one image volume and TR, instead of power deposition.

In this first study, we chose to use the original forms of pulse sequences for FAIR ASL and VASO. Over the past decade, many improvements have been developed for these methods, including vascular crushing gradients, QUIPSS (QUIPSS II and Q2TIPS), multiple post-labeling delays, background suppression, pseudo-continuous labeling for ASL (Alsop et al., 2014), and the inflow-based VASO (iVASO) approach (Donahue et al., 2009c; Donahue et al., 2010; Hua et al., 2009b, 2011a; Hua et al., 2009c, 2011b) for VASO. We are currently working to incorporate some of these improvements into the proposed approach. For instance, crusher gradients (Le Bihan et al., 1988) or the motion-sensitized driven equilibrium (MSDE) preparation (Balu et al., 2011; Hua et al., 2013a; Wang et al., 2007; Wang et al., 2010) can be added to suppress macro-vascular signal contaminations in ASL. The combined sequence can also be adapted with the QUIPSS modifications (Luh et al., 1999; Wong et al., 1998) to control the labeling bolus width. Scans at multiple post-labeling delays (TI) (Buxton et al., 1998; Dai et al., 2012; Francis et al., 2008; Gonzalez-At et al., 2000; Gunther et al., 2001; Petersen et al., 2006; Wang et al., 2013) can be achieved by deploying multiple readout modules within one scan (TR) or using separate scans for each TI, in order to obtain direct information on vascular transit times and to reduce errors in CBF quantification due to transit time variations.

However, similar to other ASL methods, this is certainly limited by factors such as TR, readout length, power deposition and total scan time. Although theoretically feasible, careful design of the timing and number of saturation and inversion pulses is needed to incorporate background suppression (Dai et al., 2008; Dixon et al., 1991; Garcia et al., 2005; Maleki et al., 2012; Ye et al., 2000) into the proposed method. FAIR ASL is a pulsed ASL (PASL) scheme. Therefore, pseudo-continuous labeling (Dai et al., 2008; Wong, 2007; Wu et al., 2007b), which generally has higher SNR than PASL, cannot be used here, which may be one of the disadvantages for the proposed method. The inversion schemes in iVASO (Donahue et al., 2009c; Donahue et al., 2010; Hua et al., 2009b, 2011a; Hua et al., 2009c, 2011b)can also be used here, which should result in enhanced SNR, and a CBV contrast dominated by the arterial compartment. Proper single TI or multiple TIs should be used to mitigate arterial transit time effects in the iVASO contrast (Donahue et al., 2009c; Donahue et al., 2010; Hua et al., 2009b, 2011a; Hua et al., 2009c, 2011b).

One drawback of the proposed 3D VASO-FAIR sequence is that the temporal resolution for the VASO scans are halved compared to the separate VASO approach, as VASO images can only be acquired at TI_1 in each NS scan but not in the SS scans where no global inversion is applied and out-of-slab blood is not properly nulled. Hence, CNR per unit time for VASO was lower in the combined method compared to the separate VASO scan (Table 1). On the other hand, since the out-of-slab blood signal is higher during the SS scans in the combined scans as compared to the blood signals in separate VASO scans, it acts as a suppressor for the CBF contamination in the VASO contrast. As a post-saturation module is already applied here to suppress the flow related artifacts in

VASO, this extra suppression effect is not obvious in the data. However, VASO $\Box$S/S in the combined scans appeared slightly lower (albeit not statistically significant) than in separate scans (Table 1), which may indicate some residual CBF contamination at TR of 3s being suppressed. This suppression effect should be more useful for VASO scans with shorter TRs in which the flow related contamination is more prominent (Donahue et al., 2009b; Lu et al., 2013).

3.5. Conclusions

A 3D perfusion imaging approach was demonstrated that combines the VASO and FAIR-ASL MRI techniques, allowing the measurement of CBV and CBF dynamics during functional stimulation in a single scan. Using a flashing checker board visual stimulation paradigm, activation patterns with signal changes ($\Box$S/S), tSNR and CNR per scan comparable to the original individual methods were detected. This approach is expected to provide a more efficient and equally sensitive alternative when both CBV and CBF responses need to be monitored during a functional task, such as needed for the quantitative BOLD fMRI studies where information about oxygen metabolism alterations can be extracted from the BOLD and hemodynamic measures.

Chapter 4: A Three-dimensional Single-scan Approach for the Measurement of Changes in Cerebral Blood Volume, Blood Flow, and Blood Oxygenation-weighted Signals during Functional Stimulation

4.1. Introduction

Functional magnetic resonance imaging (fMRI) techniques based on blood-oxygenation-level-dependent (BOLD) contrast have been used extensively for mapping functional neuroanatomy. The origin of the BOLD effect reflects the changes in the concentration of deoxygenated hemoglobin, which acts as an intrinsic paramagnetic contrast agent and reduces the local MR signal by creating microscopic field gradients in and around the blood vessels. Therefore during neuronal activation, other than the site of activation, large draining veins further downstream can also show large BOLD signal changes. As a result, the major drawback of BOLD contrast is its poor spatial specificity. In fact, the BOLD effect in tissue is very complicated and reflect ensemble changes in physiological parameters such as cerebral blood volume (CBV), blood flow (CBF), and cerebral metabolic rate of oxygen ($CMRO_2$).

A number of alternative MRI techniques that use single physiological quantities as a neuronal activity marker have been developed to measure cerebral blood flow and blood volume *separately*. Arterial spin labeling (ASL) method uses magnetically labeled (inverted) blood water as an endogenous tracer, and can measure both baseline CBF, as well as activation-dependent changes in CBF with strong arteriolar and capillary signal-weighting thus improving spatial specificity and providing a useful complement to standard BOLD functional imaging. The vascular-space-occupancy (VASO) MRI (Lu et

al., 2003) has been used to measure functionally induced changes in CBV. Based on the T1 difference between blood and brain tissue, VASO MRI employs a spatially nonselective inversion pulse to invert both blood and tissue signals and acquires MR images at the time when blood signal recovers to zero (nulled), which can be used to calculate CBV changes.

Quantitative BOLD approaches have been developed to estimate $CMRO_2$ dynamics from BOLD, CBF and CBV responses, normally using separate scans. Calibrated BOLD methods use Davis's model and estimate $CMRO_2$ changes from BOLD and CBF measurements during separate vascular and neuronal tasks, where the vascular stimulation is used as the calibration condition for BOLD signals (Blockley et al., 2013; Davis et al., 1998; Hoge et al., 1999; Lin et al., 2008, 2009; Lin et al., 2011). However, the measurement of CBV is usually inferred from the CBF measurement using Grubb's equation with a constant exponent (Grubb et al., 1974), which is commonly assumed to be identical in vascular and neuronal tasks. Recent studies have shown that this power-law relationship can vary substantially under different conditions (Blockley et al., 2009; Chen and Pike, 2009; Donahue et al., 2009e; Hua et al., 2010; Hua et al., 2011c; Ito et al., 2001; Lin et al., 2008; Rostrup et al., 2005), and calibrated BOLD studies are expected to benefit from using dynamic CBV measurements and can overcome uncertainties related to the flow-volume coupling coefficient (Lin et al., 2008). A different BOLD model proposed by Lu and van Zijl (Lu et al., 2004b), and later used and refined by others, considers both intravascular and extravascular signal contribution to the BOLD effect, and estimates $CMRO_2$ changes from separately measured BOLD, CBF and CBV responses during neuronal tasks (no vascular task is involved in this model) (Donahue et

al., 2009a; Hua et al., 2011c; Huber et al., 2013; Lin et al., 2008, 2009; Lin et al., 2011; Lu et al., 2004b; Uh et al., 2011).

It is important to measure BOLD, CBV and CBF hemodynamics to capture microvascular status changes and further estimate oxygen metabolism alterations during functional stimulations. The ability to measure these parameters in a single scan would be potentially useful to improve image acquisition efficiency, and more importantly reduce the sensitivity to temporal variations due to factors such as subject head motion, task performance, and physiologic changes among the scans. (Yang et al., 2004) previously introduced an MRI technique to simultaneously map BOLD-, CBF-, and CBV-weighted MRI signals at 3 Tesla. Several technical development and applications have followed the original proposal(Gu et al., 2005). More recently, (Krieger et al., 2013) modified and implemented a similar sequence at 7 Tesla. Those studies were implemented in two-dimensional (2D) mode to acquire a single slice or at most three slices in one repetition time (TR) thus with very limited brain coverage. Simultaneous multi-slice BOLD and CBF measurement are mostly applied in the calibrated BOLD studies using either dual-echo or dual excitation ASL (Ances et al., 2011; Bulte et al., 2009; Chen and Parrish, 2009; Chiarelli et al., 2007; Gauthier et al., 2011; Hoge et al., 1999; Leontiev et al., 2007; Mark et al., 2011; Mohtasib et al., 2012; Perthen et al., 2008; Schmithorst et al., 2014) with gradient echo (GRE) echo-planar-imaging (EPI) readout where a short echo time (TE) provides predominately flow-weighted contrast, whereas a longer TE centered on tissue water $T2^*$ provides BOLD contrast. However, there is no additional information about CBV changes in those studies as the measurement of CBV is directly inferred from

the CBF measurement using Grubb's equation with a constant exponent (Grubb et al., 1974).

As shown in Chapter 3, we proposed a 3D whole-brain MRI "VASO-FAIR" approach, the work of which has been recently published (Cheng et al., 2014). It exploits the same principle as (Yang et al.), and can measure CBV and CBF responses in one single scan. It combines the vascular-space-occupancy (VASO) (Lu et al., 2003) and flow-sensitive alternating inversion recovery (FAIR) arterial spin labeling (ASL) techniques (Kim, 1995; Kwong et al., 1995) with a common inversion pulse. A single-shot 3D fast gradient echo (GRE, also known as turbo field echo, TFE or TurboFLASH) sequence was used for image acquisition at two TIs, which consists of low flip angle pulse trains and has much less geometric distortion as well as fewer signal dropouts than the traditional GRE echo-planar-imaging (EPI) sequence. For VASO fMRI, this readout minimizes the BOLD contamination by allowing a very short TE (< 2ms) to be used. For CBF measurement, it eliminates the artifactual inter-slice perfusion signals variation due to the different post-labeling delay time that are slice-dependent in 2D acquisition sequences. When compared with the original separately performed VASO and FAIR-ASL scans, the proposed approach has been demonstrated to achieve similar image quality, activation patterns and relative signal changes (ΔS/S) during functional stimulation, as well as comparable tSNR and CNR values per scan, thus providing a more efficient and equally sensitive alternative when both CBV and CBF responses need to be monitored during a functional task (Cheng et al., 2014).

A three-dimensional T2-weighted spin-echo (SE) BOLD fMRI pulse sequence (dubbed as "3D T2prep-GRE") was previously proposed by (Hua et al., 2013b) at 7T,

where the SE BOLD contrast was induced using a T2 preparation scheme. Compared with the conventional 2D multi-slice SE EPI BOLD method, the 3D T2prep-GRE BOLD sequence permits parallel imaging in two phase encoding direction, has lower specific absorption rate (SAR) which allows larger spatial coverage with greater acquisition efficiency, and is less sensitive to susceptibility artifacts across the whole brain. Such concept of using T2 preparation to generate BOLD contrast can be combined with many other sequences and is transferable to other filed strengths.

Here, we propose an acquisition strategy, dubbed three-dimensional Triple-acquisition after Inversion Preparation or 3D-TRIP, that can incorporate these two 3D whole-brain methods for measuring CBV, CBF, and BOLD signal changes in a single scan. The T2 preparation module was placed immediately before a third acquisition module to induce the SE BOLD contrast. We will validate the proposed method using visual functional experiments in normal human brains on a 3 Tesla MRI scanner by comparing functional results from the combined sequence and the respective individual scans.

4.2. Materials and Methods

Pulse Sequence and Simulations

Figure 4.1 illustrates the combined 3D-TRIP pulse sequence. It adopts the same framework as the VASO-FAIR sequence (Cheng et al., 2014), which consists of interleaving slab-selective (SS) and non-selective (NS) inversion prepared scans where CBV-weighted VASO images are obtained at the blood-nulling time TI_1 after NS inversion, and FAIR images are collected at a later time TI_2 in both SS and NS scans.

CBF-weighted signals are then computed from pairs of FAIR images. As in the VASO-FAIR sequence, we applied the same magnetization transfer (MT) module before the inversion pulses to boost the tissue signal-to-noise ratios (SNRs) and contrast-to-noise ratios (CNRs) (Cheng et al., 2014; Hua et al., 2009a; Hua et al., 2013a). Here, a T2-preparation pre-pulse train immediately followed by a third imaging module was added after the FAIR acquisitions at TI3 in both SS and NS scans, in which T2-weighted SE BOLD images are acquired. Two refocusing pulses were used in T2-preparation to compensate phase variations and to suppress inflow effects (Hua et al., 2013b). A spoiler gradient was applied at the end of the T2-preparation pre-pulses to dephase residual transverse magnetization (Hua et al., 2013b). Same as the VASO-FAIR and T2prep BOLD sequences, a single-shot 3D fast gradient echo (GRE, also known as turbo field echo, TFE or TurboFLASH) readout with centric (low-high) phase encoding profile was employed in all three imaging modules. As the MR signal acquired at the center of k-space ($kz = ky = 0$ for 3D) determines the gross signal intensity in the image, the centric (low-high) phase encoding scheme ensures that k-space center will be acquired at the first echo, which is set at the blood nulling TI for VASO, and has the ideal T2-weighted contrast following T2-preparation for SE BOLD.
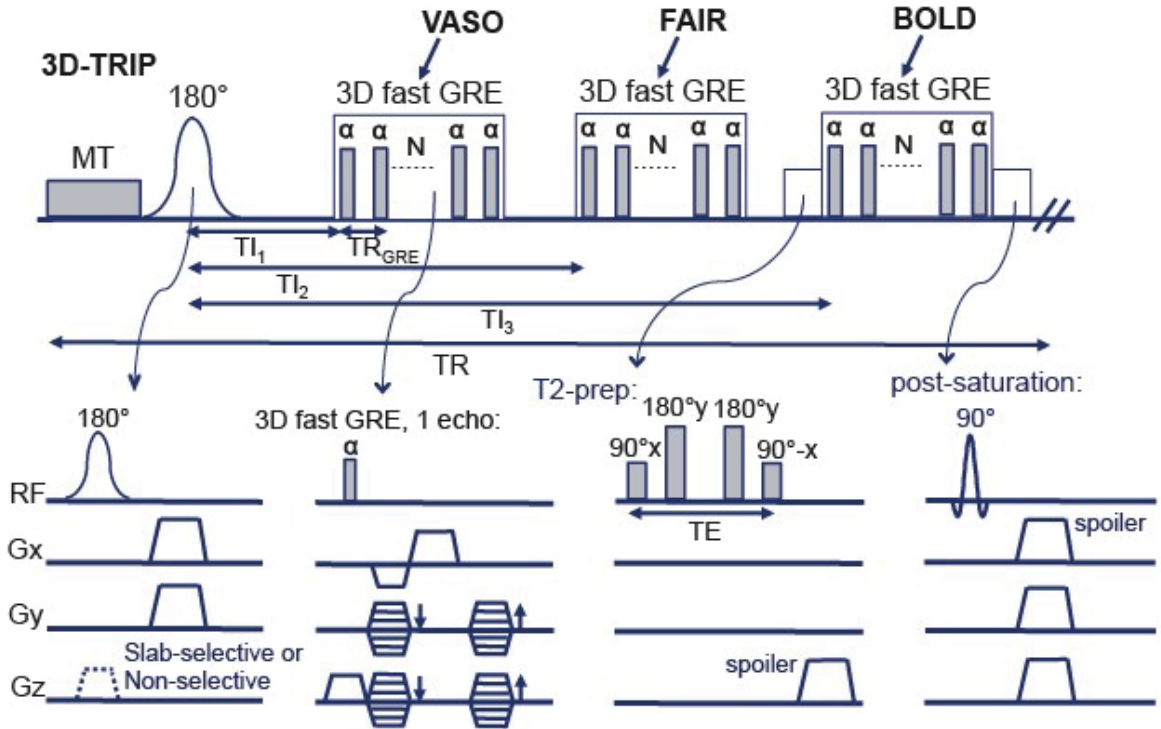
Fig. 4.1. Pulse sequence of the combined 3D-TRIP approach. A pair of interleaving slice-selective (SS) and nonselective (NS) scans are shown. A magnetization transfer (MT) prepulse is added before the adiabatic FOCI inversion pulses. The imaging module used here is a 3D fast GRE readout for VASO, FAIR ASL, and BOLD images, in which VASO signal is acquired at blood nulling time TI_1, ASL signal at time TI_2, and BOLD signal at time TI_3. A T2 preparation module ($90°x$–$180°y$–$180°y$–$90°$-x) is applied immediately before the BOLD readout to induce the T2 weighting in the BOLD signal. A post-saturation module comprising of a non-selective $90°$ saturation pulse and spoiler gradients is applied immediately after the FAIR ASL readout.

A spatially nonselective saturation (90° RF pulse followed by spoiler gradients) module was deployed immediately after the third readout to set all residual magnetization (blood and tissue) to zero. Similar to what has been shown in the VASO-FAIR sequence (Cheng et al., 2014), the purpose for this post-saturation module is to both suppress the inflow effect and to ensure that blood spins in and outside the inversion slab applied in the SS scan will have the same steady-state blood nulling condition in the following NS scan. Bloch simulation was performed using the same imaging parameters described in Experiments to estimate blood-nulling TIs in VASO images both in separate and combined scans. The same simulations were used to evaluate steady state GM and CSF signals. A 20% signal drop after the MT saturation pulse was assumed for GM (typical values under similar saturation schemes (Hua et al., 2009a)), and we assume there is no MT effect for CSF. Steady-state magnetization values for GM, CSF and blood are summarized in Table 4.1. In FAIR ASL, the magnetization values were simulated from raw data before the surround subtraction. The table only shows the out-of-slab blood magnetization at SS and NS scans for FAIR-ASL and BOLD, as both in- and out-of-slab blood signals are expected to be nulled at VASO scans, and in-slab blood signals are identical for SS and NS scans in the combined sequence and will have the same magnetization as the out-of-slab blood in NS scans. For BOLD acquisition at TI_3, since the intravascular signals (sum of in-slab and out-of-slab blood signal) will be different in SS and NS scans as expected from simulations, we will only use BOLD images obtained from the SS scans instead of using both scans consecutively for the combined sequence.

Table 4.1. Summary of steady-state signals for different tissue types from Bloch simulation (percentage of the equilibrium magnetization).

	VASO GM	VASO CSF	FAIR Blood, SS/ NS	FAIR GM	FAIR CSF	BOLD Blood, SS/NS	BOLD GM	BOLD CSF
Separate scans	24.0	-17.9	92.04/34.55	51.2	2.4	30.8	45.9	71.4
Combined scans	19.7	-6.6	54.47/37.7	53.4	16.0	17.3/15.9	28.4	23.9

Typical T_1 and T_2 values for blood, gray matter (GM) and cerebrospinal fluid (CSF) in healthy human brain at 3T were used: $T_{1,blood}$ = 1624ms (Lu et al., 2004a), $T_{1,GM}$ = 1122ms (Lu et al., 2005b), $T_{1,\,CSF}$ = 3817ms (Lu et al., 2005b), $T_{2,GM}$ = 80ms (Lu et al., 2005b), $T_{2,blood}$ = 55ms (Zhao et al., 2007), $T_{2,CSF}$ = 1442ms (Donahue et al., 2006a).

Experiments

The protocol was approved by the Johns Hopkins Medicine Institutional Review Board. Subjects gave written informed consent before participating. Experiments were performed on a 3T human MRI scanner (Philips Healthcare, Best, The Netherlands), using a body coil for RF transmission and a 32-channel head coil for reception. Six healthy volunteers were scanned for this study. Four fMRI experiments with visual stimulation (yellow/blue flashing checkerboard, 32s visual stimulation interleaved with 56s cross-hair fixation, repeated 4 times) were performed on each participant: (a) 3D-TRIP (TR/TI_1/TI_2/TI_3=4.0/0.6/1.5/2.4s, effective TE for BOLD = 60ms). A 400ms 2.5µT block-shaped MT prepulse with a frequency offset at -40 ppm (Hua et al., 2013a) was applied immediately before the inversion pulses in both NS and SS scans. (b) VASO (TR/TI = 4.0/0.88s). The same MT prepulse and post-saturation module as in 3D-TRIP were applied. (c) FAIR (TR/TI = 4.0/1.5s). d) 3D T2prep BOLD (TR = 4.0s, effective TE = 60ms). In both the combined and separate T2prep BOLD sequence, same T2 preparation module (nonselective 90°x–180°y–180°y–90°-x, hard pulses, duration or effective TE = 60ms) was applied immediately before the BOLD readout to induce T2-weighted BOLD contrast. A spoiler gradient was applied at the end of the T2prep module on the slab-selective gradient axis. The order of the experiments was randomized across participants. Optimal blood-nulling times were calculated for both 3D-TRIP (TI_1) and the separate VASO scan (TI) based on the Bloch simulations (described above) in order to account for the influence from the 3D fast GRE readout and the post-saturation module. Note that due to the different numbers of readout modules thus different recovery times after the post-saturation module (before next inversion) in the two sequences (thus

different steady states), TI_1 in the combined 3D-TRIP sequence is different from TI in VASO, which leads to different inflow times (TI) for VASO. This should not have a major influence on the VASO signals since the inflow effect should be largely suppressed by the post-saturation module when a body coil is used for RF transmit with a relatively long TR (Cheng et al., 2014; Hua et al., 2013a). Frequency offset corrected inversion (FOCI) pulses (Ordidge et al., 1996) were used for inversion in all scans, which are expected to produce sharper edges for spatially selective inversion than hyperbolic secant (HS) pulses (Hua et al., 2011a; Hua et al., 2011b). Common imaging parameters: voxel size = 5mm isotropic, 16 slices, field of view (FOV) = 192x192 mm^2, TR$_{GRE}$ (TR between two consecutive echoes in 3D GRE)/TE = 3.6/1.6ms, flip angle = 7°, turbo direction = radial, parallel imaging (SENSE) acceleration factor = 3x2 (APxFH), no partial Fourier sampling, readout duration for one image volume = 391 ms. Based on the thickness of the imaging volume (80mm), the thickness of the SS inversion slab was chosen to be 100 mm. A whole-brain 3D magnetization prepared rapid acquisition gradient echo (MPRAGE) scan (voxel size = 0.65mm isotropic, 231 slices) was also performed for anatomical reference.

Data Processing

The Statistical Parametric Mapping (SPM 12, University College London, UK) software package and several in-house Matlab R2012a (Mathworks, Natick, MA, USA) routines were used for data analysis. All fMRI images were corrected for motion and baseline drift. Gray matter, white matter, and CSF masks for each subject were generated using the MPRAGE images and SPM 12, and then coregistered with the fMRI images. CBF-

weighted images were obtained using a surround subtraction method, in which the SS/NS FAIR ASL images are subtracted with linear interpolation between the surrounding NS/SS images, respectively (Lu et al., 2006). A general linear model (GLM) was used to detect activated voxels (P < 0.01, t-score ≤ -1.5 for VASO, t-score ≥ 1.5 for FAIR and BOLD). A SNR threshold of 20 for VASO (Donahue et al., 2006b) and BOLD images was used. Due to the low SNR in the subtracted FAIR ASL images, a SNR threshold of 1 was used. The relative signal change ($\Delta S/S$) in each voxel was quantified as the difference between average signals during the baseline and activation periods normalized by the average baseline signal. In order to avoid the transitional periods when calculating average signals, images acquired during the first 24s and 8s during the baseline and activation periods, respectively, were excluded. Statistical t-score was calculated as the voxel-wise average value from the voxels in the visual cortex that are both activated in the separate and combined scans. Temporal SNR (tSNR) was calculated as the voxel-wise average baseline signal divided by the standard deviation along the time course during the baseline period. When comparing the tSNR values between separate and combined approach, since the temporal resolution for VASO and BOLD scans are halved in the combined sequence (we only use VASO images acquired in NS scans at TI_1 and BOLD images acquired in SS scans at TI_3), the VASO and BOLD images obtained from the individually performed scans were under-sampled by a factor of 2. Contrast-to-noise ratio (CNR) per unit time was taken as the product of absolute value of relative signal change ($\Delta S/S$), tSNR, and square root of number of image volumes acquired during the entire scan. In FAIR ASL, tSNR and CNR were calculated from CBF-weighted perfusion images after the surround subtraction.

4.3. Results

The fMRI results of VASO, FAIR and BOLD scan from the combined 3D-TRIP sequence are shown in Figure 4.2 and compared further with the respective separate scans as listed in Table 4.2. Representative activation maps from these three modalities are all overlaid onto the same anatomical images. The voxels meeting activation criteria (highlighted with their t-scores) are mostly localized in the visual cortex (representative images for VASO in Figures 4.2a, for FAIR in Figures 4.2b, and for BOLD in Figures 4.2c; 16 slices acquired, 4 slices shown). BOLD-weighted signals showed larger areas of significant functional activation than CBF- and CBV-weighted signals. A few spurious activations outside the visual regions were observed in some of the subjects, but these were excluded from further analysis as the focus of this study is to compare the separate and combined scans in the visual cortex. In the subsequent quantitative comparisons, only voxels that are activated in both separate and combined scans were used.

The time courses averaged over all slices and all subjects matched well between the separate and combined scans for VASO (Figure 4.2d), FAIR (Figure 4.2e), and BOLD images (Figure 4.3f). Note that VASO relative signal change is negative during neuronal activation due to the concomitant vasodilation that results in tissue signal reduction. The well known BOLD undershoot after stimulus cessation is evident in both the combined and separate scans. When compared with separate VASO, FAIR, and BOLD scan, the relative signal changes ($\Delta S/S$) and t-scores were both statistically comparable (P>0.1). For VASO images, tSNR was significantly higher (P<0.05) in the combined scans. However, CNR per unit time was comparable (P>0.1), as only half of VASO scans were acquired in the combined scan. For BOLD images, tSNR in combined

BOLD scan was slightly higher ($P<0.05$). CNR per unit time was not significantly different ($P>0.1$). For perfusion images, tSNR and CNR were comparable ($P>0.1$) between separate and combined scans.
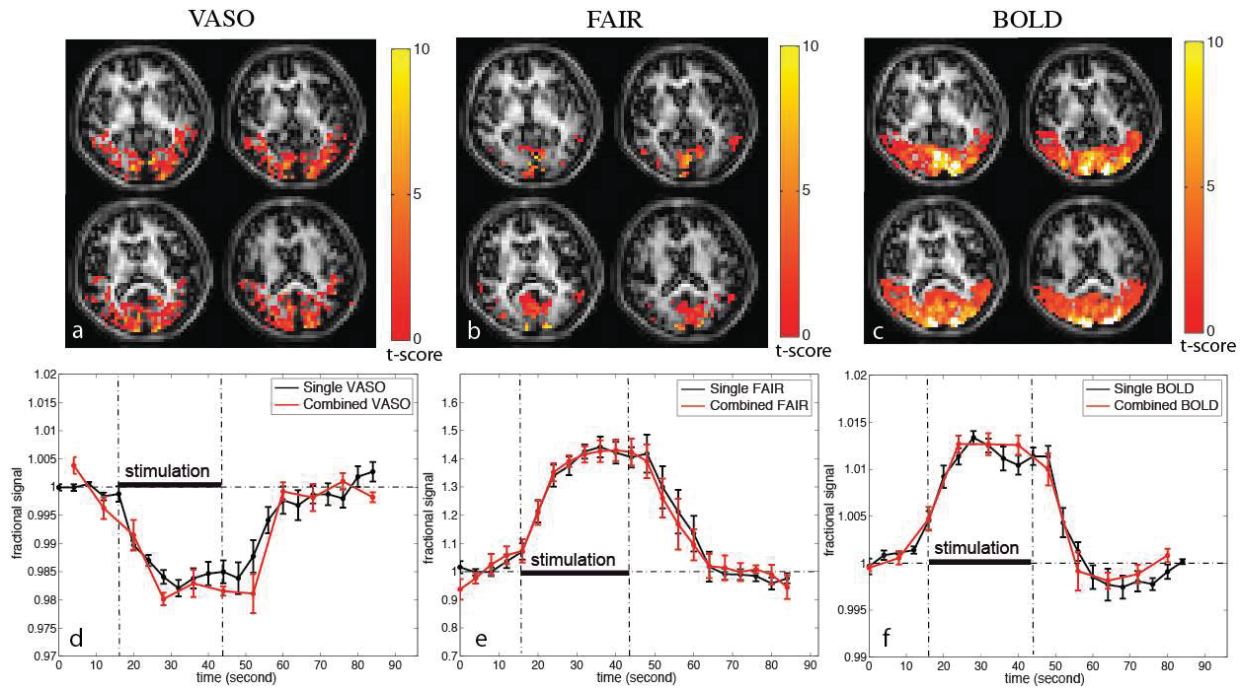
Fig. 4.2. Comparison of functional MRI results between the combined and separate scans. Representative activation maps overlaid on common anatomical images from the combined sequence (a) VASO scan, (b) FAIR ASL scan, and (c) BOLD scan are shown. The activated voxels are highlighted with their t-scores. Time courses averaged over common voxels activated in both separate (black circle) and combined (red triangle) scans (averaged over subjects, n = 6) for VASO, FAIR, and BOLD are shown in (d), (e), and (f), respectively. Error bars represent inter-subject variations. The vertical dotted lines indicate the start and end of visual stimulation. Four blocks of baseline and stimulation periods were averaged to one block.

Table 4.2. Summary of quantitative fMRI results from all subjects (n = 6).

	VASO in combined scan	Separate VASO	FAIR in combined scan	Separate FAIR	BOLD in combined scan	Separate BOLD
ΔS/S(%)	-1.84±0.22	-1.61±0.39	41.8±5.2	41.4±6.1	1.26±0.23	1.18±0.19
t-score	3.1±0.4	3.7±0.8	2.2±1.3	2.3±1.7	5.2±1.3	5.5±1.4
tSNR	58.0±6.6	47.5±5.3	1.34±0.13	1.83±0.49	97.5±5.3	86.5±8.6
CNR per unit time	7.68±1.40	7.57±1.23	5.95±1.35	7.30±1.77	8.8±1.9	10.3±2.2

Mean values ± standard deviation over all subjects. ΔS/S, t-score, tSNR and CNR were calculated as defined in Methods. Only common voxels activated in both separate and combined VASO or FAIR or BOLD scans were included. All FAIR ASL results were calculated from the subtracted images (difference maps or perfusion weighted images), and the ΔS/S are corrected for partial volume effects. When comparing the tSNR values, the VASO and BOLD images obtained from the separate scans were under-sampled by a factor of 2.

Relative CBV and CBF changes upon visual stimulation were quantified based on the measured VASO and FAIR $\Delta S/S$, respectively. Using the theory and parameters from (Donahue et al., 2006a; Hua et al., 2011c; Lu et al., 2003), the relative CBV change was calculated as 30.0%±7.3% (separate scan, mean ± standard deviation) and 34.4%±4.2% (combined scan), whereas the relative CBF change was 41.4%±6.1% (separate scan) and 41.8% ± 5.2% (combined scan). We corrected the partial-volume effects from WM and CSF in the relative CBF changes using the generated GM, WM, and CSF probability maps after segmentation. We found a voxel composition of approximately 75% GM, 20% WM, and 5% CSF for voxels in the visual cortex area. Therefore by assuming 1/3 of the baseline GM CBF value in the WM, the relative CBF change after correction was 50.7%±7.5% (separate scan) and 51.2% ± 6.4% (combined scan). OEF and CMRO2 changes were calculated from BOLD, CBV, and CBF data using the theory described previously (Lu et al. 2004b). Note that as T2-prep BOLD fMRI measures T2-weighted SE BOLD signals, the GRE BOLD signal changes in the quantitative BOLD model were approximated by three times of the measured SE BOLD signal changes. (Boxerman et al., 1995; Donahue 2006a; Yablonskiy and Haccke, 1994). If assuming a baseline CBV of 0.054 ml/ml tissue, resting arterial and venous oxygenation $Y_{a,rest} = 0.98$ and $Y_{v,rest} = 0.61$, respectively, which corresponds to a baseline oxygen extraction fraction (OEF) of 0.38, the estimated OEF value during activation is 0.27±0.01, indicating a 28.5% decrease upon activation, and the relative increase in cerebral metabolic rate of oxygen ($CMRO_2$) is 12.6±6.7%.

4.4. Discussion

We developed a 3D whole-brain imaging technique to simultaneously measure signal changes related to cerebral blood volume, blood flow, and blood oxygenation upon functional stimulation in a single MRI scan. This combined sequence is expected to provide a more efficient and equally sensitive approach for the quantitative BOLD studies where information about oxygen metabolism alterations can be extracted from these complementary hemodynamic signals associated with CBV, CBF, and blood oxygenation. Compared to sequentially obtaining CBV, CBF, and BOLD measurements using individual scans, this technique will not only improve the acquisition efficiency, but also reduce potential confounding effects resulting from head motion, task performance variation and physiologic fluctuations between MRI scans. Compared with the original separate VASO, FAIR, and BOLD scans, the proposed approach demonstrated similar activation patterns, t-scores, and relative signal changes ($\Delta S/S$) during functional stimulation. The fact that $\Delta S/S$ in the separate and combined scans are consistent indicates that they are measuring the same contrast (CBV-, CBF- and oxygenation-weighted signal changes for VASO, FAIR, and BOLD, respectively). Bloch simulation demonstrated that the GM signals in the VASO and BOLD scans in the combined method are both lower than those in the corresponding separate scans (Table 4.1), however tSNRs were significantly higher in the combined scans from the experimental data (Table 4.2), this could be explained by the fact that physiological noise is dominant in fMRI, thus a slight loss in MR signal may not lead to a decrease in tSNR (Cheng et al., 2014; Gonzalez-Castillo et al., 2011; Kruger and Glover, 2001; Kruger et al., 2001; Triantafyllou et al., 2005). Also, as can be seen from the Bloch simulation (Table 4.1), both VASO and BOLD in the combined method have less CSF

93

contamination due to the smaller CSF signal amplitude, which may further lower the noise levels. Indeed, we found that the noise levels (calculated as the standard deviation along the time course during the baseline period) in VASO and BOLD images were lower in the combined scans from all six subjects. The steady state FAIR-ASL GM signals are similar between the combined and separate scans from Bloch simulation (Table 4.1), and tSNR and CNR of the perfusion images are comparable from our data (Table 4.2).

Simultaneous BOLD and CBF measurement are mostly applied in the calibrated BOLD studies using either dual-echo or dual excitation ASL with multi-slice gradient-echo (GRE) echo-planar-imaging (EPI) readout where a short echo time (TE) provides predominately flow-weighted contrast, whereas a longer TE centered on tissue water T2* provides BOLD contrast (Ances et al., 2011; Bulte et al., 2009; Chen and Parrish, 2009; Chiarelli et al., 2007; Gauthier et al., 2011; Hoge et al., 1999; Leontiev et al., 2007; Mark et al., 2011; Mohtasib et al., 2012; Perthen et al., 2008; Schmithorst et al., 2014). This is also the case for the MRI technique previously introduced by (Yang et al., 2004)and later modified by (Krieger et al., 2013) to simultaneous acquire BOLD, CBV-, and CBF-weighted MRI signals. However, there may still be resultant BOLD effects in the CBV- and CBF- weighted images. Multiple EPI readouts will be needed to extrapolate both VASO and ASL images to TE = 0 ms and correct for BOLD signal contaminations (Krieger et al., 2013; Schulte et al., 2001; Yang et al., 2004). In our combined VASO-FAIR-BOLD approach, we adopted a 3D fast GRE imaging sequence, which minimizes the BOLD contamination to both VASO and ASL perfusion signals by allowing a very short TE (< 2ms) to be used (Cheng et al., 2014; Hua et al., 2013a), and has less

geometric distortion and fewer signal loss than the GRE-EPI sequence. Furthermore, T2-weighted BOLD contrast in the combined sequence is generated by the T2 preparation module immediately before the readout sequence, which eliminates the "dead time" and substantially improves acquisition efficiency (Hua et al., 2013b). In this proof-of-concept study, we used an effective TE = 60 ms in the T2 preparation module for BOLD images in both the separate and combined scans. However an effective TE of 80 ms that are closer to the tissue T2 value at 3T is expected to generate the optimal BOLD contrast at such field strength (Lu et al., 2005b; Ugurbil et al., 1993). Moreover, the equivalent TE to induce the same $\Delta S/S$ in a double echo CPMG sequence is expected to be longer than that in a sequence with only one refocusing pulse (Ogawa et al., 1993). This means that an echo time even longer than 80 ms may be necessary for optimizing $\Delta S/S$ in the acquired BOLD images using the T2-preparation.

The statistical activation maps of the fMRI results from the combined 3D sequence show different spatial patterns, where BOLD-weighted signals exhibited larger areas of significant functional activation than CBF- and CBV-weighted signals. VASO and ASL signal changes have a strong arteriolar and capillary signal weighting because the highest fractional changes in CBV and CBF occur in these compartments. In contrast, BOLD signal changes also occur in downstream venules and veins other than the actual site of neuronal activity. The spin-echo induced T2-weighted BOLD contrast, when compared with standard T2*-weighted GRE technique, is expected to show better functional localization to the capillary bed, due to the fact that the susceptibility-induced static dephasing effects of the extravascular spins around larger vessels are refocused by the 180° pulses in SE BOLD, but around capillaries where water diffusion is a random

process and is not negligible, the 180° pulses do not fully refocus the signal thus creating the extravascular SE BOLD contrast that is weighted toward the microvasculature (Boxerman et al., 1995; Kennan et al., 1994). However at field strengths such as 3T, blood signal from large veins is still significant, and the SE BOLD effect may still be dominated by intravascular contribution (Norris, 2012; Uludag et al., 2009) which may explain the large activation region observed from our BOLD experiments. Partial volume effects due to the relatively low spatial resolution (5mm isotropic) used in this study may also partially contribute. In fact, the superior spatial specificity of SE BOLD has turned out to be effective only at high field ($\geq$7T) (Duong et al., 2003; Fujita, 2001; Harel et al., 2006; Lee et al., 1999; Stables et al., 1998; Uludag et al., 2009; Yacoub et al., 2003; Yacoub et al., 2007; Zhao et al., 2006), where relative contribution from the extravascular compartment will be come dominant (Cheng et al., 2015; Donahue et al., 2011; Duong et al., 2003; van der Zwaag et al., 2009) and large draining veins will have minimal BOLD effect due the dramatic shortening of blood T2, but signals in the arteriolar and capillary compartment still persist, thus providing specificity advantages over conventional GRE-EPI. Thus, our proposed combined sequence might be even more helpful at ultra high field, where the T2prep module induces SE BOLD contrast with improved specificity, while simultaneously monitoring CBV and CBF reactivity with higher SNR and lower SAR which allows larger spatial coverage with fewer signal dropouts across the whole brain.

In this proof-of-concept study, we chose a spatial resolution of 5mm isotropic to boost the sensitivity (SNR) of the measurements, and to demonstrate the principles of the 3D-TRIP method with a reasonable temporal resolution for the functional experiments.

Similar to what has been shown previously in the "VASO-FAIR" method (Cheng et al., 2014), this may lead to significant partial-volume effects from WM and CSF in the GM signals. Partial volume effect from WM may bring down the overall FAIR ASL perfusion and VASO signal changes measured in our data. On the other hand, the residual inflow and partial volume effect from CSF usually result in more negative VASO signal changes (Donahue et al., 2006a; Scouten and Constable, 2007, 2008), thus making the VASO signal changes and estimated CBV changes comparable to literature values (Cheng et al., 2014). From the Bloch simulations (see Table 4.1), the steady state CSF signals in the combined scan are less negative in VASO, more positive in FAIR ASL, and less positive in BOLD than the respective separate scans. For FAIR ASL, the partial volume effect from CSF should not affect the difference signal (perfusion) as CSF signals in label and control scans should be comparable. For BOLD signal, this may at least partially explain the smaller (albeit not statistically significant) ΔS/S in the separate BOLD scan (Table 4.2). For CSF influences on the VASO signal change, simulations indicate that the CSF contamination in the VASO signal change is slightly smaller in the combined scan due to the less negative CSF signal if assuming no fractional change in the CSF volume: assuming a 30% increase of CBV upon activation, the relative VASO signal change from the simulations is -1.70% in a pure GM voxel for both separate and combined VASO scans, and is -1.74% (VASO in combined scan) and -1.79% (separate VASO scan) in a voxel with 5% CSF and 95% GM in volume. However, as it is not entirely clear whether and how much the local CSF volume alters occur in the cortex during neuronal activation, and different values have been reported from several studies: no significant change, 5-6% decrease, increase of 2%, and decrease of 2.45% (Hua et al., 2011a), We therefore

simulated the other three cases (+2%, -2% and -6%) to get an impression of the partial volume effect from CSF. If CSF volume increases 2%, the VASO relative signal change from simulation is -2.00% (separate) and -1.89% (combined); if CSF volume decreases 2%, the $\Delta S/S$ is -1.58% (separate VASO scan) and -1.59%(VASO in combined scan); if CSF volume decreases 6%, the $\Delta S/S$ is -1.16% (separate VASO scan) and -1.29% (VASO in combined scan). Although this partial volume effect should not undermine the comparison between the separate and combined approaches here, for future quantitative physiological studies, finer spatial resolution, which can be achieved by adapting the readout pulse sequence and utilizing fast imaging techniques such as parallel imaging and partial Fourier sampling, may be used to alleviate this problem.

While most of the quantitative BOLD approaches normally perform separate scans to estimate $CMRO_2$ dynamics from BOLD, CBF and CBV responses, the proposed 3D combined approach can detect changes in these hemodynamic signals in a single scan, which would not only shorten the total scan time but more importantly reduce the sensitivity to temporal variations among the fMRI experiments. Based on the measured BOLD, CBV, and CBF relative changes from the combined sequence, we quantified the oxygen extraction fraction (OEF) value during activation to be 0.27 ± 0.01 (N = 6, mean $\pm$ STD), indicating a 28.5% decrease upon visual stimulation, and changes in cerebral metabolic rate of oxygen ($CMRO_2$) to be $12.6\pm6.7\%$, after correcting for the partial-volume effects in the CBF response. Since the BOLD signal acquired from the 3D combined sequence has T2 weighting, and as the primary goal of the current study is to show the feasibility of the proposed combined sequence, we simply assume that the gradient-echo (GRE) based extravascular BOLD effect is approximately three times of

the spin-echo (SE) BOLD effect (extravascular $\Delta R2^* \approx 3 \; \Delta R2$) as shown in previous literature (Boxerman et al., 1995; Donahue et al., 2006a). This is obviously a simplification of the phenomenon that the T2-weighted BOLD contrast is created by the water diffusion, and the static dephasing regime of the extravascular water spins will be refocused in a SE-BOLD experiment. For future studies, careful modeling of extravascular SE BOLD effect is needed for a more accurate quantification of oxygen metabolism using the proposed combined sequence.

Power deposition does not seem to be a major limiting factor in the combined pulse sequence used here, mainly due to the low FA in the 3D GRE readout and the relatively long TR and readout duration. The specific absorption rate (SAR) is about 0.78W/kg (<26% of the FDA limit for head exposure) for the proposed 3D VASO-FAIR-BOLD sequence with the parameters used in this study. If the MT pre-pulse is turned off only (with other parameters identical), SAR will decrease to about 0.48 W/kg (<16% of the FDA limit). If the T2 preparation module is turned off only (with other parameters identical), SAR will decrease to about 0.5 W/kg (<17% of the FDA limit). Note that the 400 ms 2.5 µT block-shaped MT prepulse can be replaced by a pulse train to lower the SAR level. The block-shaped refocusing pulses in the T2 preparation module can be replaced by adiabatic pulses to further lower the SAR level. With the same imaging parameters used here, the 3D-TRIP sequence can acquire up to 30 slices with a SAR level less than 0.93 W/kg (<31% of the FDA limit) at 3T. In this case, the actual bottleneck is the long readout pulse train for one image volume and TR, instead of power deposition.

One drawback of the proposed 3D-TRIP sequence is that the temporal resolution for the VASO and BOLD scans are halved compared to the separate VASO and BOLD

approach, as VASO images can only be acquired at TI_1 in each non-selective (NS) inversion prepared scan but not in the slab-selective (SS) scan where no global inversion is applied and out-of-slab blood is not properly nulled, and we only use BOLD images obtained at TI_3 in the SS scans from the combined sequence, as simulation (see Table 4.1) shows that the intravascular signals (sum of in-slab and out-of-slab blood signal) at TI_3 will be different in SS and NS scans, which could complicate the interpretation of the functional results of the combined scan. One possible way to alleviate this is to adopt a motion-sensitized-driven-equilibrium (MSDE) module instead of the T2 preparation, with motion-sensitized crushing gradients inserted. For future studies, this could be beneficial for two reasons: 1. Destroy the flowing blood signals before acquiring the BOLD images, thus reduce the signal variations between the interleaving SS and NS scans, and may use both imaging volumes acquired; 2. Improve the spatial specificity of BOLD signal changes since the intravascular blood signal are destroyed thus leaving BOLD contribution mostly from the extravascular compartment, which could be especially useful for quantitative BOLD modeling.

4.5. Conclusions

A 3D perfusion imaging approach was demonstrated that combines the VASO, FAIR-ASL and SE-BOLD MRI techniques, allowing the measurement of CBV, CBF, and blood-oxygenation dynamics during functional stimulation in a single scan. Using a flashing checkerboard visual stimulation paradigm, activation patterns with signal changes (ΔS/S), tSNR and CNR per scan comparable to the original individual methods was detected. This approach is expected to provide a more efficient and equally sensitive

alternative for the quantitative BOLD fMRI studies where information about oxygen metabolism alterations can be extracted from these complementary hemodynamic signals associated with CBV, CBF, and blood oxygenation.

Chapter 5: Conclusions and Future Work

In this chapter, we summarize the major findings and conclusions in this dissertation. Future work for further improvement of the proposed techniques and potential applications is discussed.

5.1. R2* Measurement Using Multi-echo VASO MRI at 7 Tesla

In Chapter 2, we applied multi-echo VASO fMRI to remove the intravascular signal and by combining with multi-echo BOLD fMRI, we measured the absolute total and extravascular (tissue) R_2^* values as well as ΔR_2^* in the parenchyma in human visual cortex at 7T. The main conclusions are:

1. Since the intravascular signals is supposed to be nulled in the VASO method, and the CBV effect occurs predominantly in the microvasculature, by using a multi-echo VASO acquisition, we should be measuring the relaxation times of the parenchymal extravascular tissue compartment. OEF changes measured in this study were also expected to be predominantly localized in the parenchyma by taking overlapping voxels activated in both BOLD and VASO scans.

2. The parenchymal extravascular R_2^* value was 44.66 ± 1.55 s^{-1} at rest, and the ratio of extravascular ΔR_2^* to total ΔR_2^* was $91 \pm 3\%$ at 7T, confirming a predominant contribution from the extravascular component of the BOLD effect.

3. Multi-echo VASO images need to be extrapolated to TE = 0 ms or using a readout with very short TE for a purer CBV effect especially at 7T, since the extravascular BOLD effects (positive) become quite large at longer TE, which

counteract the negative VASO signals. This is also confirmed from our data, as the VASO $\Delta S/S$ is negative for very short TE, but reverses sign at longer TEs.

4. CBV increased by $35.8 \pm 3.2\%$ (n = 6, mean $\pm$ SEM) during visual stimulation, calculated from a $-1.94 \pm 0.17\%$ (n = 6, mean $\pm$ SEM) VASO signal change using the extrapolated VASO images at TE = 0 ms and assuming a baseline CBV value of 0.052ml blood/ml tissue.

5. Based on the static dephasing regime theory, Y_v^{act} and OEF during activation were quantified to be 0.75 ± 0.01 and 0.24 ± 0.01 (n = 6, mean $\pm$ SEM), respectively, indicating an approximately 37% OEF decrease during visual stimulation, consistent with values reported at lower field strengths.

When compared with total and extravascular parenchymal R_2^* values reported at various field strengths (1.5T, 3T and 7T) in the literature, The R_2^* values measured here are in good agreement with the Donahue study, but differ considerably from the ones reported in the van der Zwaag study. One plausible explanation may be that both the Donahue and current studies were conducted in the visual cortex with comparable spatial resolution, whereas the van der Zwaag study measured R_2^* values in the motor cortex with a much finer spatial resolution ($1x1x3$ mm^3). Our results also showed that the BOLD effect is dominated by the extravascular component (91%) at 7T, in line with previous literatures. The experimental results are consistent with the theoretical calculations that the intravascular BOLD signal will be significantly reduced relative to the extravascular signal at higher field due to the faster R_2^* decay of venous blood.

The contribution from physiological noises in fMRI signals has been shown to increase with field strength and voxel size. In order to check this for our study, we measured the coefficients of variation for the R_2* values, which were found to be comparable to those reported at 3T and 1.5T in a previous study adopting similar methodology. However, a larger voxel size was used in that study. From this we conclude that the noise contribution in the R_2* measurements at 7T would be larger than 3T and 1.5T if the same voxel size were used. We also noticed that the total R_2* values measured in subjects 4 and 6 were slightly lower than the corresponding extravascular R_2* values (total R_2* is expected to be higher than extravascular R_2* due to additional blood contributions), although the difference was within noise range. This also occurred for one subject reported in previous 3T data but not 1.5T. We attribute this partly to the many possible contributions to R_2*, making it difficult to measure this parameter with great accuracy, and partly to the possible insufficient nulling of intravascular blood signals. In this 7T study, even though we applied a hyperbolic secant adiabatic pulse for the spatially nonselective inversion in VASO, there could still be some imperfectness in terms of the inversion efficiency of the 180° pulse. More repeats and averaging may be necessary for robust R_2* measurement on a single-subject level, and careful optimization of the inversion pulses at 7T may also be beneficial.

A potential source of errors in this study when estimating Y_v^{act} and OEF using the static dephasing regime comes from the literature values assumed for the model parameters. We performed an error analysis by estimating OEF using parameter values over the normal physiological range for baseline CBV, microvascular Hct, and $\Delta\chi_{deoxy}$. Although this error analysis showed that the estimated OEF values in this study are only

moderately affected by these assumptions, further measurement of these physiological parameters in each participant would certainly improve the accuracy for OEF quantification.

5.2. Three-dimensional Single-scan Approaches for the Measurement of CBV, CBF, and BOLD Responses

In Chapter 3, we proposed a 3D whole-brain MRI pulse sequence (dubbed "3D VASO-FAIR") to simultaneously detect CBV and CBF responses upon functional stimulation in a single MRI scan. In Chapter 4, an acquisition strategy (dubbed "3D-TRIP") that incorporates the VASO-FAIR sequence and the 3D T2-prep GRE BOLD method was implemented, allowing for the measurement of CBV, CBF, and BOLD signal changes in a single scan. The main conclusions are:

1. A new fMRI approach, dubbed 3D VASO-FAIR, was proposed that can detect CBV and CBF responses in a single scan. VASO-FAIR uses an interleaving slab-selective (SS) and non-selective (NS) scans where the CBV-weighted VASO images are acquired at the blood nulling time TI in the NS scans, and CBF-weighted perfusion images are acquired at a longer TI_2 in both SS and NS scans.

2. A single-shot 3D fast gradient-echo (GRE) readout with centric (low-high) phase encoding profile was employed in all imaging modules. This readout has been showed previously with minimal geometrical distortion and signal dropouts, low power deposition due to small flip angles, and negligible T_2^* contamination in VASO fMRI because of the very short echo time (TE) used.

3. The MT module was applied before the inversion pulses in the VASO-FAIR

sequence to prepare a smaller magnetization values for tissue so as to boost the SNR and CNR of the VASO images.

4. The post-saturation module was employed immediately after the FAIR-ASL readout to build a steady-state after the first TR, and to ensure that blood spins in and outside the inversion slab applied in the SS scan will have the same steady-state blood nulling condition in the following NS scan.

5. The 3D VASO-FAIR sequence was implemented on a 3T human MRI scanner, and functional experiments with visual stimulation were performed to compare the combined sequence and original separate scans in order to validate accuracy of the combined scan.

6. The spatial patterns of activation are similar between the combined and separate VASO and FAIR scans. The time courses averaged over all slices and all subjects matched well between the separate and combined scans for both VASO and FAIR. The relative signal changes ($\Delta S/S$), tSNR and CNR per scan were all statistically comparable (P>0.1). CNR per unit time for VASO was higher in the separate scan (P<0.01) than in the 3D VASO-FAIR scan, as only half of VASO scans were acquired in the combined scan. CNR per unit time for FAIR was comparable (P>0.1) between separate and combined scans.

7. Relative CBV and CBF changes upon visual stimulation were quantified based on the measured VASO and FAIR $\Delta S/S$, respectively. The relative CBV change was calculated as 37.1%±3.9% (separate scan) and 34.8%±6.3% (combined scan), whereas the relative CBF change was 38.6%±6.1% (separate scan) and 42.7% ± 8.3% (combined scan), which were statistically comparable.

8. A new 3D acquisition strategy, dubbed "3D-TRIP", was implemented that extends the VASO-FAIR sequence and incorporate a 3D T2-prep GRE BOLD method to simultaneously measure BOLD, CBV, and CBF reactivity during functional stimulation. Similar to VASO-FAIR, it uses an interleaving SS and NS scans where the CBV-weighted VASO images are acquired at the blood nulling time TI in the SS scans, CBF-weighted perfusion images are acquired at a longer TI_2 in both SS and NS scans, oxygenation-weighted BOLD images are acquired at TI_3 in the SS scans.

9. Since the same single-shot 3D fast GRE imaging scheme was used in which the echo time (TE_{GRE}) during readout was very short, a T2 preparation module (nonselective $90°x–180°y–180°y–90°$-x, hard pulses, duration or effective TE = 60ms) was placed immediately before the third acquisition module to induce the T2-weighted BOLD contrast in the proposed combined sequence.

10. Similarly, MT module was applied before the inversion pulses to boost the SNR and CNR of the VASO images, and the post-saturation module was employed to suppress the inflow effect and to ensure that blood spins in and outside the inversion slab applied in the SS scan will have the same steady-state blood nulling condition in the following NS scan.

11. For BOLD acquisition at TI_3, since the intravascular signals (sum of in-slab and out-of-slab blood signal) will be different in SS and NS scans as expected from simulations, we will only use BOLD images obtained from the SS scans instead of using both scans consecutively for the combined sequence.

12. The time courses averaged over all slices and all subjects matched well between the separate and combined scans for VASO, FAIR, and BOLD images. When compared with separate VASO, FAIR, and BOLD scan, the relative signal changes ($\Delta S/S$) and t-scores were both statistically comparable ($P>0.1$). For VASO images, tSNR was significantly higher ($P<0.05$) in the combined scans. However, CNR per unit time was comparable ($P>0.1$), as only half of VASO scans were acquired in the combined scan. For BOLD images, tSNR in combined BOLD scan was slightly higher ($P<0.05$). CNR per unit time was not significantly different ($P>0.1$). For perfusion images, tSNR and CNR were comparable ($P>0.1$) between separate and combined scans.

13. The relative CBV changes were calculated as 30.0%±7.3% (separate scan, mean ± standard deviation) and 34.4%±4.2% (combined scan), whereas the relative CBF changes were 41.4%±6.1% (separate scan) and 41.8% ± 5.2% (combined scan). The BOLD relative changes were 1.18%±0.19% (separate scan) and 1.26%±0.23% (combined scan).

14. We corrected the partial-volume effects from WM and CSF in the relative CBF changes using the GM, WM, and CSF probability maps after segmentation. We found a voxel composition of approximately 75% GM, 20% WM, and 5% CSF for voxels in the visual cortex area. Therefore by assuming 1/3 of the baseline GM CBF value in the WM, the relative CBF change was 50.7%±7.5% (separate scan) and 51.2% ± 6.4% (combined scan) after correction.

15. Based on the BOLD, CBV, and CBF responses measured from the combined sequence, we also quantified the oxygen metabolism alterations using the

approximation that the gradient-echo (GRE) based extravascular BOLD effect is about three times of the spin-echo (SE) BOLD effect (extravascular $\Delta R2^* \approx 3$ $\Delta R2$) at 3T. The estimated oxygen extraction fraction (OEF) value during activation is 0.27 ± 0.01, indicating a 28.5% decrease upon activation based on the assumed baseline OEF of 0.38, and the relative increase in cerebral metabolic rate of oxygen ($CMRO_2$) is $12.6 \pm 6.7\%$.

We developed two 3D whole-brain single-scan imaging techniques to simultaneously detect CBV, CBF, and BOLD reactivity upon functional stimulation. Compared to sequentially obtaining these hemodynamic responses using individual scans, these techniques will not only improve the acquisition efficiency, but also reduce potential confounding effects resulting from head motion, task performance variation and physiologic fluctuations between MRI scans. We demonstrated that for both proposed sequences, similar image quality, activation patterns, relative signal changes ($\Delta S/S$), tSNRs and CNRs were achieved when compared to separately acquired scans. These single-scan approaches are expected to be useful especially for the quantitative BOLD methods in which concurrent BOLD, CBV, and CBF measurements are desired to further estimate oxygen metabolism alterations during functional stimulations.

One drawback for both proposed 3D single-scan sequences is that the temporal resolution for VASO is halved compared to the separate VASO approach, as VASO images can only be acquired at TI_1 in each non-selective (NS) inversion prepared scan but not in the slab-selective (SS) scan where no global inversion is applied and out-of-slab blood is not properly nulled. For the combined sequence proposed in Chapter 4, we

only used BOLD images obtained in the SS scans thereby halving the temporal resolution for BOLD. One possible way to alleviate this is to adopt a motion-sensitized-driven-equilibrium (MSDE) module instead of the T2 preparation, with motion-sensitized crushing gradients inserted to destroy the flowing intravascular blood signals before acquiring the BOLD images, thus reduce the variations between SS and NS scans while reserving the T2-weighted contrast.

We chose a spatial resolution of 5mm isotropic to boost the sensitivity (SNR) of the measurements, and to demonstrate the principles of the 3D combined methods with a reasonable temporal resolution for the functional experiments. This may lead to significant partial-volume effects from WM and CSF in the GM signals. Partial volume effect from WM may bring down the overall FAIR ASL perfusion, BOLD and VASO signal changes measured in our data. On the other hand, the residual inflow and partial volume effect from CSF usually result in more negative VASO signal changes, thus making the VASO signal changes and estimated CBV changes comparable to literature values. For FAIR ASL, the partial volume effect from CSF should not affect the difference signal (perfusion) as CSF signals in label and control scans should be comparable. For BOLD signal, this may reduce the $\Delta S/S$ in the BOLD scan. To evaluate the CSF influences on the VASO signal change can be difficult, as it is not entirely clear whether and how much the local CSF volume alters occur in the cortex during neuronal activation. Although this partial volume effect should not undermine the comparison between the separate and combined approaches here, for future quantitative physiological studies, finer spatial resolution, which can be achieved by adapting the readout pulse sequence and utilizing fast imaging techniques such as parallel imaging and partial

Fourier sampling, may be used to alleviate this problem.

Power deposition does not seem to be a major limiting factor in the combined pulse sequences used here, mainly due to the low FA in the 3D GRE readout and the relatively long TR and readout duration. Moreover, the block-shaped MT prepulse can be replaced by a pulse train to lower the SAR level, and the block-shaped refocusing pulses in the T2 preparation module can be replaced by adiabatic pulses to further lower the SAR. The actual bottleneck here is rather the long readout pulse train for one 3D image volume and TR in a single-shot acquisition scheme. For future studies, fast reconstruction methods such as compressed sensing could be used to reduce the readout pulse train lengths.

We chose to use the original forms of pulse sequences for FAIR ASL and VASO. Over the past decade, many improvements have been developed for these methods, including vascular crushing gradients, QUIPSS (QUIPSS II and Q2TIPS), background suppression, pseudo-continuous labeling for ASL, and the inflow-based VASO (iVASO) approach for VASO. We are currently working to incorporate some of these improvements into the proposed approach. For instance, crusher gradients or the motion-sensitized driven equilibrium (MSDE) preparation can be added to suppress macro-vascular signal contaminations in ASL. The combined sequences can also be adapted with the QUIPSS modifications to control the labeling bolus width. Although theoretically feasible, careful design of the timing and number of saturation and inversion pulses is needed to incorporate background suppression into the proposed method. FAIR ASL is a pulsed ASL (PASL) scheme. Therefore, pseudo-continuous labeling, which generally has higher SNR than PASL, cannot be used here. This may be one of the

disadvantages for the proposed methods. The inversion schemes in iVASO can also be used here, which should result in enhanced SNR, and a CBV contrast dominated by the arterial compartment.

When estimating the CMRO2 value from the 3D combined sequence, since the BOLD signal has T2 weighting instead of T2*, and as the primary goal of the current study is to show the feasibility of the proposed combined sequence, we simply assume that the gradient-echo (GRE) based extravascular BOLD effect is approximately three times of the spin-echo (GRE) BOLD effect (extravascular $\Delta R2^* \approx 3\Delta R2$) as shown in previous literature. This is obviously a simplification of the phenomenon that the T2-weighted BOLD contrast is created by the water diffusion, and the static dephasing regime of the extravascular water spins will be refocused in a SE-BOLD experiment. For future studies, careful modeling of extravascular SE BOLD effect is necessary for a more accurate quantification of oxygen metabolism using the proposed combined sequence.

While most of the quantitative BOLD approaches normally perform separate scans to estimate $CMRO_2$ dynamics from BOLD, CBF and CBV responses, the proposed 3D combined approaches can detect changes in these hemodynamic signals in a single scan, which would not only shorten the total scan time but more importantly reduce the sensitivity to temporal variations among the fMRI experiments. An important clinical application of such single-scan approaches is to probe cerebral pathophysiology in patients with brain tumors and carotid artery disease, where the ability to detect multiple physiological parameters within a reasonable imaging time is desirable. Another potential application is to detect intrinsic brain activities in the resting-state fMRI, since measuring spontaneous CBV and CBF fluctuations would not be possible if using individually

performed fMRI scans due to the potential changes in physiological and mental states between the scans, therefore such single-scan approaches with 3D whole-brain acquisitions will be strongly desired where BOLD-, CBV-, and CBF-based resting-state brain networks can be derived and correlated.

In summary, the work outlined in this dissertation demonstrates promising potential. We believe that the quantified parenchymal extravascular R_2^* values at 7T will provide complementary information to the existing BOLD fMRI literatures, and that the proposed 3D single-scan approaches can improve conventional individually performed fMRI methods to capture microvascular status changes in the brain in a time efficient manner and establishes a fast, non-invasive protocol that could open a new area of research for both tasked-based and resting-state functional brain physiology and clinical pathology studies.

Bibliography

Alsop, D.C., Detre, J.A., 1996. Reduced transit-time sensitivity in noninvasive magnetic resonance imaging of human cerebral blood flow. J Cereb Blood Flow Metab 16, 1236-1249.

Alsop, D.C., Detre, J.A., Golay, X., Gunther, M., Hendrikse, J., Hernandez-Garcia, L., Lu, H., Macintosh, B.J., Parkes, L.M., Smits, M., van Osch, M.J., Wang, D.J., Wong, E.C., Zaharchuk, G., 2014. Recommended implementation of arterial spin-labeled perfusion MRI for clinical applications: A consensus of the ISMRM perfusion study group and the European consortium for ASL in dementia. Magn Reson Med.

Ances, B., Vaida, F., Ellis, R., Buxton, R., 2011. Test-retest stability of calibrated BOLD-fMRI in HIV- and HIV+ subjects. Neuroimage 54, 2156-2162.

Balaban, R.S., Chesnick, S., Hedges, K., Samaha, F., Heineman, F.W., 1991. Magnetization transfer contrast in MR imaging of the heart. Radiology 180, 671-675.

Balu, N., Yarnykh, V.L., Chu, B., Wang, J., Hatsukami, T., Yuan, C., 2011. Carotid plaque assessment using fast 3D isotropic resolution black-blood MRI. Magn Reson Med 65, 627-637.

Bloch F, Hansen W, Packard M. 1946. Nuclear induction. Phys Rev 69:127-127.

Blockley, N.P., Francis, S.T., Gowland, P.A., 2009. Perturbation of the BOLD response by a contrast agent and interpretation through a modified balloon model. Neuroimage 48, 84-93.

Blockley, N.P., Griffeth, V.E., Simon, A.B., Buxton, R.B., 2013. A review of calibrated blood oxygenation level-dependent (BOLD) methods for the measurement of task-induced changes in brain oxygen metabolism. NMR Biomed 26, 987-1003.

Blockley, N.P., Jiang, L., Gardener, A.G., Ludman, C.N., Francis, S.T., Gowland, P.A., 2008. Field strength dependence of R1 and R2* relaxivities of human whole blood to ProHance, Vasovist, and deoxyhemoglobin. Magn Reson Med 60, 1313-1320.

Boxerman, J.L., Hamberg, L.M., Rosen, B.R., Weisskoff, R.M., 1995. MR contrast due to intravascular magnetic susceptibility perturbations. Magn Reson Med 34, 555-566.

Brookes, M.J., Morris, P.G., Gowland, P.A., Francis, S.T., 2007. Noninvasive measurement of arterial cerebral blood volume using Look-Locker EPI and arterial spin labeling. Magn Reson Med 58, 41-54.

Brooks, D.J., Beaney, R.P., Leenders, K.L., Marshall, J., Thomas, D.J., Jones, T., 1985. Regional cerebral oxygen utilization, blood flow, and blood volume in benign intracranial hypertension studied by positron emission tomography. Neurology 35, 1030-1034.

Bulte, D.P., Drescher, K., Jezzard, P., 2009. Comparison of hypercapnia-based calibration techniques for measurement of cerebral oxygen metabolism with MRI. Magn Reson Med 61, 391-398.

Buxton, R.B., Frank, L.R., Wong, E.C., Siewert, B., Warach, S., Edelman, R.R., 1998. A general kinetic model for quantitative perfusion imaging with arterial spin labeling. Magn Reson Med 40, 383-396.

Chen, J.J., Pike, G.B., 2009. BOLD-specific cerebral blood volume and blood flow changes during neuronal activation in humans. NMR Biomed 22, 1054-1062.

Chen, N.K., Oshio, K., Panych, L.P., Rybicki, F.J., Mulkern, R.V., 2004. Spatially selective T2 and T2 * measurement with line-scan echo-planar spectroscopic imaging. J Magn Reson 171, 90-96.

Chen, Y., Parrish, T.B., 2009. Caffeine's effects on cerebrovascular reactivity and coupling between cerebral blood flow and oxygen metabolism. Neuroimage 44, 647-652.

Cheng, Y., van Zijl, P.C., Hua, J., 2015. Measurement of parenchymal extravascular R2* and tissue oxygen extraction fraction using multi-echo vascular space occupancy MRI at 7 T. NMR Biomed 28, 264-271.

Cheng, Y., van Zijl, P.C., Pekar, J.J., Hua, J., 2014. Three-dimensional acquisition of cerebral blood volume and flow responses during functional stimulation in a single scan. Neuroimage.

Chiarelli, P.A., Bulte, D.P., Wise, R., Gallichan, D., Jezzard, P., 2007. A calibration method for quantitative BOLD fMRI based on hyperoxia. Neuroimage 37, 808-820.

Chien, D., Levin, D.L., Anderson, C.M., 1994. MR gradient echo imaging of intravascular blood oxygenation: T2* determination in the presence of flow. Magn Reson Med 32, 540-545.

Dai, W., Garcia, D., de Bazelaire, C., Alsop, D.C., 2008. Continuous flow-driven inversion for arterial spin labeling using pulsed radio frequency and gradient fields. Magn Reson Med 60, 1488-1497.

Dai, W., Robson, P.M., Shankaranarayanan, A., Alsop, D.C., 2012. Reduced resolution transit delay prescan for quantitative continuous arterial spin labeling perfusion imaging. Magn Reson Med 67, 1252-1265.

Davis, T.L., Kwong, K.K., Weisskoff, R.M., Rosen, B.R., 1998. Calibrated functional MRI: mapping the dynamics of oxidative metabolism. Proc Natl Acad Sci U S A 95, 1834-1839.

Deistung, A., Rauscher, A., Sedlacik, J., Stadler, J., Witoszynskyj, S., Reichenbach, J.R., 2008. Susceptibility weighted imaging at ultra high magnetic field strengths: theoretical considerations and experimental results. Magn Reson Med 60, 1155-1168.

Detre, J.A., Wang, J., Wang, Z., Rao, H., 2009. Arterial spin-labeled perfusion MRI in basic and clinical neuroscience. Curr Opin Neurol 22, 348-355.

Dixon, W.T., Sardashti, M., Castillo, M., Stomp, G.P., 1991. Multiple inversion recovery reduces static tissue signal in angiograms. Magn Reson Med 18, 257-268.

Dobre, M.C., Ugurbil, K., Marjanska, M., 2007. Determination of blood longitudinal relaxation time (T1) at high magnetic field strengths. Magn Reson Imaging 25, 733-735.

Donahue, M.J., Blicher, J.U., Ostergaard, L., Feinberg, D.A., MacIntosh, B.J., Miller, K.L., Gunther, M., Jezzard, P., 2009a. Cerebral blood flow, blood volume, and oxygen metabolism dynamics in human visual and motor cortex as measured by whole-brain multi-modal magnetic resonance imaging. J Cereb Blood Flow Metab 29, 1856-1866.

Donahue, M.J., Hoogduin, H., van Zijl, P.C., Jezzard, P., Luijten, P.R., Hendrikse, J., 2011. Blood oxygenation level-dependent (BOLD) total and extravascular signal changes and DeltaR2* in human visual cortex at 1.5, 3.0 and 7.0 T. NMR Biomed 24, 25-34.

Donahue, M.J., Hua, J., Pekar, J.J., van Zijl, P.C., 2009b. Effect of inflow of fresh blood on vascular-space-occupancy (VASO) contrast. Magn Reson Med 61, 473-480.

Donahue, M.J., Lu, H., Jones, C.K., Edden, R.A., Pekar, J.J., van Zijl, P.C., 2006a. Theoretical and experimental investigation of the VASO contrast mechanism. Magn Reson Med 56, 1261-1273.

Donahue, M.J., Lu, H., Jones, C.K., Pekar, J.J., van Zijl, P.C., 2006b. An account of the discrepancy between MRI and PET cerebral blood flow measures. A high-field MRI investigation. NMR Biomed 19, 1043-1054.

Donahue, M.J., MacIntosh, B.J., Sideso, E., Bright, M., Kennedy, J., Handa, A., Jezzard, P., 2009c. Absolute cerebral blood volume (CBV) quantification without contrast agents using inflow vascular-space-occupancy (iVASO)

with dynamic subtraction. Proc 17th Annual Meeting ISMRM Honolulu, Hawai'i, USA, 0628.

Donahue, M.J., Piechnik, S.K., Tijssen, R., Gallichan, D., Miller, K.L., Jezzard, P., 2009d. A theoretical and experimental investigation of vascular-space-occupancy (VASO) blood nulling times: influence of hematocrit and oxygenation on null times and CBV quantification. Proc 17th Annual Meeting ISMRM Hawaii, USA, 1576.

Donahue, M.J., Sideso, E., MacIntosh, B.J., Kennedy, J., Handa, A., Jezzard, P., 2010. Absolute arterial cerebral blood volume quantification using inflow vascular-space-occupancy with dynamic subtraction magnetic resonance imaging. J Cereb Blood Flow Metab 30, 1329-1342.

Donahue, M.J., Stevens, R.D., de Boorder, M., Pekar, J.J., Hendrikse, J., van Zijl, P.C., 2009e. Hemodynamic changes after visual stimulation and breath holding provide evidence for an uncoupling of cerebral blood flow and volume from oxygen metabolism. J Cereb Blood Flow Metab 29, 176-185.

Duong, T.Q., Yacoub, E., Adriany, G., Hu, X., Ugurbil, K., Kim, S.G., 2003. Microvascular BOLD contribution at 4 and 7 T in the human brain: gradient-echo and spin-echo fMRI with suppression of blood effects. Magn Reson Med 49, 1019-1027.

Epstein, F.H., Mugler, J.P., 3rd, Brookeman, J.R., 1996. Spoiling of transverse magnetization in gradient-echo (GRE) imaging during the approach to steady state. Magn Reson Med 35, 237-245.

Ernst RR 1987. Methodology of magnetic resonance imaging. Q Rev Biophys 19:183-220.

Essig, M., Shiroishi, M.S., Nguyen, T.B., Saake, M., Provenzale, J.M., Enterline, D., Anzalone, N., Dorfler, A., Rovira, A., Wintermark, M., Law, M., 2013. Perfusion MRI: the five most frequently asked technical questions. AJR Am J Roentgenol 200, 24-34.

Francis, S.T., Bowtell, R., Gowland, P.A., 2008. Modeling and optimization of Look-Locker spin labeling for measuring perfusion and transit time changes in activation studies taking into account arterial blood volume. Magn Reson Med 59, 316-325.

Fujita, N., 2001. Extravascular contribution of blood oxygenation level-dependent signal changes: a numerical analysis based on a vascular network model. Magn Reson Med 46, 723-734.

Gai, N.D., Talagala, S.L., Butman, J.A., 2011. Whole-brain cerebral blood flow mapping using 3D echo planar imaging and pulsed arterial tagging. J Magn Reson Imaging 33, 287-295.

Garcia, D.M., Duhamel, G., Alsop, D.C., 2005. Efficiency of inversion pulses for background suppressed arterial spin labeling. Magn Reson Med 54, 366-372.

Gati, J.S., Menon, R.S., Ugurbil, K., Rutt, B.K., 1997. Experimental determination of the BOLD field strength dependence in vessels and tissue. Magn Reson Med 38, 296-302.

Gauthier, C.J., Madjar, C., Tancredi, F.B., Stefanovic, B., Hoge, R.D., 2011. Elimination of visually evoked BOLD responses during carbogen inhalation: implications for calibrated MRI. Neuroimage 54, 1001-1011.

Golay, X., Silvennoinen, M.J., Zhou, J., Clingman, C.S., Kauppinen, R.A., Pekar, J.J., van Zij, P.C., 2001. Measurement of tissue oxygen extraction ratios from venous blood T(2): increased precision and validation of principle. Magn Reson Med 46, 282-291.

Gonzalez-At, J.B., Alsop, D.C., Detre, J.A., 2000. Cerebral perfusion and arterial transit time changes during task activation determined with continuous arterial spin labeling. Magn Reson Med 43, 739-746.

Gonzalez-Castillo, J., Roopchansingh, V., Bandettini, P.A., Bodurka, J., 2011. Physiological noise effects on the flip angle selection in BOLD fMRI. NeuroImage 54, 2764-2778.

Grandin, C.B., Bol, A., Smith, A.M., Michel, C., Cosnard, G., 2005. Absolute CBF and CBV measurements by MRI bolus tracking before and after acetazolamide challenge: repeatabilily and comparison with PET in humans. Neuroimage 26, 525-535.

Grgac, K., van Zijl, P.C., Qin, Q., 2013. Hematocrit and oxygenation dependence of blood (1)H2O T1 at 7 tesla. Magn Reson Med 70, 1153-1159.

Griffeth, V.E., Buxton, R.B., 2011. A theoretical framework for estimating cerebral oxygen metabolism changes using the calibrated-BOLD method: modeling the effects of blood volume distribution, hematocrit, oxygen extraction fraction, and tissue signal properties on the BOLD signal. Neuroimage 58, 198-212.

Grubb, R.L., Jr., Raichle, M.E., Eichling, J.O., Ter-Pogossian, M.M., 1974. The effects of changes in PaCO2 on cerebral blood volume, blood flow, and vascular mean transit time. Stroke 5, 630-639.

Gu, H., Lu, H., Ye, F.Q., Stein, E.A., Yang, Y., 2006. Noninvasive quantification of cerebral blood volume in humans during functional activation. Neuroimage 30, 377-387.

Gu, H., Stein, E.A., Yang, Y., 2005. Nonlinear responses of cerebral blood volume, blood flow and blood oxygenation signals during visual stimulation. Magn Reson Imaging 23, 921-928.

Gunther, M., Bock, M., Schad, L.R., 2001. Arterial spin labeling in combination with a look-locker sampling strategy: inflow turbo-sampling EPI-FAIR (ITS-FAIR). Magn Reson Med 46, 974-984.

Gunther, M., Oshio, K., Feinberg, D.A., 2005. Single-shot 3D imaging techniques improve arterial spin labeling perfusion measurements. Magn Reson Med 54, 491-498.

Haacke, E.M., Lai, S., Reichenbach, J.R., Kuppusamy, K., Hoogenraad, F.G., Takeichi, H., Lin, W., 1997. In vivo measurement of blood oxygen saturation using magnetic resonance imaging: a direct validation of the blood oxygen level-dependent concept in functional brain imaging. Hum Brain Mapp 5, 341-346.

Harel, N., Lin, J., Moeller, S., Ugurbil, K., Yacoub, E., 2006. Combined imaging-histological study of cortical laminar specificity of fMRI signals. Neuroimage 29, 879-887.

Lauterburg, P. 1973. Image formation by induced local interactions-examples employing nuclear magnetic-resonance. Nature 242:190-191.

Hoge, R.D., Atkinson, J., Gill, B., Crelier, G.R., Marrett, S., Pike, G.B., 1999. Investigation of BOLD signal dependence on cerebral blood flow and oxygen consumption: the deoxyhemoglobin dilution model. Magn Reson Med 42, 849-863.

Hua, J., Donahue, M.J., Zhao, J.M., Grgac, K., Huang, A.J., Zhou, J., van Zijl, P.C., 2009a. Magnetization transfer enhanced vascular-space-occupancy (MT-VASO) functional MRI. Magn Reson Med 61, 944-951.

Hua, J., Jones, C.K., Qin, Q., van Zijl, P.C., 2013a. Implementation of vascular-space-occupancy MRI at 7T. Magn Reson Med 69, 1003-1013.

Hua, J., Qin, Q., Donahue, M.J., Zhou, J., Pekar, J.J., van Zijl, P.C., 2009b. Functional MRI using arteriolar cerebral blood volume changes. Proc 17th Annual Meeting ISMRM Honolulu, Hawai'i, USA, 0012.

Hua, J., Qin, Q., Donahue, M.J., Zhou, J., Pekar, J.J., van Zijl, P.C., 2011a. Inflow-based vascular-space-occupancy (iVASO) MRI. Magn Reson Med 66, 40-56.

Hua, J., Qin, Q., Pekar, J.J., van Zijl, P.C., 2009c. Measuring absolute arteriolar cerebral blood volume (CBVa) in human brain gray matter (GM) without contrast agent. Proc 17th Annual Meeting ISMRM Honolulu, Hawai'i, USA, 1533.

Hua, J., Qin, Q., Pekar, J.J., van Zijl, P.C., 2011b. Measurement of absolute arterial cerebral blood volume in human brain without using a contrast agent. NMR Biomed 24, 1313-1325.

Hua, J., Qin, Q., van Zijl, P.C., Pekar, J.J., Jones, C.K., 2013b. Whole-brain three-dimensional T2-weighted BOLD functional magnetic resonance imaging at 7 Tesla. Magn Reson Med.

Hua, J., Qin, Q., van Zijl, P.C., Pekar, J.J., Jones, C.K., 2014. Whole-brain three-dimensional T2-weighted BOLD functional magnetic resonance imaging at 7 Tesla. Magn Reson Med 72, 1530-1540.

Hua, J., Stevens, R.D., Donahue, M.J., Huang, A.J., Pekar, J.J., van Zijl, P.C., 2010. Cerebral blood volume changes in arterial and post-arterial compartments and their relationship with cerebral blood flow alteration during brief breath-holding and visual stimulation in human brain. Proc 18th Annual Meeting ISMRM Stockholm, Sweden, 2749.

Hua, J., Stevens, R.D., Huang, A.J., Pekar, J.J., van Zijl, P.C., 2011c. Physiological origin for the BOLD poststimulus undershoot in human brain: vascular compliance versus oxygen metabolism. J Cereb Blood Flow Metab 31, 1599-1611.

Huber, L., Goense, J., Kennerley, A.J., Trampel, R., Guidi, M., Reimer, E., Ivanov, D., Neef, N., Gauthier, C.J., Turner, R., Moller, H.E., 2015. Cortical lamina-dependent blood volume changes in human brain at 7 T. Neuroimage 107, 23-33.

Huber, L., Ivanov, D., Krieger, S.N., Streicher, M.N., Mildner, T., Poser, B.A., Moller, H.E., Turner, R., 2013. Slab-selective, BOLD-corrected VASO at 7 tesla provides measures of cerebral blood volume reactivity with high signal-to-noise ratio. Magn Reson Med.

Ito, H., Takahashi, K., Hatazawa, J., Kim, S.G., Kanno, I., 2001. Changes in human regional cerebral blood flow and cerebral blood volume during visual stimulation measured by positron emission tomography. J Cereb Blood Flow Metab 21, 608-612.

Jain, V., Abdulmalik, O., Propert, K.J., Wehrli, F.W., 2012. Investigating the magnetic susceptibility properties of fresh human blood for noninvasive oxygen saturation quantification. Magn Reson Med 68, 863-867.

Jin, T., Kim, S.G., 2008. Improved cortical-layer specificity of vascular space occupancy fMRI with slab inversion relative to spin-echo BOLD at 9.4 T. Neuroimage 40, 59-67.

Jin, T., Kim, S.G., 2010. Change of the cerebrospinal fluid volume during brain activation investigated by T(1rho)-weighted fMRI. Neuroimage 51, 1378-1383.

Jochimsen, T.H., Norris, D.G., Mildner, T., Moller, H.E., 2004. Quantifying the intra- and extravascular contributions to spin-echo fMRI at 3 T. Magn Reson Med 52, 724-732.

Kennan, R.P., Zhong, J., Gore, J.C., 1994. Intravascular susceptibility contrast mechanisms in tissues. Magn Reson Med 31, 9-21.

Kim, S.G., 1995. Quantification of relative cerebral blood flow change by flow-sensitive alternating inversion recovery (FAIR) technique: application to functional mapping. Magn Reson Med 34, 293-301.

Koehler, R.C., Roman, R.J., Harder, D.R., 2009. Astrocytes and the regulation of cerebral blood flow. Trends Neurosci 32, 160-169.

Krieger, S.N., Huber, L., Egan, G., Turner, R., 2013. Simultaneous acquisition of cerebral blood volume, blood flow and blood oxygenation weighted MRI signals at 7T. Proc 21st Annual Meeting ISMRM Salt Lake City, Utah, USA.

Kruger, G., Glover, G.H., 2001. Physiological noise in oxygenation-sensitive magnetic resonance imaging. Magn Reson Med 46, 631-637.

Kruger, G., Kastrup, A., Glover, G.H., 2001. Neuroimaging at 1.5 T and 3.0 T: comparison of oxygenation-sensitive magnetic resonance imaging. Magn Reson Med 45, 595-604.

Kuhl, D.E., Alavi, A., Hoffman, E.J., Phelps, M.E., Zimmerman, R.A., Obrist, W.D., Bruce, D.A., Greenberg, J.H., Uzzell, B., 1980. Local cerebral blood volume in head-injured patients. Determination by emission computed tomography of 99mTc-labeled red cells. J Neurosurg 52, 309-320.

Kwong, K.K., Chesler, D.A., Weisskoff, R.M., Donahue, K.M., Davis, T.L., Ostergaard, L., Campbell, T.A., Rosen, B.R., 1995. MR perfusion studies with T1-weighted echo planar imaging. Magn Reson Med 34, 878-887.

Le Bihan, D., Breton, E., Lallemand, D., Aubin, M.L., Vignaud, J., Laval-Jeantet, M., 1988. Separation of diffusion and perfusion in intravoxel incoherent motion MR imaging. Radiology 168, 497-505.

Lee, S.P., Silva, A.C., Ugurbil, K., Kim, S.G., 1999. Diffusion-weighted spin-echo fMRI at 9.4 T: microvascular/tissue contribution to BOLD signal changes. Magn Reson Med 42, 919-928.

Leenders, K.L., Perani, D., Lammertsma, A.A., Heather, J.D., Buckingham, P., Healy, M.J., Gibbs, J.M., Wise, R.J., Hatazawa, J., Herold, S., et al., 1990. Cerebral blood flow, blood volume and oxygen utilization. Normal values and effect of age. Brain 113 (Pt 1), 27-47.

Leontiev, O., Dubowitz, D.J., Buxton, R.B., 2007. CBF/CMRO2 coupling measured with calibrated BOLD fMRI: sources of bias. Neuroimage 36, 1110-1122.

Li, D., Wang, Y., Waight, D.J., 1998. Blood oxygen saturation assessment in vivo using T2* estimation. Magn Reson Med 39, 685-690.

Li, T.Q., van Gelderen, P., Merkle, H., Talagala, L., Koretsky, A.P., Duyn, J., 2006. Extensive heterogeneity in white matter intensity in high-resolution T2*-weighted MRI of the human brain at 7.0 T. Neuroimage 32, 1032-1040.

Lin, A.L., Fox, P.T., Yang, Y., Lu, H., Tan, L.H., Gao, J.H., 2008. Evaluation of MRI models in the measurement of CMRO2 and its relationship with CBF. Magn Reson Med 60, 380-389.

Lin, A.L., Fox, P.T., Yang, Y., Lu, H., Tan, L.H., Gao, J.H., 2009. Time-dependent correlation of cerebral blood flow with oxygen metabolism in activated human visual cortex as measured by fMRI. Neuroimage 44, 16-22.

Lin, A.L., Lu, H., Fox, P.T., Duong, T.Q., 2011. Cerebral Blood Volume Measurements - Gd_DTPA vs. VASO - and Their Relationship with Cerebral Blood Flow in Activated Human Visual Cortex. Open Neuroimag J 5, 90-95.

Lin, C., Bernstein, M.A., 2008. 3D magnetization prepared elliptical centric fast gradient echo imaging. Magn Reson Med 59, 434-439.

Lu, H., 2008. Magnetization "reset" for non-steady-state blood spins in Vascular-Space-Occupancy (VASO) fMRI. Proc 16th Annual Meeting ISMRM Toronto, Canada. , 406.

Lu, H., Clingman, C., Golay, X., van Zijl, P.C., 2004a. Determining the longitudinal relaxation time (T1) of blood at 3.0 Tesla. Magn Reson Med 52, 679-682.

Lu, H., Donahue, M.J., van Zijl, P.C., 2006. Detrimental effects of BOLD signal in arterial spin labeling fMRI at high field strength. Magn Reson Med 56, 546-552.

Lu, H., Ge, Y., 2008. Quantitative evaluation of oxygenation in venous vessels using T2-Relaxation-Under-Spin-Tagging MRI. Magn Reson Med 60, 357-363.

Lu, H., Golay, X., Pekar, J.J., Van Zijl, P.C., 2003. Functional magnetic resonance imaging based on changes in vascular space occupancy. Magn Reson Med 50, 263-274.

Lu, H., Golay, X., Pekar, J.J., Van Zijl, P.C., 2004b. Sustained poststimulus elevation in cerebral oxygen utilization after vascular recovery. J Cereb Blood Flow Metab 24, 764-770.

Lu, H., Hua, J., van Zijl, P.C., 2013. Noninvasive functional imaging of cerebral blood volume with vascular-space-occupancy (VASO) MRI. NMR Biomed 26, 932-948.

Lu, H., Law, M., Johnson, G., Ge, Y., van Zijl, P.C., Helpern, J.A., 2005a. Novel approach to the measurement of absolute cerebral blood volume using vascular-space-occupancy magnetic resonance imaging. Magn Reson Med 54, 1403-1411.

Lu, H., Nagae-Poetscher, L.M., Golay, X., Lin, D., Pomper, M., van Zijl, P.C., 2005b. Routine clinical brain MRI sequences for use at 3.0 Tesla. J Magn Reson Imaging 22, 13-22.

Lu, H., van Zijl, P.C., 2005. Experimental measurement of extravascular parenchymal BOLD effects and tissue oxygen extraction fractions using multi-echo VASO fMRI at 1.5 and 3.0 T. Magn Reson Med 53, 808-816.

Lu, H., van Zijl, P.C., Hendrikse, J., Golay, X., 2004c. Multiple acquisitions with global inversion cycling (MAGIC): a multislice technique for vascular-space-occupancy dependent fMRI. Magn Reson Med 51, 9-15.

Lu, H., Xu, F., Grgac, K., Liu, P., Qin, Q., van Zijl, P., 2012. Calibration and validation of TRUST MRI for the estimation of cerebral blood oxygenation. Magn Reson Med 67, 42-49.

Luh, W.M., Wong, E.C., Bandettini, P.A., Hyde, J.S., 1999. QUIPSS II with thin-slice TI1 periodic saturation: a method for improving accuracy of quantitative perfusion imaging using pulsed arterial spin labeling. Magn Reson Med 41, 1246-1254.

Maleki, N., Dai, W., Alsop, D.C., 2012. Optimization of background suppression for arterial spin labeling perfusion imaging. MAGMA 25, 127-133.

Mandeville, J.B., Marota, J.J., Kosofsky, B.E., Keltner, J.R., Weissleder, R., Rosen, B.R., Weisskoff, R.M., 1998. Dynamic functional imaging of relative cerebral blood volume during rat forepaw stimulation. Magn Reson Med 39, 615-624.

Mansfield P, Pykett IL, Morris PG. 1978. Human whole body line-scan imaging by NMR. Br J Radiol 51:921-922.

Mark, C.I., Fisher, J.A., Pike, G.B., 2011. Improved fMRI calibration: precisely controlled hyperoxic versus hypercapnic stimuli. Neuroimage 54, 1102-1111.

Mintun, M.A., Lundstrom, B.N., Snyder, A.Z., Vlassenko, A.G., Shulman, G.L., Raichle, M.E., 2001. Blood flow and oxygen delivery to human brain during functional activity: theoretical modeling and experimental data. Proc Natl Acad Sci U S A 98, 6859-6864.

Mohtasib, R.S., Lumley, G., Goodwin, J.A., Emsley, H.C., Sluming, V., Parkes, L.M., 2012. Calibrated fMRI during a cognitive Stroop task reveals reduced metabolic response with increasing age. Neuroimage 59, 1143-1151.

Mugler, J.P., 3rd, Brookeman, J.R., 1990. Three-dimensional magnetization-prepared rapid gradient-echo imaging (3D MP RAGE). Magn Reson Med 15, 152-157.

Nagayama K, Wuthrich K, Bachmann P, Ernst RR. 1977. Two-dimensional J-resolved 1H nmr spectroscopy for studies of biological macromolecules. Biochem Biophys Res Commun 78:99-105

Nielsen, J.F., Hernandez-Garcia, L., 2013. Functional perfusion imaging using pseudocontinuous arterial spin labeling with low-flip-angle segmented 3D spiral readouts. Magn Reson Med 69, 382-390.

Norris, D.G., 2012. Spin-echo fMRI: The poor relation? Neuroimage 62, 1109-1115.

Ogawa, S., Menon, R.S., Tank, D.W., Kim, S.G., Merkle, H., Ellermann, J.M., Ugurbil, K., 1993. Functional brain mapping by blood oxygenation level-dependent contrast magnetic resonance imaging. A comparison of signal characteristics with a biophysical model. Biophys J 64, 803-812.

Oja, J.M., Gillen, J.S., Kauppinen, R.A., Kraut, M., van Zijl, P.C., 1999. Determination of oxygen extraction ratios by magnetic resonance imaging. J Cereb Blood Flow Metab 19, 1289-1295.

Ordidge, R.J., Wylezinska, M., Hugg, J.W., Butterworth, E., Franconi, F., 1996. Frequency offset corrected inversion (FOCI) pulses for use in localized spectroscopy. Magn Reson Med 36, 562-566.

Peppiatt, C.M., Howarth, C., Mobbs, P., Attwell, D., 2006. Bidirectional control of CNS capillary diameter by pericytes. Nature 443, 700-704.

Perthen, J.E., Lansing, A.E., Liau, J., Liu, T.T., Buxton, R.B., 2008. Caffeine-induced uncoupling of cerebral blood flow and oxygen metabolism: a calibrated BOLD fMRI study. Neuroimage 40, 237-247.

Petersen, E.T., Lim, T., Golay, X., 2006. Model-free arterial spin labeling quantification approach for perfusion MRI. Magn Reson Med 55, 219-232.

Piechnik, S.K., Evans, J., Bary, L.H., Wise, R.G., Jezzard, P., 2009. Functional changes in CSF volume estimated using measurement of water T2 relaxation. Magn Reson Med 61, 579-586.

Poser, B.A., Norris, D.G., 2011. Application of whole-brain CBV-weighted fMRI to a cognitive stimulation paradigm: robust activation detection in a stroop task experiment using 3D GRASE VASO. Hum Brain Mapp 32, 974-981.

Powers, W.J., Hirsch, I.B., Cryer, P.E., 1996. Effect of stepped hypoglycemia on regional cerebral blood flow response to physiological brain activation. Am J Physiol 270, H554-559.

Purcell E, Torrey H, Pound R. 1946. Resonance absorption by nuclear magnetic moments in a solid. Phys Rev 60:37-38

Qin, Q., Grgac, K., van Zijl, P.C., 2011. Determination of whole-brain oxygen extraction fractions by fast measurement of blood T(2) in the jugular vein. Magn Reson Med 65, 471-479.

Qin, Q., Huang, A.J., Hua, J., Desmond, J.E., Stevens, R.D., van Zijl, P.C., 2014. Three-dimensional whole-brain perfusion quantification using pseudo-continuous arterial spin labeling MRI at multiple post-labeling delays: accounting for both arterial transit time and impulse response function. NMR Biomed 27, 116-128.

Rooney, W.D., Johnson, G., Li, X., Cohen, E.R., Kim, S.G., Ugurbil, K., Springer, C.S., Jr., 2007. Magnetic field and tissue dependencies of human brain longitudinal 1H2O relaxation in vivo. Magn Reson Med 57, 308-318.

Rostrup, E., Knudsen, G.M., Law, I., Holm, S., Larsson, H.B., Paulson, O.B., 2005. The relationship between cerebral blood flow and volume in humans. Neuroimage 24, 1-11.

Schmithorst, V.J., Hernandez-Garcia, L., Vannest, J., Rajagopal, A., Lee, G., Holland, S.K., 2014. Optimized simultaneous ASL and BOLD functional imaging of the whole brain. J Magn Reson Imaging 39, 1104-1117.

Schulte, A.C., Speck, O., Oesterle, C., Hennig, J., 2001. Separation and quantification of perfusion and BOLD effects by simultaneous acquisition of functional I(0)- and T2(*)-parameter maps. Magn Reson Med 45, 811-816.

Scouten, A., Constable, R.T., 2007. Applications and limitations of whole-brain MAGIC VASO functional imaging. Magn Reson Med 58, 306-315.

Scouten, A., Constable, R.T., 2008. VASO-based calculations of CBV change: accounting for the dynamic CSF volume. Magn Reson Med 59, 308-315.

Sharan, M., Jones, M.D., Jr., Koehler, R.C., Traystman, R.J., Popel, A.S., 1989. A compartmental model for oxygen transport in brain microcirculation. Ann Biomed Eng 17, 13-38.

Silva, A.C., Williams, D.S., Koretsky, A.P., 1997. Evidence for the exchange of arterial spin-labeled water with tissue water in rat brain from diffusion-sensitized measurements of perfusion. Magn Reson Med 38, 232-237.

Silvennoinen, M.J., Clingman, C.S., Golay, X., Kauppinen, R.A., van Zijl, P.C., 2003. Comparison of the dependence of blood R2 and R2* on oxygen saturation at 1.5 and 4.7 Tesla. Magn Reson Med 49, 47-60.

Song, A.W., Wong, E.C., Tan, S.G., Hyde, J.S., 1996. Diffusion weighted fMRI at 1.5 T. Magn Reson Med 35, 155-158.

Spees, W.M., Yablonskiy, D.A., Oswood, M.C., Ackerman, J.J., 2001. Water proton MR properties of human blood at 1.5 Tesla: magnetic susceptibility, T(1), T(2), T*(2), and non-Lorentzian signal behavior. Magn Reson Med 45, 533-542.

Stables, L.A., Kennan, R.P., Gore, J.C., 1998. Asymmetric spin-echo imaging of magnetically inhomogeneous systems: theory, experiment, and numerical studies. Magn Reson Med 40, 432-442.

Thomas, D.L., Lythgoe, M.F., Calamante, F., Gadian, D.G., Ordidge, R.J., 2001. Simultaneous noninvasive measurement of CBF and CBV using double-echo FAIR (DEFAIR). Magn Reson Med 45, 853-863.

Triantafyllou, C., Hoge, R.D., Krueger, G., Wiggins, C.J., Potthast, A., Wiggins, G.C., Wald, L.L., 2005. Comparison of physiological noise at 1.5 T, 3 T and 7 T and optimization of fMRI acquisition parameters. Neuroimage 26, 243-250.

Ugurbil, K., Garwood, M., Ellermann, J., Hendrich, K., Hinke, R., Hu, X., Kim, S.G., Menon, R., Merkle, H., Ogawa, S., et al., 1993. Imaging at high magnetic fields: initial experiences at 4 T. Magn Reson Q 9, 259-277.

Ugurbil, K., Hu, X., Chen, W., Zhu, X.H., Kim, S.G., Georgopoulos, A., 1999. Functional mapping in the human brain using high magnetic fields. Philos Trans R Soc Lond B Biol Sci 354, 1195-1213.

Ugurbil, K., Toth, L., Kim, D.S., 2003. How accurate is magnetic resonance imaging of brain function? Trends Neurosci 26, 108-114.

Uh, J., Lin, A.L., Lee, K., Liu, P., Fox, P., Lu, H., 2011. Validation of VASO cerebral blood volume measurement with positron emission tomography. Magn Reson Med 65, 744-749.

Uludag, K., Muller-Bierl, B., Ugurbil, K., 2009. An integrative model for neuronal activity-induced signal changes for gradient and spin echo functional imaging. Neuroimage 48, 150-165.

van der Zwaag, W., Francis, S., Head, K., Peters, A., Gowland, P., Morris, P., Bowtell, R., 2009. fMRI at 1.5, 3 and 7 T: characterising BOLD signal changes. Neuroimage 47, 1425-1434.

van Gelderen, P., de Zwart, J.A., Duyn, J.H., 2008. Pittfalls of MRI measurement of white matter perfusion based on arterial spin labeling. Magn Reson Med 59, 788-795.

van Osch, M.J., Teeuwisse, W.M., van Walderveen, M.A., Hendrikse, J., Kies, D.A., van Buchem, M.A., 2009. Can arterial spin labeling detect white matter perfusion signal? Magn Reson Med 62, 165-173.

van Zijl, P.C., Eleff, S.M., Ulatowski, J.A., Oja, J.M., Ulug, A.M., Traystman, R.J., Kauppinen, R.A., 1998. Quantitative assessment of blood flow, blood volume and blood oxygenation effects in functional magnetic resonance imaging. Nat Med 4, 159-167.

Visser, F., Zwanenburg, J.J., Hoogduin, J.M., Luijten, P.R., 2010. High-resolution magnetization-prepared 3D-FLAIR imaging at 7.0 Tesla. Magn Reson Med 64, 194-202.

Wang, D.J., Alger, J.R., Qiao, J.X., Gunther, M., Pope, W.B., Saver, J.L., Salamon, N., Liebeskind, D.S., Investigators, U.S., 2013. Multi-delay multi-parametric arterial spin-labeled perfusion MRI in acute ischemic stroke - Comparison with dynamic susceptibility contrast enhanced perfusion imaging. Neuroimage Clin 3, 1-7.

Wang, J., Yarnykh, V.L., Hatsukami, T., Chu, B., Balu, N., Yuan, C., 2007. Improved suppression of plaque-mimicking artifacts in black-blood carotid atherosclerosis imaging

using a multislice motion-sensitized driven-equilibrium (MSDE) turbo spin-echo (TSE) sequence. Magn Reson Med 58, 973-981.

Wang, J., Yarnykh, V.L., Yuan, C., 2010. Enhanced image quality in black-blood MRI using the improved motion-sensitized driven-equilibrium (iMSDE) sequence. J Magn Reson Imaging 31, 1256-1263.

Weisskoff, R.M., Kiihne, S., 1992. MRI susceptometry: image-based measurement of absolute susceptibility of MR contrast agents and human blood. Magn Reson Med 24, 375-383.

Weisskoff, R.M., Zuo, C.S., Boxerman, J.L., Rosen, B.R., 1994. Microscopic susceptibility variation and transverse relaxation: theory and experiment. Magn Reson Med 31, 601-610.

Wolff, S.D., Balaban, R.S., 1989. Magnetization transfer contrast (MTC) and tissue water proton relaxation in vivo. Magn Reson Med 10, 135-144.

Wong, E.C., 2007. Vessel-encoded arterial spin-labeling using pseudocontinuous tagging. Magn Reson Med 58, 1086-1091.

Wong, E.C., Buxton, R.B., Frank, L.R., 1997. Implementation of quantitative perfusion imaging techniques for functional brain mapping using pulsed arterial spin labeling. NMR Biomed 10, 237-249.

Wong, E.C., Buxton, R.B., Frank, L.R., 1998. Quantitative imaging of perfusion using a single subtraction (QUIPSS and QUIPSS II). Magn Reson Med 39, 702-708.

Wright, G.A., Hu, B.S., Macovski, A., 1991. 1991 I.I. Rabi Award. Estimating oxygen saturation of blood in vivo with MR imaging at 1.5 T. J Magn Reson Imaging 1, 275-283.

Wu, W.C., Buxton, R.B., Wong, E.C., 2007a. Vascular space occupancy weighted imaging with control of residual blood signal and higher contrast-to-noise ratio. IEEE Trans Med Imaging 26, 1319-1327.

Wu, W.C., Fernandez-Seara, M., Detre, J.A., Wehrli, F.W., Wang, J., 2007b. A theoretical and experimental investigation of the tagging efficiency of pseudocontinuous arterial spin labeling. Magn Reson Med 58, 1020-1027.

Xu, F., Ge, Y., Lu, H., 2009. Noninvasive quantification of whole-brain cerebral metabolic rate of oxygen (CMRO2) by MRI. Magn Reson Med 62, 141-148.

Yablonskiy, D.A., Ackerman, J.J., Raichle, M.E., 2000. Coupling between changes in human brain temperature and oxidative metabolism during prolonged visual stimulation. Proc Natl Acad Sci U S A 97, 7603-7608.

Yablonskiy, D.A., Haacke, E.M., 1994. Theory of NMR signal behavior in magnetically inhomogeneous tissues: the static dephasing regime. Magn Reson Med 32, 749-763.

Yacoub, E., Duong, T.Q., Van De Moortele, P.F., Lindquist, M., Adriany, G., Kim, S.G., Ugurbil, K., Hu, X., 2003. Spin-echo fMRI in humans using high spatial resolutions and high magnetic fields. Magn Reson Med 49, 655-664.

Yacoub, E., Shmuel, A., Logothetis, N., Ugurbil, K., 2007. Robust detection of ocular dominance columns in humans using Hahn Spin Echo BOLD functional MRI at 7 Tesla. Neuroimage 37, 1161-1177.

Yacoub, E., Shmuel, A., Pfeuffer, J., Van De Moortele, P.F., Adriany, G., Andersen, P., Vaughan, J.T., Merkle, H., Ugurbil, K., Hu, X., 2001. Imaging brain function in humans at 7 Tesla. Magn Reson Med 45, 588-594.

Yacoub, E., Van De Moortele, P.F., Shmuel, A., Ugurbil, K., 2005. Signal and noise characteristics of Hahn SE and GE BOLD fMRI at 7 T in humans. Neuroimage 24, 738-750.

Yang, Y., Gu, H., Stein, E.A., 2004. Simultaneous MRI acquisition of blood volume, blood flow, and blood oxygenation information during brain activation. Magn Reson Med 52, 1407-1417.

Ye, F.Q., Frank, J.A., Weinberger, D.R., McLaughlin, A.C., 2000. Noise reduction in 3D perfusion imaging by attenuating the static signal in arterial spin tagging (ASSIST). Magn Reson Med 44, 92-100.

Ye, F.Q., Mattay, V.S., Jezzard, P., Frank, J.A., Weinberger, D.R., McLaughlin, A.C., 1997. Correction for vascular artifacts in cerebral blood flow values measured by using arterial spin tagging techniques. Magn Reson Med 37, 226-235.

Zhao, F., Wang, P., Hendrich, K., Ugurbil, K., Kim, S.G., 2006. Cortical layer-dependent BOLD and CBV responses measured by spin-echo and gradient-echo fMRI: insights into hemodynamic regulation. Neuroimage 30, 1149-1160.

Zhao, F., Wang, P., Kim, S.G., 2004. Cortical depth-dependent gradient-echo and spin-echo BOLD fMRI at 9.4T. Magn Reson Med 51, 518-524.

Zhao, J.M., Clingman, C.S., Narvainen, M.J., Kauppinen, R.A., van Zijl, P.C., 2007. Oxygenation and hematocrit dependence of transverse relaxation rates of blood at 3T. Magn Reson Med 58, 592-597.

CURRICULUM VITAE

YING CHENG   E-mail: yingcheng88@gmail.com

THE JOHNS HOPKINS UNIVERSITY   Cell: 443-220-9688

F.M. KIRBY RESEARCH CENTER

707 N. BROADWAY

BALTIMORE, MD 21205

USA

Personal

Name: Ying Cheng
Date of Birth: December 13, 1988
Nationality: P.R. China

Education

August 2010 – Present	The Johns Hopkins University, Baltimore, MD, U.S.A.	Ph.D.
	Major in Biomedical Engineering	
	Mentor: Dr. Peter C.M. van Zijl	

August 2006 – July 2010	Northeastern University, Shenyang, Liaoning, China P.R.	B.S.
	Major in Biomedical Engineering	

Professional Experience

F.M. Kirby Research Center for Functional Brain Imaging,
Kennedy Krieger Institute, Johns Hopkins University School of Medicine, Baltimore, MD
Graduate Research Assistant
01/2011 to present

Department of Radiology and Radiological Science,
Research Rotation (Supervisors: Drs. Peter Barker and Richard Edden)
09/2010-12/2010

Philips Medical Systems,
Software Engineer Intern
06/2009-09/2009

Teaching Experience

Teaching Assistant	Signals, Systems, and Controls Biomedical Engineering, The Johns Hopkins University	Spring 2014
Teaching Assistant	Introduction to Scientific Computing Biomedical Engineering, The Johns Hopkins University	Spring 2015

Publications

Peer Reviewed Journal Papers:

Ying Cheng, Qin Qin, Peter van Zijl, James Pekar, Jun Hua. A three-dimensional single-scan approach for the measurement of changes in cerebral blood volume, blood flow, and blood oxygenation-weighted signals during functional stimulation. *In Revision.*

Ying Cheng, Peter van Zijl, James Pekar, Jun Hua. Three-dimensional acquisition of cerebral blood volume and flow responses during functional stimulation in a single scan. *NeuroImage, 2014 Dec;103:533-41.*

Ying Cheng, Peter van Zijl, Jun Hua. Measurement of parenchymal extravascular R2* using multi-echo VASO at 7T. *NMR in Biomedicine, 2015 Feb;28(2):264-71*

Jarunee Intrapiromkul, He Zhu, **Ying Cheng**, Peter B. Barker, Richard A.E. Edden. Determining the in vivo transverse relaxation time of GABA in the human brain at 7T. *Journal of Magnetic Resonance Imaging, 2012*; 38(5): 1224-1229.

Richard A.E. Edden, Jarunee Intrapiromkul, He Zhu, **Ying Cheng**, Peter B. Barker. Measuring T2 in vivo with J-difference editing: Application to GABA at 3 Tesla. *Magnetic Resonance in Medicine, 2011;* 35(1): 229-234.

Yue Zhao, Xiaoyu Cui, **Ying Cheng**. High-performance and real-time volume rendering in CUDA. *Biomedical Engineering and Informatics, 2009. BMEI'09.*

Book Chapters:

Jun Hua, **Ying Cheng**, Peter van Zijl (2016). The Vascular-space-occupancy (VASO) MRI. *In MR & CT Perfusion Imaging: Clinical Applications and Theoretical Principles (Roland Bammer, editor), Chapter 91. Wolters Kluwer.*

Conference Proceedings:

Ying Cheng, Qin Qin, Peter van Zijl, James Pekar, Jun Hua. Three-dimensional acquisition of cerebral blood volume, blood flow, and blood oxygenation-weighted responses during functional stimulation in a single scan. *Proceedings of International Society for Magnetic Resonance in Medicine*, 2015. Oral Presentation.

Ying Cheng, Kilian Weiss, Peter van Zijl, Kathy Zackowski, Craig K. Jones. Using chemical exchange saturation transfer (CEST) to detect glycogen-depleting exercise-induced changes in vivo. *Proceedings of International Society for Magnetic Resonance in Medicine*, 2014.

Ying Cheng, Peter van Zijl, Jun Hua. Measurement of parenchymal extravascular R2* using multi-echo VASO MRI at 7T. *Proceedings of International Society for Magnetic Resonance in Medicine*, 2012. Oral Presentation.

Invited Talks

Ying Cheng. Development of MRI Techniques for Simultaneous Assessment of Cerebral Blood Volume, Blood Flow, and Blood Oxygenation. *05/2015. Philips Research North America, Briarcliff, NY, USA.*

Ying Cheng. Development of MRI Techniques for Simultaneous Assessment of Cerebral Blood Volume, Blood Flow, and Blood Oxygenation. *03/2015. Department of Medical Physics, Memorial Sloan-Kettering Cancer Center, New York City, NY, USA.*

Ying Cheng, Kilian Weiss, Peter van Zijl, Kathy Zackowski, Craig K. Jones. Using chemical exchange saturation transfer (CEST) to detect glycogen-depleting exercise-induced changes in vivo. 10/2014. *Annual Johns Hopkins Radiology Division of MR Research Retreat, Cambridge, MD, USA.*

Ying Cheng, Peter van Zijl, Jun Hua. Concurrent 3D Acquisition of Cerebral Blood Volume and Blood Flow Responses during Functional Stimulation. 10/2012. *Annual Johns Hopkins Radiology Division of MR Research Retreat, Cambridge, MD, USA.*

Awards & Fellowships

2015   Summa cum laude Award, International Society for Magnetic Resonance in Medicine (ISMRM)

2012—2015   Educational Stipend, International Society for Magnetic Resonance in Medicine (ISMRM)

2010—2011 NIH Biomedical Engineering Training Grant

2009—2010 HP Scholarship, Hewlett-Packard Ltd.

2007—2009 National Scholarship (Top 0.3% nationwide), Ministry of Education, China.

Relevant Skills

Experience of Software Development: C++ (5+ years); MATLAB and Python (5+ years); Java (3+ years); 5+ years of MRI pulse sequence development using Philips Paradise (GOAL-C) pulse programming tool on Philips MR scanners at 3T and 7T.